Error Analysis and Adaptive Control for Gas Flow in Networks

vorgelegt von

Jeroen Johannes Stolwijk, MSc

geboren in Leiden

von der Fakultät II - Mathematik und Naturwissenschaften

der Technischen Universität Berlin

zur Erlangung des akademischen Grades

Doktor der Naturwissenschaften

Dr. rer. nat.

genehmigte Dissertation

Promotionsausschuss:

Vorsitzender:	Prof. Dr. Martin Skutella
Gutachter:	Prof. Dr. Volker Mehrmann
Gutachterin:	Prof. Dr. Nicole Marheineke
Gutachter:	JProf. Dr. Martin Schmidt

Tag der wissenschaftlichen Aussprache: 28. September 2018

Berlin 2019

Acknowledgments

First of all, I would like to thank my PhD adviser Prof. Dr. Volker Mehrmann for the fruitful and inspiring discussions, the helpful advice, and for proofreading the preliminary manuscripts. I would also like to thank Eduardo Cejudo, Dr. Pia Domschke, Aseem Dua, Prof. Dr. Jens Lang, Martijn Nagtegaal, and JProf. Dr. Martin Schmidt for our pleasant and productive collaboration. Furthermore, I am grateful to all my colleagues of both the working group Numerical Analysis at the TU Berlin and the Transregio-Collaborative Research Center (TRR-CRC) 154 for the interesting (lunch time, corridor, etc.) discussions. Special thanks go to Kerstin Ullrich and Christina Weber for carefully handling all the administrative issues. Last but not least, I would like to thank my friends, family, and, especially, my wife Patricia for their continuous support.

This work was supported by the German Research Foundation (DFG) within project B03 in the TRR-CRC 154 *Mathematical Modeling, Simulation and Optimization using the Example of Gas Networks*. Moreover, the research in Chapter 5 was supported by the DFG within project B01 in the TRR-CRC 154 and Jens Lang was also supported by the Excellence Initiative of the German Federal and State Governments via the Darmstadt Graduate School of Excellence Energy Science and Engineering. Furthermore, the research in Chapter 6 was supported by the Bavarian State Government as part of the Energie Campus Nürnberg as well as the DFG within project B08 in the TRR-CRC 154.

Zusammenfassung

In dieser Arbeit werden einheitliche Schätzer für die verschiedenen Fehler, welche eine numerische Lösung enthalten könnte, nämlich Modellierungs-, Diskretisierungs-, Iterations-, Datenunsicherheits- und Rundungsfehler, hergeleitet. Anschließend werden die Fehler auf einem Netzwerk adaptiv gesteuert, um den Gesamtfehler unter eine vorgegebene Toleranz zu bringen, während der Rechenaufwand niedrig gehalten wird. Als Beispielprobleme werden die Simulation und Optimierung von Gasflüssen durch Rohrnetzwerke betrachtet. Der Gasfluss wird durch die Euler-Gleichungen der Strömungsmechanik, welche ein System von hyperbolischen partiellen Differentialgleichungen sind, modelliert. Dieses System wird durch geeignete Anfangs-, Rand- und Kopplungsbedingungen ergänzt und unter Verwendung verschiedener Diskretisierungsverfahren für transiente Gasströmungen, z. B. des sehr effizienten impliziten Box-Schemas, diskretisiert. Aufgrund der hohen Rechenkomplexität zur Simulation oder Optimierung dieses Systems partieller Differentialgleichungen werden oft Vereinfachungen unter Verwendung geeigneter Annahmen vorgenommen, was zu einer Modellhierarchie führt. Rein algebraische Modelle können in Teilen des Netzes mit geringer Gasdynamik verwendet werden, während komplexere Modelle z. B. unmittelbar nach einem Kompressor verwendet werden sollten. In dieser Arbeit wird eine Fehler- und Sensitivitätsanalyse für viele Modelle in dieser Hierarchie durchgeführt. Da die Modellierungs- und Diskretisierungsfehler in der Literatur bereits umfassend untersucht wurden, liegt der erste Fokus auf den Rundungs- und Datenunsicherheitsfehlern. Diese Fehler werden über eine Rückwärtsfehleranalyse für die gewonnenen nichtlinearen Gleichungssysteme berechnet. Dazu wird eine neue komponentenweise Konditionszahl eingeführt und deren Vorteil gegenüber der klassischen normweise Konditionszahl demonstriert. Die entwickelte Sensitivitätsanalyse wird u. a. auf ein exemplarisches Y-förmiges Gasnetzwerk angewendet, in dem der Einfluss veränderter Randbedingungen auf den Netzwerkzustand untersucht wird. Um einen geeigneten Kompromiss zwischen Genauigkeit und Rechenkomplexität zu finden, werden die verschiedenen Fehler auf jedem Rohr adaptiv gesteuert. Dazu werden neue Greedy-ähnliche Raum/Zeit/Modell-Verfeinerungsstrategien entwickelt, welche einen Netzwerkübersicht haben und das Verhalten des Gases besser berücksichtigen als die Strategie, die derzeit in der Gasfluss-Simulationssoftware ANACONDA implementiert ist. Sowohl ein synthetisches als auch ein realistisches Experiment zeigen, dass die neuen Strategien den

Rechenaufwand im Vergleich zur aktuellen Verfeinerungsstrategie bei gleicher Fehlertoleranz signifikant reduzieren. Darüber hinaus wird gezeigt, dass eine adaptive Fehlersteuerung (unter Verwendung von Bulk-Kriterien, die häufig in der adaptiven Finite-Elemente-Methode verwendet werden) auch innerhalb eines Optimierungsalgorithmus angewendet werden kann, was wiederum zu einer Verringerung des Rechenaufwands führt. Es wird bewiesen dass, auch wenn man Vergröberungen zulässt, nach einer endlichen Anzahl von Iterationen eine ε-zulässige Lösung gefunden wird. Man beachte, dass die entwickelten Fehlerschätzer und adaptiven Fehlersteuerungstechniken nicht auf Gasnetze beschränkt sind, sondern beispielsweise auch auf Wasser-, Strom- oder Verkehrsnetze angewendet werden können.

Abstract

In this thesis, uniform estimators are derived for the different errors that a numerical solution could contain, namely modeling, discretization, iteration, data uncertainty, and rounding errors. Subsequently, the errors are adaptively controlled on a network in order to bring the total error below a prescribed tolerance while keeping the computational cost low. As example problems, the simulation and optimization of gas flow through pipeline networks are considered. The gas flow is modeled by the Euler equations of fluid dynamics, which are a system of hyperbolic partial differential equations. This system is complemented by suitable initial, boundary, and coupling conditions and discretized using different schemes, e.g., the implicit box scheme, which is an effective discretization method for transient gas flow models. Due to the high computational complexity of this system of partial differential equations, simplifications are often made using appropriate assumptions, resulting in a model hierarchy. Purely algebraic models may be used in parts of the network with low gas dynamics, whereas more involved models should be used, e.g., right after a compressor. In this thesis, an error and sensitivity analysis for many models in this hierarchy is performed. Since the modeling and discretization errors have already been extensively studied in the literature, the first focus lies on the rounding and data uncertainty errors. These errors are computed via a backward error analysis for the obtained nonlinear systems of equations. For this, a novel componentwise condition number is introduced and the advantage over the classical normwise condition number is demonstrated. The developed sensitivity analysis is applied, inter alia, on an exemplary Y-shaped gas network, where the effect of changing boundary conditions on the network state is investigated. In order to find a convenient trade-off between accuracy and computational complexity, the different errors on every pipe are adaptively controlled. For this, new Greedy-like spatial/temporal/model refinement strategies are developed, which have a network overview and take the behavior of the gas better into account than the strategy that is currently implemented in the gas flow simulation software ANACONDA. Both a synthetic and a realistic experiment show that the new strategies significantly reduce the computational cost as compared to the current refinement strategy while maintaining the same error tolerance. Moreover, it is shown that adaptive error control (using bulk criteria, which are frequently employed in the adaptive finite element method) can also be applied within an optimization algorithm, which again results in a reduction of the computational cost. It is proven that,

also when one allows for coarsenings, an ε-feasible solution is obtained after a finite number of iterations. Note that the developed error estimators and adaptive error control techniques are not limited to gas networks, but can also be applied to, e.g., water, electricity, or traffic networks.

Declaration of Personal Contribution to the Articles

Chapters 3, 5, and 6 are essentially copies of the articles

[94] J. J. Stolwijk and V. Mehrmann. Error analysis and model adaptivity for flows in gas networks. *An. Ştiinţ. Univ. "Ovidius" Constanţa Ser. Mat.*, 26(2):231–266, 2018. DOI: 10.2478/auom-2018-0027,

[34] P. Domschke, A. Dua, J. J. Stolwijk, J. Lang, and V. Mehrmann. Adaptive refinement strategies for the simulation of gas flow in networks using a model hierarchy. *Electron. Trans. Numer. Anal.*, 48:97–113, 2018. URL: http://etna.mcs.kent.edu/volumes/2011-2020/vol48/abstract.php?vol=48&pages=97-113,

[74] V. Mehrmann, M. Schmidt, and J. J. Stolwijk. Model and discretization error adaptivity within stationary gas transport optimization. *Vietnam J. Math.*, 46(4):779–801, 2018. DOI: 10.1007/s10013-018-0303-1,

respectively, which are here presented in their postprint version. The co-authors of these articles are

- Dr. Pia Domschke, Technische Universität Darmstadt,
- Aseem Dua, Technische Universität Berlin,
- Prof. Dr. Jens Lang, Technische Universität Darmstadt,
- Prof. Dr. Volker Mehrmann, Technische Universität Berlin,
- JProf. Dr. Martin Schmidt, Friedrich-Alexander-Universität Erlangen-Nürnberg.

Most of the research in Chapter 3 has been performed by Jeroen Stolwijk, whereas Volker Mehrmann provided the research topics and the supervision. Chapter 5 is the result of a close cooperation between, in particular, Pia Domschke, Aseem Dua, and Jeroen Stolwijk. The synthetic experiment in Section 5.4.1 has been implemented mainly by Aseem Dua, while Pia Domschke is the main contributor to the realistic gas network simulation in Section 5.4.2. The scientific ideas mainly stem from Aseem Dua and Jeroen Stolwijk. They also wrote most of the article. The research has been supervised by Jens Lang and Volker Mehrmann. Regarding Chapter 6, Martin Schmidt was mainly

responsible for Section 6.2 and Jeroen Stolwijk for Section 6.3. Section 6.4 and the implementation of the grid and model adaptation algorithm in Python has been a close cooperation between Martin Schmidt and Jeroen Stolwijk. The computational results in Section 6.5 were provided by Martin Schmidt. The entire research process has been closely supervised by Volker Mehrmann. All the remaining chapters of this thesis are Jeroen Stolwijk's own work.

Contents

Nomenclature & Acronyms

Mathematical Notation

$\doteq$	equal to, except for higher order terms
$\dot{\leqq}$	less than or equal to, except for higher order terms
$\boldsymbol{d}$	(uncertain) data/parameter vector
d_i	component i of vector $\boldsymbol{d}$
E_{abs}	absolute error
E_{rel}	relative error
f	one-dimensional function
F	multi-dimensional function
F'_x	Jacobian matrix of F w.r.t. x
h	spatial stepsize
$\mathscr{J}_c$	set of compressor stations
k	componentwise relative amplification vector
κ_{abs}	absolute condition number
κ_{rel}	relative condition number
$\kappa(f;d)$	condition number of f w.r.t. d
M	target functional
μ	mean of a random variable
N	sample size
n	number of parameters
σ	standard deviation of a random variable
τ	temporal stepsize
$\mathbf{u}$	rounding unit in finite precision arithmetic

Physical Quantities

A	cross-sectional area of the pipeline [m^2]
atm	standard atmospheric pressure (1.01325 bar)
bar	metric unit of pressure; equal to 100,000 N/m^2
c	speed of sound [m/s]
c_v	volumetric heat capacity [$\text{J}/(\text{m}^3\cdot\text{K})$]
D	diameter of the pipeline [m]
e	internal energy $c_v T + gh$ [J]
η	dynamic viscosity
g	gravitational acceleration on earth [m/s^2]

h	height above sea level [m]
h	hour
h'	slope of the pipeline
k	roughness [m]
k_w	heat conductivity coefficient [W/(m · K)]
λ	Darcy friction factor [1]
L	pipe length [m]
p	pressure [N/m^2]
p_c	pseudocritical pressure [N/m^2]
p_{in}	inlet pressure [N/m^2]
q	mass flow rate $A\rho v$ [kg/s]
$\bar{q}$	mass flux ρv [kg/(m^2·s)]
q_0	volume flow rate under standard conditions (air pressure of 1 atm, temperature of 0 °C) [m^3/s]
r	radius of the pipeline [m]
ρ	density [kg/m^3]
ρ_{in}	inlet density [kg/m^3]
ρ_0	density under standard conditions (air pressure of 1 atm, temperature of 0 °C) [kg/m^3]
R	specific gas constant [J/(kg·K)]
t	time [s]
t_f	final time [s]
T	temperature [K]
$\bar{T}$	constant temperature [K]
T_c	pseudocritical temperature [K]
T_{in}	inlet temperature [K]
T_w	pipeline wall temperature [K]
v	velocity [m/s]
v_{in}	inlet velocity [m/s]
x	coordinate along the pipeline [m]
x_0	begin point of the pipeline [m]
z	compressibility factor [1]

Acronyms

AGA	American Gas Association
Alg.	Algorithm
cf.	confer *(Latin)*: see, by way of comparison
DAE	differential-algebraic equation
e.g.	exempli gratia *(Latin)*: for example
Eq.	Equation
etc.	etcetera
h.o.t.	higher order terms
i.e.	id est *(Latin)*: that is
km	kilometer

MCS	Monte Carlo simulation
ODE	ordinary differential equation
p.	page
PDE	partial differential equation
pp.	pages
URQ	univariate reduced quadrature

Chapter 1

Introduction

The numerical solution of a simulation or an optimization problem inevitably contains errors from all or some of the following sources: modeling, discretization, iteration, rounding, and data uncertainty errors; see, e.g., [57]. Namely, if a mathematical model is used to describe a physical process, then the model is rarely an exact representation of reality. Thus, a modeling error is made. Also, a mathematically involved model can be simplified using certain assumptions on the problem, which yields an additional modeling error. Moreover, if the model contains ordinary or partial differential equations, then the solution can often not be obtained analytically. A discretization method should be applied to find an approximate solution, introducing a discretization error. After the discretization of the model, a (linear or nonlinear) system of equations is obtained, which is usually solved using an iterative method. Due to the preliminary stopping of this method, an iteration error is incurred. Furthermore, the computations are performed nowadays almost exclusively on computers, such that rounding errors are made due to its inherent floating-point arithmetic. Finally, model parameters can often only be determined approximately, which results in a data uncertainty error. In order for the result to be reliable, the total error should be below a prescribed tolerance. On the other hand, in order to make real-time decisions, the computational cost should be limited. Hence, an appropriate trade-off between accuracy and computational complexity should be made.

Throughout this thesis, the simulation and optimization of gas transport through pipeline networks are taken as example problems. Natural gas plays a crucial role in the energy supply of the world. It is sufficiently and readily available, it is traded, and it is storable. For example, after oil, natural gas was the second most used energy supplier in Germany in 2017 with a share of more than 20% of the total energy consumption [20]. The extensive European pipeline network that is used for the transportation of natural gas is depicted in Figure 1.1. Directed by EU regulations from 1998 and 2003, the European gas market has been liberalized with the goals of increasing the competition between gas transmission operators and ensuring the security of the gas supply [64, pp. 48, 327, 328]. The high demand for natural gas and the importance

of a dependable gas supply illustrate the need for accurate and reliable gas network simulations. Therefore, considerable research on the mathematical modeling, simulation, and optimization of gas flow through pipeline networks has been performed in the last decades, see, e.g., [1, 4, 5, 25, 28, 43, 44, 56, 61, 73, 82, 91], where different simulation models for the flow through a pipe or a network of pipes and compressor stations have been proposed. Since the simulation models are a key factor in optimization tools, adequate accuracy and high efficiency are very important. So, using error estimation, typically the grid is adapted in space and time and as a new component of the simulation process we will discuss the adaptation of the model within a model hierarchy.

An error analysis on a gas flow model hierarchy has been performed in [33, 39]. Here, only the discretization and model error with respect to a functional of interest have been analyzed. The rounding, data uncertainty, and iteration errors are usually not considered in the literature, since they are often implicitly assumed to be small. However, if the considered problem is ill-conditioned, then small rounding errors and a low data uncertainty can result in a large error in the solution. Therefore, the main focus of the error analysis in this thesis is the calculation of the condition number of the considered discretized models, which are (usually large) nonlinear systems of equations. Classically, the normwise relative condition number of a nonlinear system is computed; see [57, 102]. However, we show that this condition number overestimates the

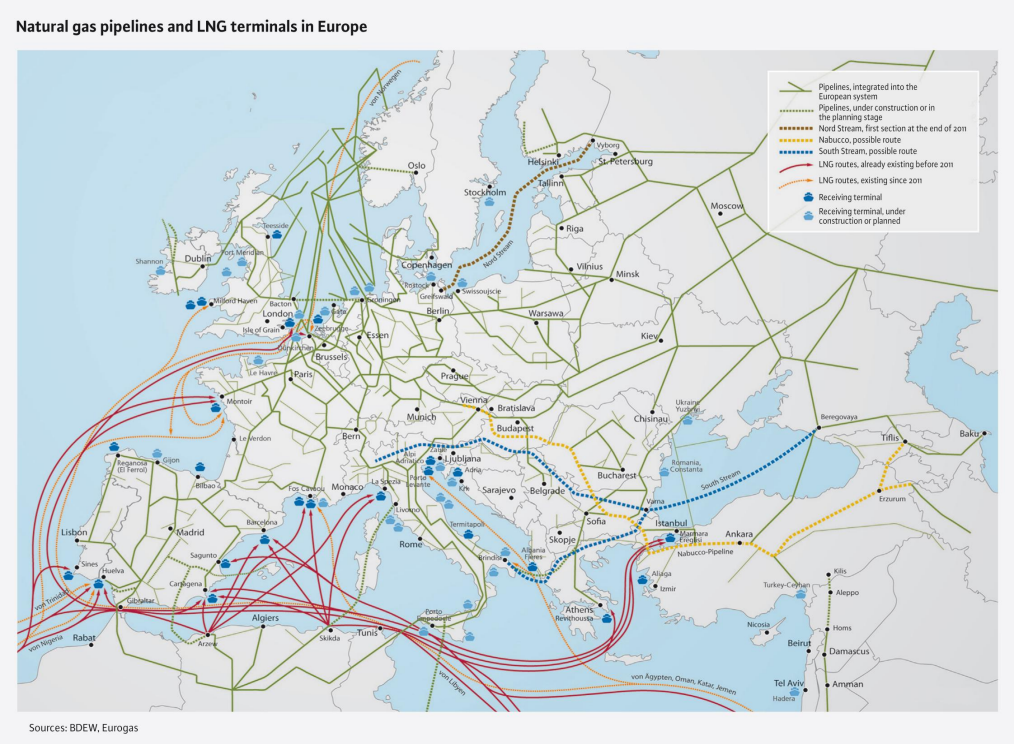

Figure 1.1: Gas pipeline network and liquefied natural gas (LNG) routes in Europe [21].

sensitivity of the problem substantially and that it is more accurate to use a novel componentwise relative condition number for nonlinear systems. In the context of gas networks, the different errors on every pipe are often controlled using adaptive techniques; see, e.g., [37, 38]. In this thesis, the performance of these current adaptive error control techniques is improved by developing new Greedy-like algorithms, which have a lower computational cost while maintaining the same error tolerance. Furthermore, it is shown that adaptive error control can also be applied within a gas flow optimization algorithm, which again reduces the computational cost. Finally, the finite termination of the optimization algorithm is proven.

This thesis has two aims, namely (1) the development of uniform error estimators for all the different error sources and (2) the adaptive control of these errors. The first aim is addressed in Chapter 3, where all the errors are written in a discrete setting with respect to the infinity-norm. This allows the errors to be balanced and adaptively controlled. Adaptive error control strategies that bring the total error below a prescribed tolerance and have a low computational cost are developed in Chapters 5 and 6, which thereby address the second aim of this thesis. The error control is performed by refining or coarsening the discretization grid and by switching up or down in a model hierarchy. The derived error estimators and the developed adaptive error control techniques are applied to different realistic gas network instances in order to test their performance and to obtain results that can be useful for gas network operators.

This thesis is structured as follows. Chapter 2 contains some preliminary definitions and results. In Chapter 3, uniform estimators are developed for all the different errors that a numerical solution could contain. These error estimators are applied to a two-level model hierarchy that describes the gas flow in networks. The transient model in this hierarchy is discretized using two different frequently used discretization schemes and the results are compared with each other. The analysis in Chapter 3 is only performed for a single pipe section. Therefore, the sensitivity analysis is extended in Chapter 4 to an exemplary Y-shaped gas network, in which the gas flow is described by three different high-level transient models. The influence of changing boundary conditions on the network state is determined. Simulations on both a realistic and an abstract gas network with twelve pipes using a three-level model hierarchy are performed in Chapter 5. Two new strategies for refinements in space, time, and model are developed and their performance is compared with a strategy that is currently used in simulation software. A compressor cost minimization problem, constrained by a stationary gas flow model for every pipe, is considered in Chapter 6. The spatial grid and the model are adapted using bulk criteria in order to find an ε-feasible solution. Under certain assumptions, we prove that this solution can be obtained after a finite number of adaptations. Some conclusions and an outlook are given in Chapter 7 and, finally, the appendix contains a forecast error analysis for two different gas networks using the gas flow simulation software ANACONDA.

Chapter 2

Preliminaries

This chapter contains some preliminary definitions and results regarding sensitivity analysis in Sections 2.1 and 2.2 and the Newton method in Section 2.3.

2.1 Sensitivity Analysis

This section presents a brief overview of the concept sensitivity analysis. Let the problem $(F;\boldsymbol{d})$, with mapping $F : D_{\boldsymbol{d}} \to \mathbb{R}^n$ and $D_{\boldsymbol{d}}$ an open subset of $\mathbb{R}^m$, be given. Thus, the problem is to compute F given input data $\boldsymbol{d}$. The aim of a sensitivity analysis is to determine the magnitude of the perturbation in F that is caused by a perturbation in the data $\boldsymbol{d}$. Usually, this amounts to calculating the condition number of F with respect to $\boldsymbol{d}$. In the following, four different kinds of condition numbers for $(F;\boldsymbol{d})$ are defined, since the perturbations in the input data can be given either normwise or componentwise and either in an absolute or in a relative fashion. For the definitions, it is convenient to introduce the notation $\dot{\leq}$, meaning "less than or equal to, except for higher order terms". A precise definition of this notation can be found, e.g., in [30], which also includes the following definition.

Definition 2.1. The *absolute normwise condition number* of the problem $(F;\boldsymbol{d})$ is the smallest number $\kappa_{\text{abs,n}}(F;\boldsymbol{d}) \geq 0$, such that

$$\|F(\tilde{\boldsymbol{d}}) - F(\boldsymbol{d})\| \dot{\leq} \kappa_{\text{abs,n}}(F;\boldsymbol{d})\|\tilde{\boldsymbol{d}} - \boldsymbol{d}\|, \quad \text{for } \tilde{\boldsymbol{d}} \to \boldsymbol{d}.$$

Analogously, the *relative normwise condition number* of $(F;\boldsymbol{d})$ is the smallest number $\kappa_{\text{rel,n}}(F;\boldsymbol{d}) \geq 0$, such that

$$\frac{\|F(\tilde{\boldsymbol{d}}) - F(\boldsymbol{d})\|}{\|F(\boldsymbol{d})\|} \dot{\leq} \kappa_{\text{rel,n}}(F;\boldsymbol{d})\frac{\|\tilde{\boldsymbol{d}} - \boldsymbol{d}\|}{\|\boldsymbol{d}\|}, \quad \text{for } \tilde{\boldsymbol{d}} \to \boldsymbol{d}.$$

Furthermore, the *absolute componentwise condition number* of $(F;\boldsymbol{d})$ is the smallest number $\kappa_{\text{abs,c}}(F;\boldsymbol{d}) \geq 0$, such that

$$\max_i |F_i(\tilde{\boldsymbol{d}}) - F_i(\boldsymbol{d})| \dot{\leq} \kappa_{\text{abs,c}}(F;\boldsymbol{d}) \max_i |\tilde{\boldsymbol{d}}_i - \boldsymbol{d}_i|, \quad \text{for } \tilde{\boldsymbol{d}} \to \boldsymbol{d}.$$

Finally, the *relative componentwise condition number* of $(F;\boldsymbol{d})$ is the smallest number $\kappa_{\text{rel,c}}(F;\boldsymbol{d}) \geq 0$, such that

$$\max_i \frac{|F_i(\tilde{\boldsymbol{d}}) - F_i(\boldsymbol{d})|}{|F_i(\boldsymbol{d})|} \dot{\leq} \kappa_{\text{rel,c}}(F;\boldsymbol{d}) \max_i \frac{|\tilde{\boldsymbol{d}}_i - \boldsymbol{d}_i|}{|\boldsymbol{d}_i|}, \quad \text{for } \tilde{\boldsymbol{d}} \to \boldsymbol{d}.$$

In general, if the condition number is small, then the problem is called *well-conditioned*, and if the condition number is large, the problem is called *ill-conditioned*. What is considered "small" and "large" depends on the specific problem. Figures 2.1 and 2.2 depict examples of an ill-conditioned and a well-conditioned problem, respectively. In Figure 2.1 a light beam, starting at the left-hand wall (the input), is aimed at a ball with a mirror at its exterior. The beam is reflected at the ball, the ceiling, and again the ball before it reaches the right-hand wall, which is here considered the result. One observes that a small perturbation of the input yields a large perturbation of the output. Thus, the problem of determining the position of the beam at the right-hand wall is ill-conditioned. On the other hand, in Figure 2.2 we consider the problem of determining the value of $f(t;a) = ae^{-t} + 1$ at $t = 8$ when parameter a is uncertain. We observe that $f(8;a)$ is only perturbed slightly when a changes, such that this problem is well-conditioned.

2.2 Sensitivity Analysis for Recursive Schemes

A recursive scheme consists of a number of steps, possibly infinitely many, where the solution $\boldsymbol{x}^i$ in every step depends on the solution $\boldsymbol{x}^{i-1}$ of the previous step. Recursive schemes appear, e.g., in the time discretization of ordinary

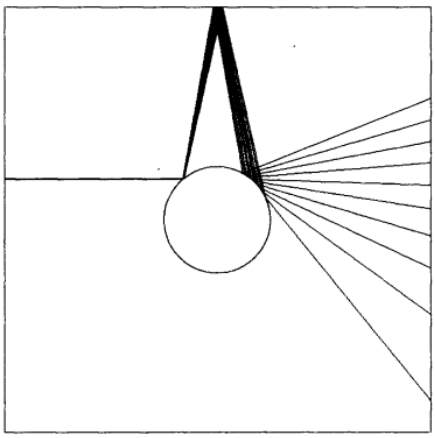

Figure 2.1: Scattering [96]. The problem of determining the position of the light beam at the right-hand wall is ill-conditioned.

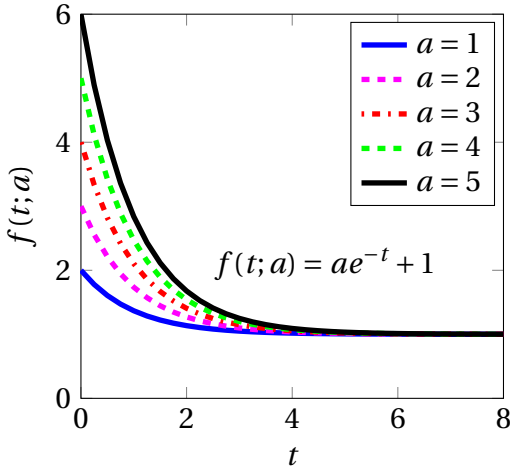

Figure 2.2: Horizontal asymptote. The problem of determining the value of $f(t;a)$ at $t = 8$ is well-conditioned.

differential equations (ODEs) and partial differential equations (PDEs), where the solution of the current time integration step depends on the solution(s) of the previous time step(s); see the flowchart depicted in Figure 2.3. The pseudocode of a recursive scheme with n steps and problem f, which is solved in every step, is given in Algorithm 2.1. If the parameter vector $\boldsymbol{d}$ contains uncertainties, then it causes uncertainties in all solutions $\boldsymbol{x}^i$, $i = 1,\dots,n$, in every step of the recursive scheme. The following theorem gives an expression for the sensitivity of the final solution $\boldsymbol{x}^n$ with respect to the uncertain data $\boldsymbol{d}$ and the initial value $\boldsymbol{x}^0$.

Theorem 2.1. *Let the absolute normwise condition number* $\kappa_{\text{abs,n}}$ *be defined as in Definition 2.1 and let a recursive scheme be given by Algorithm 2.1. Then, the* data uncertainty error *in* $\boldsymbol{x}^n$ *due to uncertain data* $\boldsymbol{d}$ *and initial value* $\boldsymbol{x}^0$ *is given by*

$$\begin{aligned}\|\tilde{\boldsymbol{x}}^n - \boldsymbol{x}^n\|_2^2 \lesapprox & \left[\sum_{i=0}^{n-1}\prod_{j=n-i}^{n}\kappa_{\text{abs,n}}^2\left(\boldsymbol{x}^j;\begin{bmatrix}\boldsymbol{d}\\ \boldsymbol{x}^{j-1}\end{bmatrix}\right)\right]\|\tilde{\boldsymbol{d}}-\boldsymbol{d}\|_2^2 \\ & + \left[\prod_{j=1}^{n}\kappa_{\text{abs,n}}^2\left(\boldsymbol{x}^j;\begin{bmatrix}\boldsymbol{d}\\ \boldsymbol{x}^{j-1}\end{bmatrix}\right)\right]\|\tilde{\boldsymbol{x}}^0-\boldsymbol{x}^0\|_2^2. \end{aligned} \tag{2.1}$$

Proof. Using Definition 2.1 for the absolute normwise condition number and problem f in line 2 of Algorithm 2.1, one may write

$$\|\tilde{\boldsymbol{x}}^n - \boldsymbol{x}^n\| \lesapprox \kappa_{\text{abs,n}}\left(\boldsymbol{x}^n;\begin{bmatrix}\boldsymbol{d}\\ \boldsymbol{x}^{n-1}\end{bmatrix}\right)\left\|\begin{bmatrix}\tilde{\boldsymbol{d}}-\boldsymbol{d}\\ \tilde{\boldsymbol{x}}^{n-1}-\boldsymbol{x}^{n-1}\end{bmatrix}\right\|,$$

where $\tilde{\boldsymbol{x}}^n = f(\tilde{\boldsymbol{x}}^{n-1},\tilde{\boldsymbol{d}})$ and $\tilde{\boldsymbol{x}}^{n-1}$ and $\tilde{\boldsymbol{d}}$ denote the perturbed values of $\boldsymbol{x}^{n-1}$ and $\boldsymbol{d}$, respectively. The 2-norm is chosen and, for notational convenience,

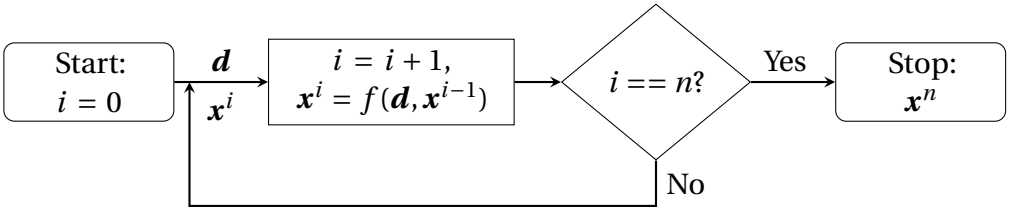

Figure 2.3: Flowchart of a typical recursive scheme appearing in time-discretized ODEs or PDEs. Uncertainties in the parameters $\boldsymbol{d}$ cause uncertainties in all solutions $\boldsymbol{x}^i$, $i = 1,\dots,n$.

Algorithm 2.1 : A general recursive scheme.

Input: initial value $\boldsymbol{x}^0$, data $\boldsymbol{d}$
1: **for** $i \leftarrow 1 : n$ **do**
2: $\quad \boldsymbol{x}^i = f(\boldsymbol{d}, \boldsymbol{x}^{i-1})$
3: **end for**
Output: $\boldsymbol{x}^n$

the expression is squared, which yields

$$\begin{aligned}\|\tilde{\boldsymbol{x}}^n - \boldsymbol{x}^n\|_2^2 \dot{\leq} \kappa_{\text{abs,n}}^2\left(\boldsymbol{x}^n; \begin{bmatrix}\boldsymbol{d}\\ \boldsymbol{x}^{n-1}\end{bmatrix}\right) \underbrace{\left\|\begin{bmatrix}\tilde{\boldsymbol{d}}-\boldsymbol{d}\\ \tilde{\boldsymbol{x}}^{n-1}-\boldsymbol{x}^{n-1}\end{bmatrix}\right\|_2^2}_{=\|\tilde{\boldsymbol{d}}-\boldsymbol{d}\|_2^2+\|\tilde{\boldsymbol{x}}^{n-1}-\boldsymbol{x}^{n-1}\|_2^2} \\ = \kappa_{\text{abs,n}}^2\left(\boldsymbol{x}^n; \begin{bmatrix}\boldsymbol{d}\\ \boldsymbol{x}^{n-1}\end{bmatrix}\right)\|\tilde{\boldsymbol{d}}-\boldsymbol{d}\|_2^2 + \kappa_{\text{abs,n}}^2\left(\boldsymbol{x}^n; \begin{bmatrix}\boldsymbol{d}\\ \boldsymbol{x}^{n-1}\end{bmatrix}\right)\|\tilde{\boldsymbol{x}}^{n-1}-\boldsymbol{x}^{n-1}\|_2^2.\end{aligned} \tag{2.2}$$

Then, it also holds that

$$\begin{aligned}\|\tilde{\boldsymbol{x}}^{n-1} - \boldsymbol{x}^{n-1}\|_2^2 \dot{\leq} \kappa_{\text{abs,n}}^2\left(\boldsymbol{x}^{n-1}; \begin{bmatrix}\boldsymbol{d}\\ \boldsymbol{x}^{n-2}\end{bmatrix}\right)\|\tilde{\boldsymbol{d}}-\boldsymbol{d}\|_2^2 \\ + \kappa_{\text{abs,n}}^2\left(\boldsymbol{x}^{n-1}; \begin{bmatrix}\boldsymbol{d}\\ \boldsymbol{x}^{n-2}\end{bmatrix}\right)\|\tilde{\boldsymbol{x}}^{n-2}-\boldsymbol{x}^{n-2}\|_2^2.\end{aligned}$$

Inserting this in (2.2), it follows that

$$\begin{aligned}&\|\tilde{\boldsymbol{x}}^n - \boldsymbol{x}^n\|_2^2 \\ \dot{\leq}& \left(\kappa_{\text{abs,n}}^2\left(\boldsymbol{x}^n; \begin{bmatrix}\boldsymbol{d}\\ \boldsymbol{x}^{n-1}\end{bmatrix}\right) + \kappa_{\text{abs,n}}^2\left(\boldsymbol{x}^n; \begin{bmatrix}\boldsymbol{d}\\ \boldsymbol{x}^{n-1}\end{bmatrix}\right)\kappa_{\text{abs,n}}^2\left(\boldsymbol{x}^{n-1}; \begin{bmatrix}\boldsymbol{d}\\ \boldsymbol{x}^{n-2}\end{bmatrix}\right)\right)\|\tilde{\boldsymbol{d}}-\boldsymbol{d}\|_2^2 \\ &+ \kappa_{\text{abs,n}}^2\left(\boldsymbol{x}^n; \begin{bmatrix}\boldsymbol{d}\\ \boldsymbol{x}^{n-1}\end{bmatrix}\right)\kappa_{\text{abs,n}}^2\left(\boldsymbol{x}^{n-1}; \begin{bmatrix}\boldsymbol{d}\\ \boldsymbol{x}^{n-2}\end{bmatrix}\right)\|\tilde{\boldsymbol{x}}^{n-2}-\boldsymbol{x}^{n-2}\|_2^2.\end{aligned}$$

Using an induction argument, the expression (2.1) is obtained. □

2.3 The Newton Method

In general, the solution of a nonlinear system of equations

$$F(\boldsymbol{x}) = 0, \quad F : \mathbb{R}^n \to \mathbb{R}^n, \tag{2.3}$$

cannot be computed analytically. Indeed, even in the one-dimensional case $n = 1$ there is no general algebraic solution for the roots of a polynomial of degree five or higher, which is known as the Abel-Ruffini theorem [59, p. 211]. However, the nonlinear system of equations (2.3) can be solved iteratively to an arbitrary precision using, e.g., the Newton method. This method computes a new iterate $\boldsymbol{x}^{i+1}$ from the current iterate $\boldsymbol{x}^i$ using the expression [63, p. 71]

$$\boldsymbol{x}^{i+1} = \boldsymbol{x}^i - F'(\boldsymbol{x}^i)^{-1}F(\boldsymbol{x}^i), \tag{2.4}$$

where F' is the Jacobian of the function F. Before discussing the convergence of the Newton method, we introduce the definition of Lipschitz continuity; see, e.g., [63, p. 67].

Definition 2.2. Let $\Omega \subset \mathbb{R}^n$, let $G : \Omega \to \mathbb{R}^m$ and let $||\cdot||$ be a norm on $\mathbb{R}^n$. G is *Lipschitz continuous on* Ω *with Lipschitz constant* γ if

$$||G(\boldsymbol{x}) - G(\boldsymbol{y})|| \leq \gamma ||\boldsymbol{x} - \boldsymbol{y}||$$

for all $\boldsymbol{x}, \boldsymbol{y} \in \Omega$.

Let the assumptions that (2.3) has a solution $\boldsymbol{x}^*$, the Jacobian $F'(\boldsymbol{x})$ is Lipschitz continuous, and $F'(\boldsymbol{x}^*)$ is nonsingular be given. It is well-known, see, e.g., [63, Theorem 5.1.2], that under these assumptions and if the initial iterate $\boldsymbol{x}^0$ is sufficiently close to the solution $\boldsymbol{x}^*$, then the Newton iteration (2.4) converges quadratically to $\boldsymbol{x}^*$, i.e., there exists a constant $K > 0$ such that

$$||\boldsymbol{x}^{i+1} - \boldsymbol{x}^*|| \leq K||\boldsymbol{x}^i - \boldsymbol{x}^*||^2, \tag{2.5}$$

with $K||\boldsymbol{x}^i - \boldsymbol{x}^*|| < 1$, for all i. A commonly used stopping criterion for the Newton iteration is a combination of relative and absolute error tolerances, denoted by τ_r and τ_a, respectively, [63, p. 73]

$$||F(\boldsymbol{x})|| \leq \tau_r ||F(\boldsymbol{x}^0)|| + \tau_a.$$

Another possibility is to stop the Newton iteration (2.4) when the difference between consecutive iterates

$$||\boldsymbol{e}^{i+1}|| = ||\boldsymbol{x}^{i+1} - \boldsymbol{x}^i||$$

is sufficiently small. We show that $||\boldsymbol{e}^{i+1}||$ is a good approximation of the error $||\boldsymbol{x}^i - \boldsymbol{x}^*||$ for $\boldsymbol{x}^i$ near the solution $\boldsymbol{x}^*$.

Corollary 2.2. *For the difference* $\boldsymbol{e}^{i+1}$ *between the consecutive iterates* $\boldsymbol{x}^{i+1}$ *and* $\boldsymbol{x}^i$ *it holds that*

$$||\boldsymbol{e}^{i+1}|| = ||\boldsymbol{x}^i - \boldsymbol{x}^*|| + O\big(||\boldsymbol{x}^i - \boldsymbol{x}^*||^2\big). \tag{2.6}$$

Proof. It follows from (2.5) that

$$||\boldsymbol{x}^{i+1} - \boldsymbol{x}^*|| = ||\boldsymbol{x}^{i+1} - \boldsymbol{x}^i + \boldsymbol{x}^i - \boldsymbol{x}^*|| = ||\boldsymbol{e}^{i+1} + \boldsymbol{x}^i - \boldsymbol{x}^*|| = O\big(||\boldsymbol{x}^i - \boldsymbol{x}^*||^2\big). \tag{2.7}$$

We use the reverse triangle inequality [27, Lemma 2.1.2], which states that for a normed vector space V

$$||\boldsymbol{x} - \boldsymbol{y}|| \geq \big|||\boldsymbol{x}|| - ||\boldsymbol{y}||\big|, \quad \forall \boldsymbol{x}, \boldsymbol{y} \in V.$$

Then, it follows from (2.7) that

$$\begin{aligned} ||\boldsymbol{e}^{i+1} + \boldsymbol{x}^i - \boldsymbol{x}^*|| &= ||\boldsymbol{e}^{i+1} - (-(\boldsymbol{x}^i - \boldsymbol{x}^*))|| \\ \geq \big|||\boldsymbol{e}^{i+1}|| - ||\boldsymbol{x}^i - \boldsymbol{x}^*||\big| &= O\big(||\boldsymbol{x}^i - \boldsymbol{x}^*||^2\big). \end{aligned}$$

Hence,

$$||\boldsymbol{e}^{i+1}|| - ||\boldsymbol{x}^i - \boldsymbol{x}^*|| = O\big(||\boldsymbol{x}^i - \boldsymbol{x}^*||^2\big),$$

from which (2.6) follows directly. □

Chapter 3

Error Analysis and Model Adaptivity for Flows in Gas Networks

3.1 Introduction

It is well known, see, e.g., [57, page 5], that the numerical solution of a computational problem contains errors from all or some of the following sources: modeling, discretization, iteration, data uncertainty, and rounding errors, see Figure 3.1 for a schematic overview. These errors should be balanced to achieve an adequate simulation result. We focus on the pure pipe flow, where the model hierarchy is easily constructed and where it can be used to find an appropriate trade-off between accuracy and computational complexity, see [3, 19, 33, 37]. We derive error estimates and a sensitivity analysis within the typical model hierarchy with respect to the discretization scheme, while also considering the iteration and rounding errors for the solution of the resulting nonlinear systems of equations. To demonstrate the new techniques and to keep the presentation simple we present a deterministic as well as statistical error and sensitivity analysis only for two specific components of the model hierarchy, a purely algebraic model and an isothermal semilinear model, but the analysis can be carried out also for more complex components in the model hierarchy. For these two models, model and discretization error estimators for an arbitrary cost functional have been derived in [33, 40]. However, the effect of data uncertainty and rounding errors on the solution of these two models has not been considered in the literature and is the main topic of this chapter.

To estimate the errors, we perform a backward error analysis, see, e.g., [57], and derive first order upper bounds as well as mean statistical estimates for the error in the solution due to data uncertainty, modeling, discretization, rounding, and iteration errors. A perturbation analysis in which also higher order error terms are included usually leads to very pessimistic upper error bounds, see [67], and is therefore not considered. We derive componentwise condition numbers and, based on these, deterministic first order error bounds. The advantage of the componentwise relative condition number over the traditional normwise condition number for nonlinear systems is demonstrated.

This chapter is organized as follows. Section 3.2 introduces different models that describe the gas flow through a pipeline. Section 3.3 gives a concise introduction into error analysis and conditioning. Moreover, several kinds of condition numbers are derived. Section 3.4 presents a sensitivity analysis for two different discretization schemes applied to the semilinear model and applies the derived condition numbers to the resulting nonlinear systems of equations. Moreover, the effect of rounding errors and the iteration error is investigated and the relative model error between the semilinear and the algebraic model is determined. In Section 3.5 both a theoretical worst case and a statistical mean error analysis for the stationary Euler equations in purely algebraic form is presented. A summary of this chapter is given in Section 3.6.

3.2 The Model Hierarchy

As a model problem for the balanced error analysis in a model hierarchy, the gas flow through a pipeline is modeled via the one dimensional Euler equations that represent a system of nonlinear hyperbolic partial differential equations for the behavior of compressible, non-viscous fluids. The model consists of, see, e.g., [69], the continuity equation, the impulse equation, and the energy

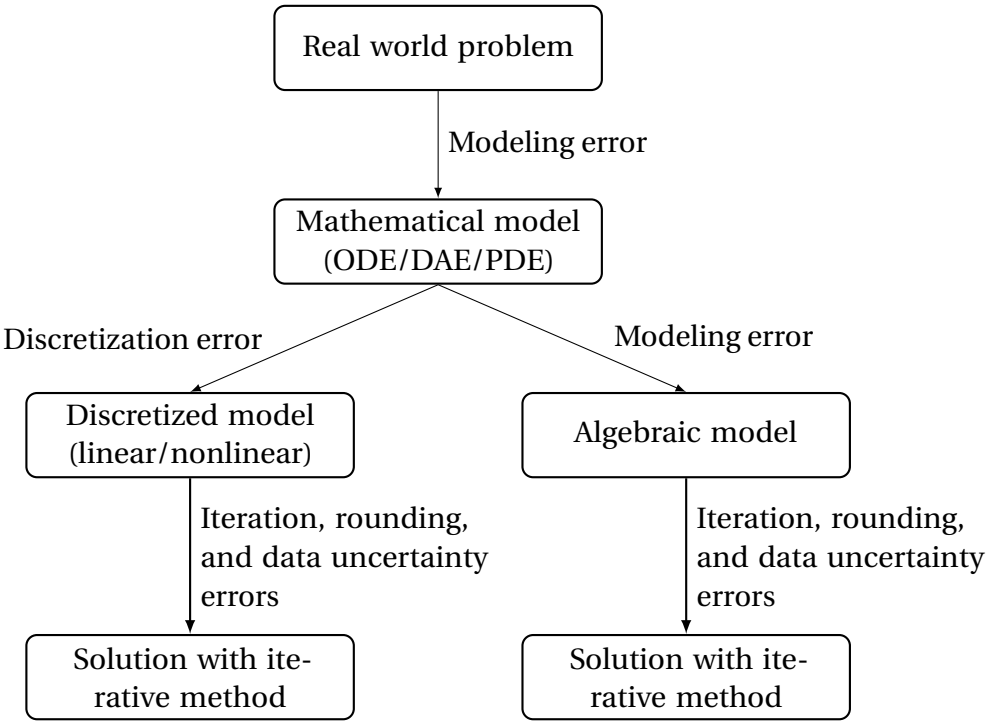

Figure 3.1: Overview of different error sources contained in the numerical simulation of a real world problem.

equation, respectively,

$$\frac{\partial \rho}{\partial t} + \frac{\partial}{\partial x}(\rho v) = 0, \tag{3.1a}$$

$$\frac{\partial}{\partial t}(\rho v) + \frac{\partial}{\partial x}(p + \rho v^2) = -\frac{\lambda}{2D}\rho v|v| - g\rho h', \tag{3.1b}$$

$$\frac{\partial}{\partial t}\Big(\rho\big(\frac{1}{2}v^2 + e\big)\Big) + \frac{\partial}{\partial x}\Big(\rho v\big(\frac{1}{2}v^2 + e\big) + pv\Big) = -\frac{k_w}{D}(T - T_w). \tag{3.1c}$$

Moreover, the state equation for real gases is added, which is given by

$$p = R\rho T z(p, T). \tag{3.2}$$

In this system of equations the variables have the following physical meaning: ρ is the density of the gas, t is the time, v the velocity of the gas, x the space coordinate along the pipeline, p the pressure of the gas, λ the pipe friction coefficient, D the diameter of the pipeline, g the gravitational constant, h the height of the pipeline, $h'(x)$ the slope of the pipeline, c_v the volumetric heat capacity, $e = c_v T + gh$ the internal (thermal plus potential) energy, T the temperature of the gas, k_w the heat conductivity coefficient, T_w the wall temperature of the pipeline, and R the gas constant. Finally, $z(p, T)$ denotes the compressibility factor for which we use the model of the American Gas Association (AGA)

$$z(p, T) = 1 + 0.257\frac{p}{p_c} - 0.533\frac{pT_c}{p_c T}, \tag{3.3}$$

where p_c and T_c denote the pseudo-critical pressure and temperature, which provides a good approximation of z for pressures up to 70 bar [2, 89]. The full Euler equations (even in the one-dimensional case (3.1)) are mathematically quite involved and their numerical solution requires large computational effort. For this reason, in particular when the solution is part of an optimization procedure, usually several simplifications are made. Such simplifications are e.g. to use an approximate semilinear model as derived in Section 3.2.1 or a purely algebraic model as considered in Section 3.2.2.

3.2.1 Derivation of the Semilinear Isothermal Model

Starting from the full one dimensional Euler equations (3.1), to derive the isothermal model, the temperature $T = T_0$ is assumed to be constant within the pipeline, such that the energy equation (3.1c) can be dropped and the isothermal Euler equations (3.1a) and (3.1b) are obtained. According to the International Standard Metric Conditions for natural gas [58], the value $T_0 = 15.0\,^{\circ}\mathrm{C}$ (which is equal to 288 K) is taken for this constant temperature. Then, in the isothermal case, the compressibility factor z in the AGA model (3.3) only depends on p and we get

$$z(p) = 1 + \alpha p, \quad \text{with} \quad \alpha = \frac{0.257}{p_c} - 0.533\frac{T_c}{p_c T_0}. \tag{3.4}$$

If one also assumes that this compressibility factor $z(p) = z_0$ is constant in p, then one can use the average

$$z_0 = \frac{z(0) + z(70\,\text{bar})}{2} = 0.928$$

as its value. For constant temperature T_0 and compressibility factor z_0, the state equation for real gases (3.2) then reduces to

$$p(\rho) = RT_0 z_0 \rho. \tag{3.5}$$

If also the entropy of the gas is assumed to be constant, which is a reasonable assumption when the temperature of the gas is constant [33, page 7], then the speed of sound is given by $c = \sqrt{\partial p / \partial \rho}$, see also [69, Eq. (14.32)]. From (3.5) it follows that

$$c = \sqrt{RT_0 z_0} = \sqrt{p/\rho}. \tag{3.6}$$

Hence, we have $\rho = p/c^2$, and inserting this in (3.1b), the momentum equation can be rewritten as

$$\frac{\partial}{\partial t}(\rho v) + \frac{\partial}{\partial x}(p(1 + v^2/c^2)) = -\frac{\lambda}{2D}\rho v|v| - g\rho h'.$$

As further simplifications often the term v^2/c^2 is neglected in the case of small gas flow velocities v, see [81], and it is assumed that $h'(x) \equiv 0$, i.e., the pipeline is assumed to be (essentially) horizontal. These simplifications result in the *isothermal semilinear model* (see [33, 80])

$$\frac{\partial \rho}{\partial t} + \frac{\partial}{\partial x}(\rho v) = 0, \tag{3.7a}$$

$$\frac{\partial}{\partial t}(\rho v) + \frac{\partial p}{\partial x} = -\frac{\lambda}{2D}\rho v|v|. \tag{3.7b}$$

Introducing the *mass flow rate* $q = A\rho v$, with a constant cross-sectional area A, and using (3.6), system (3.7) may be rewritten in the form

$$\frac{\partial p}{\partial t} + \frac{c^2}{A}\frac{\partial q}{\partial x} = 0, \tag{3.8a}$$

$$\frac{\partial q}{\partial t} + A\frac{\partial p}{\partial x} = -\frac{\lambda c^2}{2DA}\frac{q|q|}{p}, \tag{3.8b}$$

$$q(x_R, t) = q_s(t), \tag{3.8c}$$

$$p(x_L, t) = p_s(t), \tag{3.8d}$$

where as boundary conditions the mass flow rate is prescribed by $q_s(t)$ at the *right-hand side of the pipeline* x_R and the pressure is prescribed by $p_s(t)$ at the *left-hand side of the pipeline* x_L. When considering all these drastic model simplifications it has to be analyzed whether these perturbations in the model have a large effect on the simulation results.

3.2.2 Derivation of the Algebraic Model

Another simplified model (presented in an even more reduced form in [19]) is obtained by neglecting the terms $\frac{\partial}{\partial x}(\rho v^2)$, $\frac{\partial}{\partial x}(\rho v^3)$, and $\frac{\partial}{\partial t}(\rho v)$ in (3.1). This results in the model

$$\frac{\partial \rho}{\partial t} + \frac{\partial}{\partial x}(\rho v) = 0, \tag{3.9a}$$

$$\frac{\partial p}{\partial x} = -\frac{\lambda}{2D}\rho v|v| - g\rho h', \tag{3.9b}$$

$$\frac{\partial}{\partial t}(\rho e) + \frac{\partial}{\partial x}(\rho v e + p v) = -\frac{k_w}{D}(T - T_w). \tag{3.9c}$$

If, as further simplification, a stationary model is assumed, i.e., the time-derivatives $\frac{\partial}{\partial t}$ are set to zero, the pipeline is again assumed to be horizontal, i.e., $h' = 0$, and the compressibility factor z is set to be constant, then a set of ordinary differential equations is obtained, which can be solved analytically via

$$\hat{q} = \rho_{\text{in}} v_{\text{in}}, \tag{3.10a}$$

$$p(x) = \sqrt{p_{\text{in}}^2 - \frac{\lambda c^2}{2r}\rho v|\rho v|(x - x_0)}, \tag{3.10b}$$

$$T(x) = (T_{\text{in}} - T_w)e^{-\frac{k_w}{Dc_v\rho v}(x - x_0)} + T_w. \tag{3.10c}$$

Here, $\hat{q} = \rho v$ is the mass flux, which is constant in space, ρ_{in} is the inlet density, v_{in} the inlet velocity, p_{in} the inlet pressure, c the constant speed of sound, r the radius of the pipeline, x_0 the starting point of the pipeline, and T_{in} the inlet temperature. Equations (3.10) are referred to as the *temperature dependent algebraic model* of the one dimensional Euler equations. Again, an isothermal simplification is obtained by taking the temperature T constant. This leaves us with (3.10a) and (3.10b), which are referred to as the *isothermal algebraic model*. A detailed derivation of this model is given in [37]. In the optimization of natural gas networks, this nonlinear algebraic model is often further approximated by piecewise linear functions, see, e.g., [47] and [64, page 115]. Although usually within the optimization methods the approximation accuracy by the piecewise linear approximations is controlled, the modeling error of the nonlinear algebraic model is usually not considered. If this modeling error is large, then the linear relaxation techniques used in the optimization methods inevitably lead to inaccurate results. This motivates our consideration of the model error in Section 3.4.5.

The discussed model hierarchy is depicted schematically in Figure 3.2. We will analyze the errors in this model hierarchy, however, it should be clear that the analysis can be extended by considering all simplifications separately and by also starting from a more detailed original model.

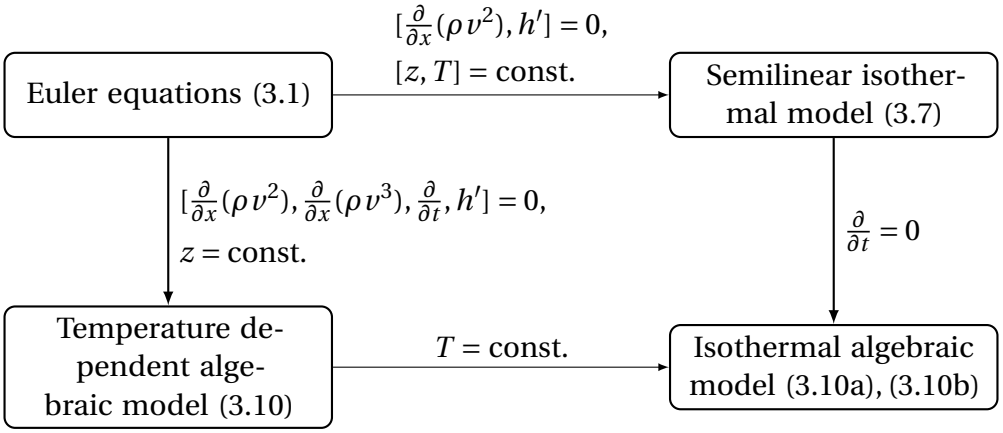

Figure 3.2: Two level model hierarchy for the simulation of flows in gas networks.

3.3 Error Analysis and Conditioning

The aim of *error analysis* is to construct an estimate or upper bound of the effect that modeling, rounding, data uncertainty, and discretization errors have on the solution of a given problem, see, e.g., [15, 57, 85]. Rounding errors in the numerical computations due to floating point arithmetic can be interpreted as perturbations in the data using a backward error analysis, see [101]. We investigate the data uncertainty error by means of a sensitivity analysis. A deterministic perturbation analysis, as given in Section 3.3.1, results in a first order upper error bound, which can possibly be very pessimistic for certain input parameter values. Therefore, it is important to compare this upper bound with an average error estimate, which can be obtained using a statistical analysis as described in Section 3.3.2.

3.3.1 Deterministic Perturbation Analysis

The term *condition number* is used to describe the sensitivity of problems to uncertainties in the input parameters [85]. Using the classical concepts of backward and forward error, we have the rule of thumb [57]

$$\text{forward error} \dot{\leq} \text{condition number} \times \text{backward error},$$

with $\dot{\leq}$ meaning "less than or equal to except for higher order terms". It insightfully shows that despite of a small backward error (which is often given by the residual), a problem can have a large forward error due to a high condition number. Formal definitions for normwise and componentwise condition numbers are given in e.g. [30].

Suppose that the solution of a problem is obtained by evaluating the differentiable function of a single variable $f(d)$. Denoting the derivative of f with

respect to d by $f'(d)$, then the quantity [57]

$$\kappa_{\text{rel}}(f;d) = \left| \frac{d\, f'(d)}{f(d)} \right|,$$

with $|.|$ denoting the absolute value, is the *relative condition number* of f and it measures, for small perturbations Δd, the relative change in the output for a given relative change in the input. On the other hand, if the solution of a problem is obtained by evaluating a differentiable function of several variables $f(\boldsymbol{d})$ with $\boldsymbol{d} \in \mathbb{R}^n$, then, using a first order Taylor series expansion, we have

$$\frac{f(\boldsymbol{d}+\boldsymbol{\Delta d}) - f(\boldsymbol{d})}{f(\boldsymbol{d})} \doteq \sum_{i=1}^{n} \frac{\partial f(\boldsymbol{d})}{\partial d_i} \frac{d_i}{f(\boldsymbol{d})} \frac{\Delta d_i}{d_i},$$

where $\doteq$ denotes a first order approximation, cf. [30, page 28]. Taking the absolute value results in the first order upper bounds

$$\begin{aligned} \frac{|f(\boldsymbol{d}+\boldsymbol{\Delta d}) - f(\boldsymbol{d})|}{|f(\boldsymbol{d})|} &\dot{\leq} \sum_{i=1}^{n} \left| \frac{\partial f(\boldsymbol{d})}{\partial d_i} \frac{d_i}{f(\boldsymbol{d})} \right| \frac{|\Delta d_i|}{|d_i|} \\ &\leq \sum_{i=1}^{n} \left| \frac{\partial f(\boldsymbol{d})}{\partial d_i} \frac{d_i}{f(\boldsymbol{d})} \right| \cdot \max_i \frac{|\Delta d_i|}{|d_i|}, \end{aligned}$$

such that the quantities, cf. [67],

$$\kappa_{\text{rel}}(f;d_i) = \left| \frac{\partial f(\boldsymbol{d})}{\partial d_i} \frac{d_i}{f(\boldsymbol{d})} \right|, \quad i = 1,\ldots,n, \tag{3.11}$$

are the *individual relative condition numbers* of f with respect to d_i and the quantity

$$\kappa_{\text{rel}}(f;\boldsymbol{d}) = \sum_{i=1}^{n} \left| \frac{\partial f(\boldsymbol{d})}{\partial d_i} \frac{d_i}{f(\boldsymbol{d})} \right| = \sum_{i=1}^{n} \kappa_{\text{rel}}(f;d_i) \tag{3.12}$$

is the relative condition number of f with respect to $\boldsymbol{d}$.

For systems of nonlinear equations, normwise relative condition numbers were first studied in [102], and the results are extended and summarized in [57]. We develop componentwise condition numbers for nonlinear systems of equations

$$F(\boldsymbol{x};\boldsymbol{d}) = 0, \tag{3.13}$$

where $F : D_{\boldsymbol{x}} \times D_{\boldsymbol{d}} \to \mathbb{R}^m$ with $D_{\boldsymbol{x}} \times D_{\boldsymbol{d}}$ an open subset of $\mathbb{R}^m \times \mathbb{R}^n$. In the following we assume that $F \in C^{1,1}$, i.e., it is (at least once) continuously differentiable with respect to both $\boldsymbol{x}$ and $\boldsymbol{d}$. Given a solution $\boldsymbol{x}^* \in \mathbb{R}^m$ we are interested in the sensitivity of $\boldsymbol{x}^*$ with respect to perturbations in the data vector $\boldsymbol{d} \in \mathbb{R}^n$, i.e., we are interested in the condition number $\kappa_{\text{rel}}(\boldsymbol{x}^*;\boldsymbol{d})$ of $\boldsymbol{x}^*$ with respect to perturbations $\tilde{\boldsymbol{d}}$ in the data $\boldsymbol{d}$. So instead of (3.13) one solves the problem

$$F(\tilde{\boldsymbol{x}};\tilde{\boldsymbol{d}}) = 0, \tag{3.14}$$

and we determine a relation between the norms $||\tilde{\boldsymbol{x}}^* - \boldsymbol{x}^*||$ for the solutions $\tilde{\boldsymbol{x}}^*, \boldsymbol{x}^*$ and the deviation in the data $||\tilde{\boldsymbol{d}} - \boldsymbol{d}||$, where the norm $||\cdot||$ should be

chosen such that it fits the problem [102, page 374]. The first order term in the Taylor series expansion gives

$$F(\tilde{\boldsymbol{x}}^*;\tilde{\boldsymbol{d}}) \doteq F(\boldsymbol{x}^*;\boldsymbol{d}) + F'_{\boldsymbol{x}}(\boldsymbol{x}^*;\boldsymbol{d})(\tilde{\boldsymbol{x}}^* - \boldsymbol{x}^*) + F'_{\boldsymbol{d}}(\boldsymbol{x}^*;\boldsymbol{d})(\tilde{\boldsymbol{d}} - \boldsymbol{d}), \tag{3.15}$$

where $F'_{\boldsymbol{x}}$ and $F'_{\boldsymbol{d}}$ denote the Jacobians of F with respect to $\boldsymbol{x}^*$ and $\boldsymbol{d}$, respectively. Since both $F(\boldsymbol{x}^*;\boldsymbol{d}) = 0$ and $F(\tilde{\boldsymbol{x}}^*;\tilde{\boldsymbol{d}}) = 0$, (3.15) can be rewritten as

$$F'_{\boldsymbol{x}}(\boldsymbol{x}^*;\boldsymbol{d})(\tilde{\boldsymbol{x}}^* - \boldsymbol{x}^*) \doteq -F'_{\boldsymbol{d}}(\boldsymbol{x}^*;\boldsymbol{d})(\tilde{\boldsymbol{d}} - \boldsymbol{d}). \tag{3.16}$$

If $F'_{\boldsymbol{x}}$ is invertible and bounded in $(\boldsymbol{x}^*;\boldsymbol{d})$, then we obtain that

$$||\tilde{\boldsymbol{x}}^* - \boldsymbol{x}^*|| \dot{\leq} ||F'_{\boldsymbol{x}}(\boldsymbol{x}^*;\boldsymbol{d})^{-1}F'_{\boldsymbol{d}}(\boldsymbol{x}^*;\boldsymbol{d})||\,||\tilde{\boldsymbol{d}} - \boldsymbol{d}||, \tag{3.17}$$

so that

$$\frac{||\tilde{\boldsymbol{x}}^* - \boldsymbol{x}^*||}{||\boldsymbol{x}^*||} \dot{\leq} \frac{||\boldsymbol{d}||\,||F'_{\boldsymbol{x}}(\boldsymbol{x}^*;\boldsymbol{d})^{-1}F'_{\boldsymbol{d}}(\boldsymbol{x}^*;\boldsymbol{d})||}{||\boldsymbol{x}^*||}\frac{||\tilde{\boldsymbol{d}} - \boldsymbol{d}||}{||\boldsymbol{d}||}, \tag{3.18}$$

where the matrix norm $||F'_{\boldsymbol{x}}(\boldsymbol{x}^*;\boldsymbol{d})^{-1}F'_{\boldsymbol{d}}(\boldsymbol{x}^*;\boldsymbol{d})||$ is the one induced by the vector norm. From (3.17) and (3.18) it follows that the normwise absolute and relative condition numbers of the solution $\boldsymbol{x}^*$ with respect to the data $\boldsymbol{d}$ are given by

$$\kappa_{\text{abs,n}}(\boldsymbol{x}^*;\boldsymbol{d}) = ||F'_{\boldsymbol{x}}(\boldsymbol{x}^*;\boldsymbol{d})^{-1}F'_{\boldsymbol{d}}(\boldsymbol{x}^*;\boldsymbol{d})|| \tag{3.19}$$

and, see [102, page 377] and [57, Eq. (25.11)],

$$\kappa_{\text{rel,n}}(\boldsymbol{x}^*;\boldsymbol{d}) = \frac{||\boldsymbol{d}||\,||F'_{\boldsymbol{x}}(\boldsymbol{x}^*;\boldsymbol{d})^{-1}F'_{\boldsymbol{d}}(\boldsymbol{x}^*;\boldsymbol{d})||}{||\boldsymbol{x}^*||}, \tag{3.20}$$

respectively. Considering individual components, one can determine the sensitivity of the i-th component x_i^* of the solution vector $\boldsymbol{x}^*$ of the problem (3.13) with respect to small perturbations in the data vector $\boldsymbol{d}$. We rewrite (3.16) as

$$\tilde{\boldsymbol{x}}^* - \boldsymbol{x}^* \doteq -F'_{\boldsymbol{x}}(\boldsymbol{x}^*;\boldsymbol{d})^{-1}F'_{\boldsymbol{d}}(\boldsymbol{x}^*;\boldsymbol{d})(\tilde{\boldsymbol{d}} - \boldsymbol{d}). \tag{3.21}$$

For the i-th component $(\tilde{\boldsymbol{x}}^* - \boldsymbol{x}^*)_i$ of the vector $\tilde{\boldsymbol{x}}^* - \boldsymbol{x}^*$ we obtain

$$\begin{aligned}(\tilde{\boldsymbol{x}}^* - \boldsymbol{x}^*)_i &\doteq -\left(F'_{\boldsymbol{x}}(\boldsymbol{x}^*;\boldsymbol{d})^{-1}F'_{\boldsymbol{d}}(\boldsymbol{x}^*;\boldsymbol{d})(\tilde{\boldsymbol{d}} - \boldsymbol{d})\right)_i \\ &\doteq -\left(F'_{\boldsymbol{x}}(\boldsymbol{x}^*;\boldsymbol{d})^{-1}F'_{\boldsymbol{d}}(\boldsymbol{x}^*;\boldsymbol{d})\right)_{i,:}(\tilde{\boldsymbol{d}} - \boldsymbol{d}),\end{aligned} \tag{3.22}$$

where $M_{i,:}$ denotes the i-th row of the matrix M. Taking the absolute value and using the Cauchy-Schwarz inequality [95, page 107] result in first order upper bounds for the absolute and relative error

$$|\tilde{x}_i^* - x_i^*| \dot{\leq} \left\|\left(F'_{\boldsymbol{x}}(\boldsymbol{x}^*;\boldsymbol{d})^{-1}F'_{\boldsymbol{d}}(\boldsymbol{x}^*;\boldsymbol{d})\right)^T_{i,:}\right\|_2 \|\tilde{\boldsymbol{d}} - \boldsymbol{d}\|_2, \tag{3.23}$$

$$\frac{|\tilde{x}_i^* - x_i^*|}{|x_i^*|} \dot{\leq} \frac{\|\boldsymbol{d}\|_2\left\|\left(F'_{\boldsymbol{x}}(\boldsymbol{x}^*;\boldsymbol{d})^{-1}F'_{\boldsymbol{d}}(\boldsymbol{x}^*;\boldsymbol{d})\right)^T_{i,:}\right\|_2}{|x_i^*|}\frac{\|\tilde{\boldsymbol{d}} - \boldsymbol{d}\|_2}{\|\boldsymbol{d}\|_2}. \tag{3.24}$$

It follows that the absolute and relative condition number of component x_i^* with respect to $\boldsymbol{d}$ are given by

$$\kappa_{\text{abs}}(x_i^*;\boldsymbol{d}) = \left\| \left(F'_{\boldsymbol{x}}(\boldsymbol{x}^*;\boldsymbol{d})^{-1}F'_{\boldsymbol{d}}(\boldsymbol{x}^*;\boldsymbol{d})\right)^T_{i,:} \right\|_2, \tag{3.25}$$

$$\kappa_{\text{rel}}(x_i^*;\boldsymbol{d}) = \frac{\|\boldsymbol{d}\|_2 \left\| \left(F'_{\boldsymbol{x}}(\boldsymbol{x}^*;\boldsymbol{d})^{-1}F'_{\boldsymbol{d}}(\boldsymbol{x}^*;\boldsymbol{d})\right)^T_{i,:} \right\|_2}{|x_i^*|}. \tag{3.26}$$

Let us now consider, analogous to [24, Example 3.7], componentwise condition numbers in both the input and the output parameters. Since we are interested in the maximum componentwise error in the output parameters, we take the infinity norm in (3.21), which yields

$$\|\Delta\boldsymbol{x}^*\|_\infty \dot{\leq} \|F'_{\boldsymbol{x}}(\boldsymbol{x}^*;\boldsymbol{d})^{-1}F'_{\boldsymbol{d}}(\boldsymbol{x}^*;\boldsymbol{d})\|_\infty \|\Delta\boldsymbol{d}\|_\infty,$$

where $\Delta\boldsymbol{x}^* = \tilde{\boldsymbol{x}}^* - \boldsymbol{x}^*$ and $\Delta\boldsymbol{d} = \tilde{\boldsymbol{d}} - \boldsymbol{d}$. Thus, the componentwise absolute condition number is given by

$$\kappa_{\text{abs,c}}(\boldsymbol{x}^*;\boldsymbol{d}) = \|F'_{\boldsymbol{x}}(\boldsymbol{x}^*;\boldsymbol{d})^{-1}F'_{\boldsymbol{d}}(\boldsymbol{x}^*;\boldsymbol{d})\|_\infty. \tag{3.27}$$

In order to derive the componentwise relative condition number, we define matrices $D_{\boldsymbol{x}^*} = \text{diag}(x_i^*)$ and $D_{\boldsymbol{d}} = \text{diag}(d_i)$, analogous to [24, Def. 3.1]. Then, (3.21) is equivalent to

$$D_{\boldsymbol{x}^*}^{-1}\Delta\boldsymbol{x}^* \doteq -D_{\boldsymbol{x}^*}^{-1}F'_{\boldsymbol{x}}(\boldsymbol{x}^*;\boldsymbol{d})^{-1}F'_{\boldsymbol{d}}(\boldsymbol{x}^*;\boldsymbol{d})D_{\boldsymbol{d}}D_{\boldsymbol{d}}^{-1}\Delta\boldsymbol{d},$$

where we assume that all components of $\boldsymbol{x}^*$ and $\boldsymbol{d}$ are nonzero, such that the inverses $D_{\boldsymbol{x}^*}^{-1}$ and $D_{\boldsymbol{d}}^{-1}$ exist. Taking the infinity norm again yields

$$\|D_{\boldsymbol{x}^*}^{-1}\Delta\boldsymbol{x}^*\|_\infty \dot{\leq} \|D_{\boldsymbol{x}^*}^{-1}F'_{\boldsymbol{x}}(\boldsymbol{x}^*;\boldsymbol{d})^{-1}F'_{\boldsymbol{d}}(\boldsymbol{x}^*;\boldsymbol{d})D_{\boldsymbol{d}}\|_\infty \|D_{\boldsymbol{d}}^{-1}\Delta\boldsymbol{d}\|_\infty. \tag{3.28}$$

Hence, the *componentwise relative condition number* of $\boldsymbol{x}^*$ with respect to $\boldsymbol{d}$ is given by

$$\kappa_{\text{rel,c}}(\boldsymbol{x}^*;\boldsymbol{d}) = \|D_{\boldsymbol{x}^*}^{-1}F'_{\boldsymbol{x}}(\boldsymbol{x}^*;\boldsymbol{d})^{-1}F'_{\boldsymbol{d}}(\boldsymbol{x}^*;\boldsymbol{d})D_{\boldsymbol{d}}\|_\infty. \tag{3.29}$$

Note that by choosing the infinity norm in (3.20), we have the relation

$$\kappa_{\text{rel,c}}(\boldsymbol{x}^*;\boldsymbol{d}) \leq \kappa_{\text{rel,n}}(\boldsymbol{x}^*;\boldsymbol{d}) \tag{3.30}$$

due to the sub-multiplicativity of the infinity norm. Surprisingly, the componentwise relative condition number (3.29) for general nonlinear problems (3.13) has not been formulated in the literature before. E.g., in [30, Example 2.17], [24, Example 3.7] the componentwise relative condition number for the more specific nonlinear system $F(\boldsymbol{x}) = \boldsymbol{d}$ is derived. In [57, 102] only the normwise relative condition number for nonlinear system (3.13) is given. We note that the amount of literature considering the conditioning of general nonlinear systems is relatively small. This observation is also made in [57, page 468].

Remark. If the nonlinear system (3.13) is solved using (a variant of) the Newton method, then in each Newton iteration the linear system

$$F'(\boldsymbol{x}_j)\Delta\boldsymbol{x}_j = -F(\boldsymbol{x}_j), \tag{3.31}$$

has to be solved, where $\Delta\boldsymbol{x}_j = \boldsymbol{x}_{j+1} - \boldsymbol{x}_j$. It is shown in [102] that the data uncertainty error in $\boldsymbol{x}^*$ depends on the sensitivity of the nonlinear system (3.13) and not on the sensitivity of the linear system (3.31).

3.3.2 Statistical Perturbation Analysis

The condition number leads to a first order worst case perturbation bound. However, in practice, this error bound is rarely attained and the actual error could be much smaller. In order to have a more detailed description of the data uncertainty error, we therefore also compute average perturbation estimates by means of a statistical sensitivity analysis.

We perform this analysis by using the Univariate Reduced Quadrature (URQ) method, see [83]. This method presents a convenient trade-off between computational complexity and accuracy. In contrast to the large sample size that is required for a Monte Carlo Simulation (MCS), the URQ method only utilizes a sample size of $2n+1$, where n is the number of uncertain data components. This makes the URQ method computationally much less expensive than a MCS. The mean μ_{x_k} and the variance $\sigma^2_{x_k}$, $k = 1,\ldots,m$, of a solution component x_k in $\boldsymbol{x}$ are approximated in the URQ method using the quadrature formulas in [83, (20) and (21)]. We use the factor

$$\phi(\boldsymbol{x};\boldsymbol{d}) = \frac{\max_k \sigma_{x_k}/\mu_{x_k}}{\max_i \sigma_{d_i}/\mu_{d_i}} \tag{3.32}$$

as a statistical measure for the average amplification of the uncertainties in the data d_i, $i = 1,\ldots,n$.

Having established normwise and componentwise condition numbers for general nonlinear systems of equations as well as an average uncertainty amplification measure, in the next sections we apply these results to study the sensitivity of the two classes of Euler equations with respect to perturbations in the data.

3.4 Error Analysis for the Semilinear Isothermal Model

In this section, an error analysis is performed for the isothermal Euler equations in semilinear form, called the *semilinear model*. Sections 3.4.1 and 3.4.2 discuss two simple discretization schemes applied to the semilinear model (3.7). These simple discretization schemes, here called the *1S-scheme* and the *MP-scheme*, are typically used in the optimization of large gas networks, see [43, 76]. A theoretical worst case and a statistical mean sensitivity

analysis for both systems is presented in Section 3.4.3. A rounding and iteration error analysis for the two resulting nonlinear systems is contained in Section 3.4.4. Finally, a first order upper bound for the relative model error between the semilinear and the algebraic model is derived in Section 3.4.5.

3.4.1 Discretization using a One-Sided Evaluation

For notational convenience, we consider one space interval $[x_L, x_R]$ as a piece of length H of a pipeline and discretize system (3.8) first in space. There are many different possibilities to obtain such a discretization. Here, we approximate the space derivative by

$$\frac{\partial q}{\partial x} \approx \frac{q(x_R,t) - q(x_L,t)}{H}. \tag{3.33}$$

Furthermore, we use the evaluation $p(x_R,t)$ as an approximation of $p(x,t)$ and $q(x,t) \approx q(x_L,t)$. Inserting the boundary conditions (3.8c), (3.8d) into (3.8a), (3.8b) results in a system of ordinary differential equations (ODEs), which is given by

$$\dot{p}(x_R,t) + \frac{c^2}{AH}\big(q_s(t) - q(x_L,t)\big) = 0, \tag{3.34a}$$

$$\dot{q}(x_L,t) + \frac{A}{H}\big(p(x_R,t) - p_s(t)\big) = -\frac{\lambda c^2}{2DA}\frac{q(x_L,t)|q(x_L,t)|}{p(x_R,t)}. \tag{3.34b}$$

Using the implicit Euler discretization scheme in time and introducing the vector $\boldsymbol{x}^i = [p(x_R,t_i), q(x_L,t_i)]^T$, yields the nonlinear system of equations

$$F_1(\boldsymbol{x}^i, \boldsymbol{d}) = \frac{1}{\tau}(x_1^i - x_1^{i-1}) + \frac{c^2}{AH}(q_s^i - x_2^i) = 0, \tag{3.35a}$$

$$F_2(\boldsymbol{x}^i, \boldsymbol{d}) = \frac{1}{\tau}(x_2^i - x_2^{i-1}) + \frac{A}{H}(x_1^i - p_s^i) + \frac{\lambda c^2}{2DA}\frac{x_2^i|x_2^i|}{x_1^i} = 0. \tag{3.35b}$$

Here, the (uncertain) data are collected in the vector

$$\boldsymbol{d} = [A, \lambda, D, c, p_s^i, q_s^i, x_1^{i-1}, x_2^{i-1}]^T. \tag{3.36}$$

These are the cross-sectional area A, the Darcy friction factor λ, the diameter D, the speed of sound c, the boundary conditions, and the solution of the previous time step $\boldsymbol{x}^{i-1}$. The first three parameters are uncertain because their values cannot be determined accurately for pipelines that lie deep in the ground for a long period of time. The speed of sound c within the gas is uncertain because the temperature T and the compressibility factor z are set to a constant in (3.6) and thus a modeling error is made. The boundary values are subject to measurement errors (or simulation errors when the pipeline is split into smaller pieces), and $\boldsymbol{x}^{i-1}$ is uncertain due to the accumulation of discretization errors, as well as the rounding and data uncertainty errors in the

previous time steps. We call this discretization scheme the *1S-scheme* in the following. It is similar to the discretization in [43, 76]; the only difference is that p and q are there both evaluated in x_R, given that the gas flows from x_L to x_R. Equations (3.35) define a two-dimensional nonlinear system with solution $\boldsymbol{x}^i$. The Jacobian $F'_{\boldsymbol{x}^i}(\boldsymbol{x}^i, \boldsymbol{d})$ of $F = [F_1, F_2]^T$ with respect to $\boldsymbol{x}^i$ is given by

$$F'_{\boldsymbol{x}^i}(\boldsymbol{x}^i, \boldsymbol{d}) = \begin{bmatrix} \frac{1}{\tau} & -\frac{c^2}{AH} \\ \frac{A}{H} - \frac{\lambda c^2}{2DA}\frac{x_2^i|x_2^i|}{(x_1^i)^2} & \frac{1}{\tau} + \frac{\lambda c^2}{DA}\frac{|x_2^i|}{x_1^i} \end{bmatrix}. \tag{3.37}$$

For the solution $\boldsymbol{x}^i$ of the nonlinear system (3.35) we use the Newton method, see, e.g., [63], with stopping criterion $\|\boldsymbol{x}_j^i - \boldsymbol{x}_{j-1}^i\|_\infty \leq \text{tol}$. In our simulations that we present below we use $\text{tol} = 10^{-3}$, the concrete parameters values

$$\tau = 15\,\text{s}, \quad p_R^{i-1} = 5 \cdot 10^6\,\text{Pa}, \quad q_L^{i-1} = 300\,\text{kg s}^{-1}, \tag{3.38a}$$

$$c = \sqrt{RT_0 z_0} = \sqrt{518.3 \cdot 288.15 \cdot 0.928} = 372\,\text{m s}^{-1}, \text{see (3.6)}, \tag{3.38b}$$

$$H = 500\,\text{m}, \quad p_s^i = 5.07 \cdot 10^6\,\text{Pa}, \quad q_s^i = 302\,\text{kg s}^{-1}, \tag{3.38c}$$

$$A = 0.785\,\text{m}^2, \quad \lambda = 0.06, \quad D = 1\,\text{m}, \tag{3.38d}$$

and starting values $\boldsymbol{x}_0^i = [5 \cdot 10^6\,\text{Pa}, 300\,\text{kg s}^{-1}]^T$. These values result in an approximate solution $\boldsymbol{x}^i$ which is given by

$$\boldsymbol{x}^i = \begin{bmatrix} p_R^i \\ q_L^i \end{bmatrix} = \begin{bmatrix} 5.01 \cdot 10^6\,\text{Pa} \\ 3.03 \cdot 10^2\,\text{kg s}^{-1} \end{bmatrix}. \tag{3.39}$$

An important question is, how sensitive this solution is with respect to small perturbations in the uncertain data $\boldsymbol{d}$ in (3.36). To determine this sensitivity, the Jacobian of F with respect to $\boldsymbol{d}$ is computed, which is given by

$$F'_{\boldsymbol{d}}(\boldsymbol{x}^i, \boldsymbol{d}) = \begin{bmatrix} \frac{c^2}{A^2 H}(x_2^i - q_s^i) & \frac{1}{H}(x_1^i - p_s^i) - \frac{\lambda c^2}{2DA^2}\frac{x_2^i|x_2^i|}{x_1^i} \\ 0 & \frac{c^2}{2DA}\frac{x_2^i|x_2^i|}{x_1^i} \\ 0 & -\frac{\lambda c^2}{2D^2 A}\frac{x_2^i|x_2^i|}{x_1^i} \\ \frac{2c}{AH}(q_s^i - x_2^i) & \frac{\lambda c}{DA}\frac{x_2^i|x_2^i|}{x_1^i} \\ 0 & -\frac{A}{H} \\ \frac{c^2}{AH} & 0 \\ -\frac{1}{\tau} & 0 \\ 0 & -\frac{1}{\tau} \end{bmatrix}^T. \tag{3.40}$$

The results of the sensitivity analysis are presented in Section 3.4.3.

3.4.2 Discretization using the Midpoint Rule

As an alternative space discretization of the system (3.8) we use the midpoint rule for the pressure $p(x,t)$ and the mass flow rate $q(x,t)$. For example, for $p(x,t)$ we obtain

$$p(x,t) \approx \frac{p(x_R,t)+p(x_L,t)}{2}.$$

Again, the boundary conditions (3.8c), (3.8d) are inserted into (3.8a), (3.8b). This results in the system of ODEs

$$\begin{aligned}
&\frac{1}{2}\dot{p}(x_R,t) + \frac{c^2}{AH}\big(q_s(t) - q(x_L,t)\big) + \frac{1}{2}\dot{p}_s(t) = 0,\\
&\frac{1}{2}\dot{q}(x_L,t) + \frac{A}{H}\big(p(x_R,t) - p_s(t)\big) + \frac{1}{2}\dot{q}_s(t)\\
&\quad + \frac{\lambda c^2}{4DA}\frac{\big(q_s(t)+q(x_L,t)\big)|q_s(t)+q(x_L,t)|}{p(x_R,t)+p_s(t)} = 0.
\end{aligned}$$

Using again the implicit Euler scheme for the time discretization yields the nonlinear system

$$F_1(\boldsymbol{x}^i,\boldsymbol{d}) = \frac{1}{\tau}(x_1^i - x_1^{i-1}) + \frac{2c^2}{AH}(q_s^i - x_2^i) + \dot{p}_s^i = 0, \tag{3.42a}$$

$$\begin{aligned}
F_2(\boldsymbol{x}^i,\boldsymbol{d}) = &\frac{1}{\tau}(x_2^i - x_2^{i-1}) + \frac{2A}{H}(x_1^i - p_s^i) + \dot{q}_s^i\\
&+ \frac{\lambda c^2}{2DA}\frac{(q_s^i + x_2^i)|q_s^i + x_2^i|}{x_1^i + p_s^i} = 0,
\end{aligned} \tag{3.42b}$$

with data vector

$$\boldsymbol{d} = [A,\lambda,D,c,p_s^i,q_s^i,\dot{p}_s^i,\dot{q}_s^i,x_1^{i-1},x_2^{i-1}]^T. \tag{3.43}$$

We call this discretization scheme the *MP-scheme*. It is equivalent to the implicit box scheme in [66]. The Jacobian $F'_{\boldsymbol{x}^i}$ of $F = [F_1,F_2]^T$ with respect to $\boldsymbol{x}^i$ in this case is given by

$$F'_{\boldsymbol{x}^i}(\boldsymbol{x}^i,\boldsymbol{d}) = \begin{bmatrix} \frac{1}{\tau} & -\frac{2c^2}{AH} \\ \frac{2A}{H} - \frac{\lambda c^2}{2DA}\frac{(q_s^i+x_2^i)|q_s^i+x_2^i|}{(x_1^i+p_s^i)^2} & \frac{1}{\tau} + \frac{\lambda c^2}{DA}\frac{|q_s^i+x_2^i|}{x_1^i+p_s^i} \end{bmatrix}. \tag{3.44}$$

We again use the Newton method for the solution $\boldsymbol{x}^i$ of (3.42) with stopping criterion $\|\boldsymbol{x}_j^i - \boldsymbol{x}_{j-1}^i\|_\infty \le \text{tol}$. For the numerical simulations presented below we use the parameter values (3.38),

$$\dot{p}_s^i = 100, \quad \dot{q}_s^i = 0.05, \tag{3.45}$$

and the starting values $\boldsymbol{x}_0^i = [5\cdot 10^6\,\text{Pa}, 300\,\text{kg s}^{-1}]^T$. This results in an approximate solution $\boldsymbol{x}^i$ given by

$$\boldsymbol{x}^i = \begin{bmatrix} p_R^i \\ q_L^i \end{bmatrix} = \begin{bmatrix} 5.01\cdot 10^6\,\text{Pa} \\ 3.03\cdot 10^2\,\text{kg s}^{-1} \end{bmatrix}. \tag{3.46}$$

In order to determine the sensitivity of $\boldsymbol{x}^i$ with respect to perturbations in the data, the Jacobian of the function F with respect to $\boldsymbol{d}$ in (3.43) is calculated as

$$F'_{\boldsymbol{d}}(\boldsymbol{x}^i,\boldsymbol{d}) = \begin{bmatrix} \frac{2c^2}{A^2H}(x_2^i - q_s^i) & \frac{2}{H}(x_1^i - p_s^i) - \frac{\lambda c^2}{2DA^2}\frac{(q_s^i+x_2^i)|q_s^i+x_2^i|}{x_1^i+p_s^i} \\ 0 & \frac{c^2}{2DA}\frac{(q_s^i+x_2^i)|q_s^i+x_2^i|}{x_1^i+p_s^i} \\ 0 & -\frac{\lambda c^2}{2D^2A}\frac{(q_s^i+x_2^i)|q_s^i+x_2^i|}{x_1^i+p_s^i} \\ \frac{4c}{AH}(q_s^i - x_2^i) & \frac{\lambda c}{DA}\frac{(q_s^i+x_2^i)|q_s^i+x_2^i|}{x_1^i+p_s^i} \\ 0 & -\frac{2A}{H} - \frac{\lambda c^2}{2DA}\frac{(q_s^i+x_2^i)|q_s^i+x_2^i|}{(x_1^i+p_s^i)^2} \\ \frac{2c^2}{AH} & \frac{\lambda c^2}{DA}\frac{|q_s^i+x_2^i|}{x_1^i+p_s^i} \\ 1 & 0 \\ 0 & 1 \\ -\frac{1}{\tau} & 0 \\ 0 & -\frac{1}{\tau} \end{bmatrix}^T . \tag{3.47}$$

The sensitivity results are presented in Section 3.4.3.

3.4.3 Sensitivity Analysis for the Two Discretizations

This section contains both a worst case first order and a statistical mean sensitivity analysis for the 1S- and the MP- discretization scheme. Moreover, we show that the normwise condition number yields a too pessimistic upper error bound.

We use the Jacobians in (3.37), (3.40), (3.44), (3.47) to calculate the individual condition numbers (3.26) of the components p_R^i and q_L^i of the solutions $\boldsymbol{x}^i$ in (3.39), (3.46) with respect to perturbations in the uncertain data. Using the parameter values in (3.38), (3.45) we obtain the results presented in Table 3.1. We find that the largest individual condition number is $\kappa_{\text{rel}}(q_L^i; p_s^i)$ for both schemes. Moreover, one observes that the mass flow rate q_L^i is more sensitive to small perturbations in the parameters than the pressure p_R^i. We note that a scaling of the parameter values or using different units, e.g. by choosing the unit metric ton rather than kg, does not change the results.

Calculating the normwise relative condition numbers (3.20) of $\boldsymbol{x}^i$ with respect to $\boldsymbol{d}$ in (3.36), (3.43) for the 1S- and the MP-scheme with parameter values (3.38), (3.45) yields $\kappa_{\text{rel,n}}^{\text{1S}}(\boldsymbol{x}^i;\boldsymbol{d}) = 1.39\cdot 10^6$, $\kappa_{\text{rel,n}}^{\text{MP}}(\boldsymbol{x}^i;\boldsymbol{d}) = 1.45\cdot 10^6$. We find that these normwise condition numbers are at least three orders of magnitude larger than the individual condition numbers in Table 3.1. Hence, the normwise condition number considerably overestimates the sensitivity of the corresponding nonlinear root finding problem, i.e., it constitutes a very pessimistic upper bound. Considering also (3.30), this leads to the conclusion

that it is more adequate to use the componentwise relative condition number in (3.29) in order to determine the sensitivity of $\boldsymbol{x}^i$ with respect to $\boldsymbol{d}$.

The componentwise condition numbers for the two different discretization schemes are calculated for spatial stepsizes $H \in [1, 1000\,\mathrm{m}]$ and for temporal stepsizes $\tau \in [10^{-2}, 30\,\mathrm{s}]$. The results are depicted in Figure 3.3. In order to get a more detailed description of the sensitivity of the nonlinear systems, we also perform a statistical mean error analysis for the 1S- and the MP-scheme using the URQ method; see Section 3.3.2. The relative standard deviations σ_{d_j}/μ_{d_j}, $j = 1, \ldots, n$, for the input parameters is set to 0.5% and the values in (3.38) are taken for the mean values μ_{d_j}. Subsequently, the relative standard deviations $\sigma_{x_k^i}/\mu_{x_k^i}$, $k = 1, 2$, of the solution $\boldsymbol{x}^i$ are computed. Factor $\phi(\boldsymbol{x}^i; \boldsymbol{d})$ in (3.32) is again calculated for $H \in [1, 1000\,\mathrm{m}]$ and $\tau \in [10^{-2}, 30\,\mathrm{s}]$. The results are depicted in Figure 3.4. We find that the differences between the mean uncertainty amplification factors ϕ and the first order worst case bounds in Figure 3.3 are relatively small. Furthermore, we observe in both figures that given H and τ, the sensitivity of the MP-scheme is smaller than that of the 1S-scheme. Using Figures 3.3 and 3.4 for a given discretization scheme, the spatial and temporal stepsizes H and τ can be chosen such that the sensitivity of the corresponding nonlinear system is low. Note that while reducing H

Table 3.1: Individual relative condition numbers in (3.26) for the 1S- and the MP-scheme. The condition numbers are computed for the solution components p_R^i and q_L^i with respect to the uncertain input parameters $\boldsymbol{d}$ in (3.36), (3.43). The values in (3.38), (3.45) are used.

	$\kappa_{\mathrm{rel}}^{\mathrm{1S}}$		$\kappa_{\mathrm{rel}}^{\mathrm{MP}}$	
	p_R^i	q_L^i	p_R^i	q_L^i
A	$2.30 \cdot 10^{-2}$	$7.65 \cdot 10^{-2}$	$2.40 \cdot 10^{-2}$	$4.07 \cdot 10^{-2}$
λ	$1.15 \cdot 10^{-2}$	$3.60 \cdot 10^{-2}$	$1.20 \cdot 10^{-2}$	$1.88 \cdot 10^{-2}$
D	$1.15 \cdot 10^{-2}$	$3.60 \cdot 10^{-2}$	$1.20 \cdot 10^{-2}$	$1.88 \cdot 10^{-2}$
c	$2.28 \cdot 10^{-2}$	$8.09 \cdot 10^{-2}$	$2.40 \cdot 10^{-2}$	$4.38 \cdot 10^{-2}$
p_s^i	$9.44 \cdot 10^{-1}$	2.94	1.00	1.57
q_s^i	$2.53 \cdot 10^{-2}$	$9.16 \cdot 10^{-1}$	$2.53 \cdot 10^{-2}$	$9.57 \cdot 10^{-1}$
$\dot{p}_s^i$	–	–	$6.23 \cdot 10^{-6}$	$4.58 \cdot 10^{-4}$
$\dot{q}_s^i$	–	–	$3.13 \cdot 10^{-6}$	$4.89 \cdot 10^{-6}$
p_R^{i-1}	$7.93 \cdot 10^{-2}$	2.87	$2.08 \cdot 10^{-2}$	1.53
q_L^{i-1}	$2.37 \cdot 10^{-3}$	$7.39 \cdot 10^{-3}$	$1.25 \cdot 10^{-3}$	$1.96 \cdot 10^{-3}$

and τ decreases the discretization error, it increases the sensitivity of the problem and thus both the error due to data uncertainty and the effect of rounding are amplified. Hence, a balance between the discretization and the data uncertainty error should be determined to find appropriate values for H and τ.

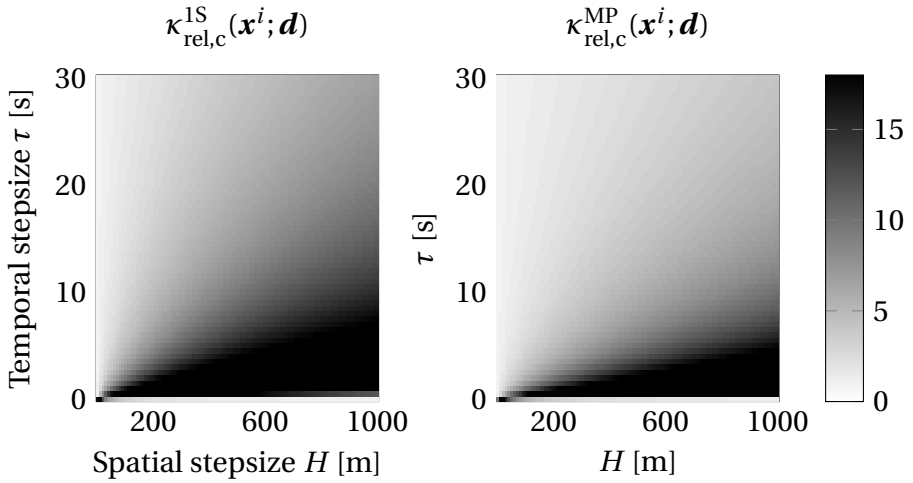

Figure 3.3: The componentwise relative condition numbers in (3.29) of the 1S-scheme (left) and the MP-scheme (right) as a function of the spatial and temporal stepsize. The condition number is computed for the solution $\boldsymbol{x}^i = [p_R^i, q_L^i]^T$ with respect to the uncertain data $\boldsymbol{d}$ in (3.36), (3.43). The numbers at the colorbar denote the values of $\kappa_{\text{rel,c}}$.

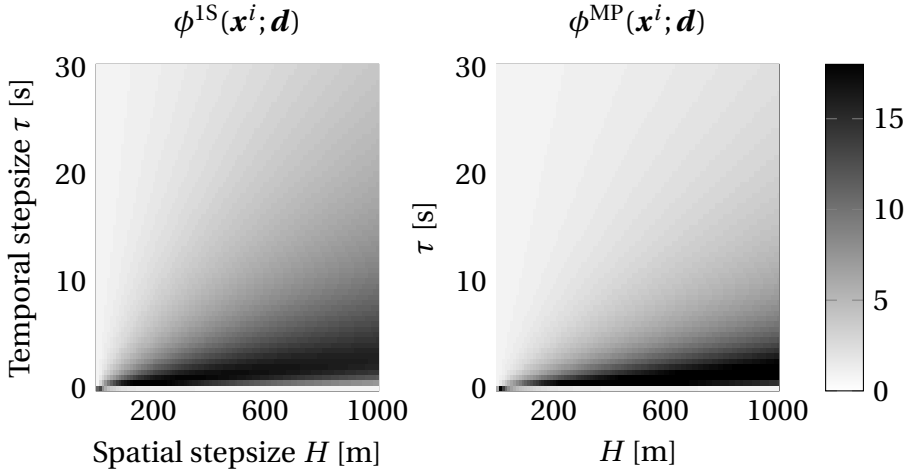

Figure 3.4: The mean uncertainty amplification factor $\phi(\boldsymbol{x}^i;\boldsymbol{d})$ in (3.32), calculated with the URQ method, for the 1S-scheme (left) and MP-scheme (right) as a function of H and τ. The values in (3.38) are taken for the mean values of the uncertain data. The numbers at the colorbar denote the values of ϕ.

3.4.4 Rounding and Iteration Error Analysis

In this section a first order upper bound for the rounding errors and the iteration error that are committed in the Newton method is derived. The result is applied to both the 1S- and the MP-scheme.

A rounding error analysis for the solution of the linear system (3.31) arising in the Newton method is presented in [103], together with a condition for which the intermediate solution $\boldsymbol{x}_j$ cannot be improved due to rounding errors, see [103, page 117]. If e_j is an upper bound for the rounding error $\|F(\boldsymbol{x}_j)-\tilde{F}(\boldsymbol{x}_j)\|$, where F is the exact function evaluation and $\tilde{F}$ is the computed function evaluation, then this condition is given by

$$\|\tilde{F}(\boldsymbol{x}_j)\| \le e_j \quad \text{or} \quad \|\tilde{F}(\boldsymbol{x}_j)\| \ge \|\tilde{F}(\boldsymbol{x}_{j-1})\|. \tag{3.48}$$

In the following we assume that the first condition of (3.48) is satisfied before the second condition of (3.48). We define the set

$$\mathscr{S} := \{\boldsymbol{x} \mid \|\tilde{F}(\boldsymbol{x})\| \le e_j\} \tag{3.49}$$

and assume that $\boldsymbol{x}^* \in \mathscr{S}$. Then, provided that the Jacobian of $\tilde{F}$ is invertible for all $\boldsymbol{x} \in \mathscr{S}$, it follows from the implicit function theorem that

$$\begin{aligned} \|\boldsymbol{x}_j - \boldsymbol{x}^*\| &\doteq \|[\tilde{F}'(\boldsymbol{x}_j)]^{-1}\| \, \|\tilde{F}(\boldsymbol{x}_j) - \tilde{F}(\boldsymbol{x}^*)\| \\ &\le \|[\tilde{F}'(\boldsymbol{x}_j)]^{-1}\| \, (\|\tilde{F}(\boldsymbol{x}_j)\| + \|\tilde{F}(\boldsymbol{x}^*)\|) \\ &\le \|[\tilde{F}'(\boldsymbol{x}_j)]^{-1}\| \, (\|\tilde{F}(\boldsymbol{x}_j)\| + e_j) \end{aligned} \tag{3.50}$$

for all $\boldsymbol{x}_j \in \mathscr{S}$. Let $\mathscr{B}(r)$ denote the ball with radius r around $\boldsymbol{x}^*$, i.e.,

$$\mathscr{B}(r) = \{\boldsymbol{x} \mid \|\boldsymbol{x} - \boldsymbol{x}^*\| < r\}.$$

It is well-known, see, e.g., [63, Theorem 5.1.1], that under certain assumptions on the function F, e.g., Lipschitz continuity of F', there exists a $\xi > 0$ such that if $\boldsymbol{x}_j \in \mathscr{B}(\xi) \setminus \mathscr{S}$, then the Newton method converges quadratically, i.e., $\|\boldsymbol{x}_{j+1} - \boldsymbol{x}^*\| = O(\|\boldsymbol{x}_j - \boldsymbol{x}^*\|^2)$. This implies that

$$\|\boldsymbol{x}_j - \boldsymbol{x}^*\| \le \|\boldsymbol{x}_j - \boldsymbol{x}_{j+1}\| + O(\|\boldsymbol{x}_j - \boldsymbol{x}^*\|^2), \quad \text{for all } \boldsymbol{x}_j \in \mathscr{B}(\xi) \setminus \mathscr{S}. \tag{3.51}$$

Thus, we have the following theorem.

Theorem 3.1. *Let a solution $\boldsymbol{x}_j$ of the nonlinear system arising in the gas flow simulation that is computed with the Newton method be given. Let η^{ri} denote the error in $\boldsymbol{x}_j$ both due to rounding errors in the solution of* (3.31) *and due to a preliminary stopping of the Newton iteration. Let e_j be an upper bound for the rounding error $\|F(\boldsymbol{x}_j) - \tilde{F}(\boldsymbol{x}_j)\|$. Suppose that $\mathscr{S} \subseteq \mathscr{B}(\xi)$ and $\boldsymbol{x}_j \in \mathscr{B}(\xi)$, then*

$$\eta^{\mathrm{ri}} \doteq \begin{cases} \|[\tilde{F}'(\boldsymbol{x}_j)]^{-1}\| \, (\|\tilde{F}(\boldsymbol{x}_j)\| + e_j) & \text{if } \boldsymbol{x}_j \in \mathscr{S}, \\ \|\boldsymbol{x}_j - \boldsymbol{x}_{j+1}\| & \text{if } \boldsymbol{x}_j \in \mathscr{B}(\xi) \setminus \mathscr{S}. \end{cases} \tag{3.52}$$

Proof. If $\boldsymbol{x}_j \in \mathscr{B}(\xi) \setminus \mathscr{S}$, then the Newton method converges quadratically despite rounding errors in the solution of (3.31), see [103, page 117]. Thus, η^{ri} is given by (3.51). On the other hand, if $\boldsymbol{x}_j \in \mathscr{S}$, then condition (3.48) is satisfied and we do not have convergence. An upper bound for η^{ri} is then given by (3.50). □

To apply this result, we compute η^{ri} for the 1S- and the MP-scheme. For the 1S-scheme we may write

$$\tilde{F}_1(\boldsymbol{x}^i, \boldsymbol{d}) = \frac{x_1^i - x_1^{i-1}}{\tau}(1+3\varepsilon) + \frac{c^2(q_s^i - x_2^i)}{AH}(1+6\varepsilon),$$
$$\tilde{F}_2(\boldsymbol{x}^i, \boldsymbol{d}) = \frac{x_2^i - x_2^{i-1}}{\tau}(1+4\varepsilon) + \frac{A(x_1^i - p_s^i)}{H}(1+5\varepsilon) + \frac{\lambda c^2 x_2^i |x_2^i|}{2DAx_1^i}(1+8\varepsilon),$$

where $|\varepsilon| \leq \mathbf{u}$ and $\mathbf{u}$ denotes the unit roundoff. Hence, we have

$$|F_1 - \tilde{F}_1| \leq \frac{|x_1^i - x_1^{i-1}|}{\tau}3\mathbf{u} + \frac{c^2|q_s^i - x_2^i|}{AH}6\mathbf{u} =: \alpha^{1\mathrm{S}},$$
$$|F_2 - \tilde{F}_2| \leq \frac{|x_2^i - x_2^{i-1}|}{\tau}4\mathbf{u} + \frac{A|x_1^i - p_s^i|}{H}5\mathbf{u} + \frac{\lambda c^2 (x_2^i)^2}{2DAx_1^i}8\mathbf{u} =: \beta^{1\mathrm{S}}$$

and, thus, $e_j^{1\mathrm{S}} = \|[\alpha^{1\mathrm{S}}, \beta^{1\mathrm{S}}]^T\|$. For the MP-scheme we obtain

$$\tilde{F}_1 = \frac{x_1^i - x_1^{i-1}}{\tau}(1+4\varepsilon) + \frac{2c^2(q_s^i - x_2^i)}{AH}(1+7\varepsilon) + \dot{p}_s^i(1+\varepsilon),$$
$$\tilde{F}_2 = \frac{x_2^i - x_2^{i-1}}{\tau}(1+5\varepsilon) + \frac{2A(x_1^i - p_s^i)}{H}(1+6\varepsilon) + \dot{q}_s^i(1+2\varepsilon)$$
$$+ \frac{\lambda c^2 (q_s^i + x_2^i)|q_s^i + x_2^i|}{2DA(x_1^i + p_s^i)}(1+11\varepsilon),$$

and, hence

$$|F_1 - \tilde{F}_1| \leq \frac{|x_1^i - x_1^{i-1}|}{\tau}4\mathbf{u} + \frac{2c^2|q_s^i - x_2^i|}{AH}7\mathbf{u} + |\dot{p}_s^i|\mathbf{u} =: \alpha^{\mathrm{MP}},$$
$$|F_2 - \tilde{F}_2| \leq \frac{|x_2^i - x_2^{i-1}|}{\tau}5\mathbf{u} + \frac{2A|x_1^i - p_s^i|}{H}6\mathbf{u} + |\dot{q}_s^i|2\mathbf{u}$$
$$+ \frac{\lambda c^2 (q_s^i + x_2^i)^2}{2DA(x_1^i + p_s^i)}11\mathbf{u} =: \beta^{\mathrm{MP}},$$

and $e_j^{\mathrm{MP}} = \|[\alpha^{\mathrm{MP}}, \beta^{\mathrm{MP}}]^T\|$. Assuming the use of IEEE standard double precision arithmetic, such that $\mathbf{u} = 2.22 \cdot 10^{-16}$, see [57, page 39], and choosing the infinity norm, we obtain the following error estimates. For the 1S-scheme with the values in (3.38) and the solution $\boldsymbol{x}^i$ in (3.39) we have $e_j^{1\mathrm{S}} = 1.16 \cdot 10^{-12}$ and $\|\tilde{F}(\boldsymbol{x}^i)\| = 1.74 \cdot 10^{-11}$. Thus, $\boldsymbol{x}^i$ is not an element of the set $\mathscr{S}$. We assume that $\boldsymbol{x}^i \in \mathscr{B}(\xi)$ such that we have $\eta^{\mathrm{ri}} \doteq 1.56 \cdot 10^{-10}$. For the MP-scheme with

the values in (3.45) and the solution $\boldsymbol{x}^i$ in (3.46) we have $e_j^{\mathrm{MP}} = 1.73 \cdot 10^{-12}$ and $\|\tilde{F}(\boldsymbol{x}^i)\| = 2.22 \cdot 10^{-11}$. Hence, $\boldsymbol{x}^i$ again is not contained in $\mathscr{S}$. We again assume that $\boldsymbol{x}^i \in \mathscr{B}(\xi)$ such that we have $\eta^{\mathrm{ri}} \doteq 7.82 \cdot 10^{-11}$. It can be concluded that for both schemes the rounding and iteration errors can be neglected in comparison with the data uncertainty error.

3.4.5 Modeling Error between the Semilinear and Algebraic Model

In this section we analyze the modeling error that is committed when the isothermal semilinear model (3.7) is simplified to the isothermal algebraic model (3.10a), (3.10b) that is obtained by assuming a stationary gas flow, see Figure 3.2.

We consider the semilinear and the algebraic model on the spatial interval $[0, L]$, with pipeline length L, and the temporal interval $[0, T]$. We define gridpoints (x_i, t^k), $i = 0, \ldots, N$ and $k = 0, \ldots, M$, with stepsizes $H = L/N$ and $\tau = T/M$. Let the solution of the semilinear model at the gridpoints be denoted by $\boldsymbol{y}^{\mathrm{sem}}(x_i, t^k)$, the solution of the discretized semilinear model with stepsizes H and τ at the gridpoints (x_i, t^k) be denoted by $\boldsymbol{y}_i^k(H, \tau)$, and the solution of the algebraic model at the gridpoints be denoted by $\boldsymbol{y}^{\mathrm{alg}}(x_i)$, with $\boldsymbol{y}(x, t) = [p(x, t), q(x, t)]^T$. We define the relative model error η^{m} between the semilinear and the algebraic model by

$$\eta^{\mathrm{m}} := \max_{i,k} \left\| D^{-1}_{\boldsymbol{y}_i^k(H/2,\tau/2)} \left(\boldsymbol{y}^{\mathrm{sem}}(x_i, t^k) - \boldsymbol{y}^{\mathrm{alg}}(x_i) \right) \right\|_\infty,$$

with $D_{\boldsymbol{x}} := \mathrm{diag}(\boldsymbol{x})$. Using the triangle inequality, we have

$$\begin{aligned} \eta^{\mathrm{m}} \leq \max_{i,k} \big(& \left\| D^{-1}_{\boldsymbol{y}_i^k(H/2,\tau/2)} \left(\boldsymbol{y}^{\mathrm{sem}}(x_i, t^k) - \boldsymbol{y}_i^k(H/2, \tau/2) \right) \right\|_\infty \\ & + \left\| D^{-1}_{\boldsymbol{y}_i^k(H/2,\tau/2)} \left(\boldsymbol{y}_i^k(H/2, \tau/2) - \boldsymbol{y}^{\mathrm{alg}}(x_i) \right) \right\|_\infty \big). \end{aligned} \tag{3.55}$$

The term $\boldsymbol{y}^{\mathrm{sem}}(x_i, t^k) - \boldsymbol{y}_i^k(H/2, \tau/2)$ in (3.55) denotes the discretization error of the semilinear model at the gridpoint (x_i, t^k). We note that the right-hand side of the semilinear model in (3.8) is only once continuously differentiable in both space and time due to the term $q|q|$. Thus, in general, the maximum attainable convergence order in space and time for finite difference schemes is one. However, if q does not change sign during the simulation, i.e., if no backflow occurs, which we assume in the following, then higher order convergence rates can be achieved. Suppose that the discretization scheme for the semilinear model converges with order γ in space and order δ in time. Then, the discretization error has an asymptotic expansion of the form

$$\boldsymbol{y}^{\mathrm{sem}}(x_i, t^k) - \boldsymbol{y}_i^k(H/2, \tau/2) = e(x_i, t^k) \left((H/2)^\gamma + (\tau/2)^\delta \right) + O\left(H^{\gamma+1} + \tau^{\delta+1} \right),$$

with coefficient function $e(x, t)$ that is independent of H and τ, cf. [50]. Hence,

we have the first order approximations

$$\boldsymbol{y}^{\mathrm{sem}}(x_i,t^k)-\boldsymbol{y}_i^k(H/2,\tau/2)\doteq e(x_i,t^k)\big((H/2)^\gamma+(\tau/2)^\delta\big), \tag{3.56}$$

$$\boldsymbol{y}^{\mathrm{sem}}(x_i,t^k)-\boldsymbol{y}_i^k(H,\tau)\doteq e(x_i,t^k)(H^\gamma+\tau^\delta). \tag{3.57}$$

Subtracting (3.56) from (3.57) and rewriting yields

$$e(x_i,t^k)\doteq\frac{\boldsymbol{y}_i^k(H,\tau)-\boldsymbol{y}_i^k(H/2,\tau/2)}{H^\gamma+\tau^\delta-(H/2)^\gamma-(\tau/2)^\delta}.$$

Inserting this into (3.56) and inserting (3.56) into (3.55) results in the first order upper bound for the relative model error

$$\begin{aligned}\eta^{\mathrm{m}}\lessdot\max_{i,k}\Big(&\frac{(H/2)^\gamma+(\tau/2)^\delta}{H^\gamma+\tau^\delta-(H/2)^\gamma-(\tau/2)^\delta}\\&\cdot\big\|D^{-1}_{\boldsymbol{y}_i^k(H/2,\tau/2)}\big(\boldsymbol{y}_i^k(H,\tau)-\boldsymbol{y}_i^k(H/2,\tau/2)\big)\big\|_\infty\\&+\big\|D^{-1}_{\boldsymbol{y}_i^k(H/2,\tau/2)}\big(\boldsymbol{y}_i^k(H/2,\tau/2)-\boldsymbol{y}^{\mathrm{alg}}(x_i)\big)\big\|_\infty\Big).\end{aligned} \tag{3.58}$$

In order to apply this result, we discretize the semilinear model with the 1S-scheme from Section 3.4.1. This discretization scheme is consistent of order 1 both in space and time. The stability of the 1S-scheme is secured by the use of the implicit Euler method in time. Hence, we have convergence of order 1 in space and time, i.e., $\gamma=\delta=1$. Using e.g. the concrete values $p_{\mathrm{in}}=5.06\cdot10^6\,\mathrm{Pa}$, $q=300\,\mathrm{kg\,s^{-1}}$ for the algebraic model and the values in (3.38) for the semilinear model, we compute the discrete semilinear solutions $\boldsymbol{y}_i^k(H,\tau)$, $\boldsymbol{y}_i^k(H/2,\tau/2)$ and the algebraic solution $\boldsymbol{y}^{\mathrm{alg}}(x_i)$. From (3.58), for these concrete data this results in $\eta^{\mathrm{m}}\lessdot1.16\,\%$.

Having analyzed different error sources for the semilinear model, in the next section we step down one level in the model hierarchy in Figure 3.2 and perform a similar analysis for the algebraic model.

3.5 Error Analysis for the Algebraic Model

In this section an error analysis is performed for the temperature dependent algebraic model in (3.10). This analysis is performed both in terms of backward and forward errors, resulting in first order upper error bounds, in Section 3.5.1 and statistically, yielding mean error estimates, in Section 3.5.2. Furthermore, it is analyzed in Section 3.5.3 under which condition the temperature dependent model can safely be simplified to the isothermal algebraic model. Further details and examples can be found in [75].

3.5.1 Deterministic Error Analysis

In this section a backward error analysis is performed for the algebraic model (3.10). The rounding errors due to finite precision arithmetic and the

uncertainties in the data are interpreted as perturbations in the input parameters. Then, the relative errors in the output parameters are calculated using the individual relative condition numbers and their magnitudes are analyzed for certain concrete input parameter values.

In the equation for the mass flux

$$\hat{q}(\boldsymbol{d}) = \rho_{\text{in}} v_{\text{in}}, \tag{3.59}$$

which is constant in space, only one multiplication is performed with relative error ε_1, which yields

$$\begin{aligned}\tilde{\hat{q}}(\rho_{\text{in}}, v_{\text{in}}) &= \rho_{\text{in}}(1+\varepsilon_{\rho_{\text{in}}}) v_{\text{in}}(1+\varepsilon_{v_{\text{in}}})(1+\varepsilon_1) \\ &= \rho_{\text{in}} v_{\text{in}}(1+\varepsilon_{\rho_{\text{in}}}+\varepsilon_{v_{\text{in}}}+\varepsilon_1+O(\varepsilon^2)) \\ &= \hat{q}(\rho_{\text{in}}, v_{\text{in}}(1+\varepsilon_2)),\end{aligned} \tag{3.60}$$

with $\varepsilon_2 = \varepsilon_{\rho_{\text{in}}} + \varepsilon_{v_{\text{in}}} + \varepsilon_1 + O(\varepsilon^2)$. Here, $\varepsilon_{\rho_{\text{in}}}$ is the relative measurement error in ρ_{in}, $\varepsilon_{v_{\text{in}}}$ the relative data error in v_{in}, and $|\varepsilon_1| < \mathbf{u}$ the relative error of the multiplication, with $\mathbf{u}$ the rounding unit in finite precision arithmetic. For the absolute relative error in $\hat{q}$, using (3.60), we obtain

$$\begin{aligned}\frac{|\hat{q}(\boldsymbol{d}) - \hat{q}(\boldsymbol{d}+\Delta\boldsymbol{d})|}{|\hat{q}(\boldsymbol{d})|} &\le \Big|\frac{\partial\hat{q}}{\partial\rho_{\text{in}}}\frac{1}{\hat{q}(\boldsymbol{d})}\underbrace{\Delta\rho_{\text{in}}}_{0}\Big| + \Big|\frac{\partial\hat{q}}{\partial v_{\text{in}}}\frac{1}{\hat{q}(\boldsymbol{d})}\Delta v_{\text{in}}\Big| + O\big((\Delta\boldsymbol{d})^2\big) \\ &= \Big|\underbrace{\Big(\frac{\partial\hat{q}}{\partial v_{\text{in}}}\frac{v_{\text{in}}}{\hat{q}(\boldsymbol{d})}\Big)}_{\frac{\rho_{\text{in}} v_{\text{in}}}{\rho_{\text{in}} v_{\text{in}}}=1}\underbrace{\frac{\Delta v_{\text{in}}}{v_{\text{in}}}}_{\varepsilon_2}\Big| + O\big((\Delta\boldsymbol{d})^2\big) \\ &= |\varepsilon_2| + \text{h.o.t.} \le |\varepsilon_{\rho_{\text{in}}}| + |\varepsilon_{v_{\text{in}}}| + |\varepsilon_1| + \text{h.o.t.},\end{aligned}$$

where h.o.t. stands for higher order terms in the ε_j. Assuming that the roundoff error ε_1 is so small that it can be neglected in comparison with errors $\varepsilon_{\rho_{\text{in}}}$ and $\varepsilon_{v_{\text{in}}}$, then we have the constraint

$$|\varepsilon_{\rho_{\text{in}}}| + |\varepsilon_{v_{\text{in}}}| \dot{\le} e_{\text{lim}},$$

where e_{lim} is a limit for the relative error in $\hat{q}$.

For the computation of the pressure

$$p(\boldsymbol{d}) = \sqrt{p_{\text{in}}^2 - \frac{\lambda c^2}{2r}\rho v|\rho v|(x-x_0)} \tag{3.61}$$

we use Algorithm 3.1. Using the Taylor series expansion $\frac{1}{1-\varepsilon} = 1+\varepsilon+O(\varepsilon^2)$, this leads to a backward error due to roundoff errors in finite precision arithmetic with unit roundoff $\mathbf{u}$, given by

$$\tilde{p}(\boldsymbol{d}) = \sqrt{(p_{\text{in}}(1+\varepsilon_{13}))^2 - \frac{\lambda(1+\varepsilon_{14})c^2}{2r}\rho v|\rho v|(x-x_0)}, \tag{3.62}$$

where

$$2|\varepsilon_{13}| = |\varepsilon_1 + \varepsilon_{11} + 2\varepsilon_{12} + O(\varepsilon^2)| \leq 4\mathbf{u} + O(\mathbf{u}^2),$$

so that $|\varepsilon_{13}| \leq 2\mathbf{u} + O(\mathbf{u}^2)$ and $|\varepsilon_{14}| \leq 13\mathbf{u} + O(\mathbf{u}^2)$. Introducing relative data errors and denoting the relative measurement error for the parameter α by ε_α, continuing with (3.62), gives

$$\tilde{p}(\boldsymbol{d})^2 = \big(p_{\text{in}}(1+\varepsilon_{15})\big)^2 - \frac{\lambda(1+\varepsilon_{16})c^2}{2r}\rho v|\rho v|\big(x(1+\varepsilon_x) - x_0(1+\varepsilon_{x_0})\big),$$

with

$$|\varepsilon_{15}| = |\varepsilon_{p_{\text{in}}} + \varepsilon_{13} + O(\varepsilon^2)| \leq |\varepsilon_{p_{\text{in}}}| + 2\mathbf{u} + \text{h.o.t.}, \tag{3.63a}$$

$$|\varepsilon_{16}| \leq |\varepsilon_\lambda| + 2|\varepsilon_c| + |\varepsilon_r| + 2|\varepsilon_\rho| + 2|\varepsilon_v| + 13\mathbf{u} + \text{h.o.t.} \tag{3.63b}$$

Thus, for the backward error of $p(\boldsymbol{d})$, considered as a function of $p_{\text{in}}, \lambda, x, x_0$, we have the expression

$$\tilde{p}(p_{\text{in}}, \lambda, x, x_0) = p\big(p_{\text{in}}(1+\varepsilon_{15}), \lambda(1+\varepsilon_{16}), x(1+\varepsilon_x), x_0(1+\varepsilon_{x_0})\big). \tag{3.64}$$

The effect of the rounding errors in the arithmetic computation of the pressure, given by $2\mathbf{u}$ and $13\mathbf{u}$ in (3.63), is in general much smaller than the measurement errors for the input parameters, which, in the worst case scenario, can be in the order of a few percent. Hence, the magnitudes of the relative backward errors $\varepsilon_{15}, \varepsilon_{16}, \varepsilon_x, \varepsilon_{x_0}$ mainly depend on the inflicted measurement errors. Using Taylor series expansion and the triangle inequality, it follows from (3.64) that an upper bound for the relative error in $p(\boldsymbol{d})$ due to the relative perturbations in the data $\boldsymbol{d} = [p_{\text{in}}, \lambda, x, x_0]^T$ caused by rounding and data uncertainty is given

Algorithm 3.1 : Computing the pressure p in (3.61)

Input: p_{in}, λ, c, r, ρ, v, x, x_0

1: $\leftarrow p_{\text{in}} \cdot p_{\text{in}}$
2: $z_2 \leftarrow c \cdot c$
3: $z_3 \leftarrow \lambda \cdot z_2$
4: $z_4 \leftarrow 2 \cdot r$
5: $z_5 \leftarrow z_3 / z_4$
6: $z_6 \leftarrow \rho \cdot v$
7: $z_7 \leftarrow x - x_0$
8: $z_8 \leftarrow z_5 \cdot z_6$
9: $z_9 \leftarrow z_8 \cdot |z_6|$
10: $z_{10} \leftarrow z_9 \cdot z_7$
11: $z_{11} \leftarrow z_1 - z_{10}$
12: $z_{12} \leftarrow \sqrt{z_{11}}$
13: $p(\boldsymbol{d}) \leftarrow z_{12}$

Output: p

by

$$\begin{aligned}\frac{|p(\boldsymbol{d})-p(\boldsymbol{d}+\Delta\boldsymbol{d})|}{p(\boldsymbol{d})} &\le \sum_{i=1}^{4}\left|\frac{\partial p(\boldsymbol{d})}{\partial d_i}\frac{d_i}{p(\boldsymbol{d})}\right|\left|\frac{\Delta d_i}{d_i}\right| + O\left((\Delta\boldsymbol{d})^2\right)\\ &= \underbrace{\left(\frac{p_{\text{in}}}{p(\boldsymbol{d})}\right)^2}_{\kappa_{\text{rel}}(p;p_{\text{in}})}|\varepsilon_{15}| + \underbrace{\frac{\lambda c^2\rho^2 v^2(x-x_0)}{4r\,p(\boldsymbol{d})^2}}_{\kappa_{\text{rel}}(p;\lambda)}|\varepsilon_{16}| + \underbrace{\frac{\lambda c^2\rho^2 v^2|x|}{4r\,p(\boldsymbol{d})^2}}_{\kappa_{\text{rel}}(p;x)}|\varepsilon_x|\\ &\quad + \underbrace{\frac{\lambda c^2\rho^2 v^2|x_0|}{4r\,p(\boldsymbol{d})^2}}_{\kappa_{\text{rel}}(p;x_0)}|\varepsilon_{x_0}| + \text{h.o.t.},\end{aligned} \tag{3.65}$$

where $\kappa_{\text{rel}}(p;p_{\text{in}}), \kappa_{\text{rel}}(p;\lambda), \kappa_{\text{rel}}(p;x), \kappa_{\text{rel}}(p;x_0)$ are the individual relative condition numbers, see (3.11), which amplify the relative backward errors. Note that the relative condition number $\kappa_{\text{rel}}(p;\boldsymbol{d})$ of p with respect to $\boldsymbol{d}$ is given by the sum of these four individual condition numbers, see (3.12). Suppose that we require $\kappa_{\text{rel}}(p;p_{\text{in}}) \le \text{tol}$, where tolerance $\text{tol} > 1$ should depend on $\varepsilon_{p_{\text{in}}}$, then the inequality

$$\frac{p_{\text{in}}^2}{p_{\text{in}}^2 - \lambda c^2\rho v|\rho v|(x-x_0)/(2r)} \le \text{tol}$$

is obtained. By rewriting this relation it follows that if $\rho v > 0$, then the algebraic model can be used safely for a maximum pipeline length

$$L = x - x_0 \le \frac{2r\,p_{\text{in}}^2(1-1/\text{tol})}{\lambda c^2\rho^2 v^2}. \tag{3.66}$$

If $\rho v \le 0$, then there is no such restriction on the pipeline length. Choosing e.g. the concrete nominal values $\boldsymbol{d}_{\text{nom}}$ given by

$$p_{\text{in}_{\text{nom}}} = 2\cdot 10^5\,\text{Pa}, \quad \lambda_{\text{nom}} = 0.03, \quad c_{\text{nom}} = 343\,\text{m}\,\text{s}^{-1}, \tag{3.67a}$$

$$r_{\text{nom}} = 0.5\,\text{m}, \quad \rho_{\text{nom}} = 1\,\text{kg}\,\text{m}^{-3}, \quad v_{\text{nom}} = 10\,\text{m}\,\text{s}^{-1}, \quad x_{0_{\text{nom}}} = 0\,\text{m}, \tag{3.67b}$$

then $\kappa_{\text{rel}}(p;x) = \kappa_{\text{rel}}(p;\lambda)$ and $\kappa_{\text{rel}}(p;x_0) = 0$. The relative condition numbers $\kappa_{\text{rel}}(p;p_{\text{in}}), \kappa_{\text{rel}}(p;\lambda), \kappa_{\text{rel}}(p;x)$ grow quickly with the pipeline length $L = x - x_0$, see Figure 3.5. The graphs have a vertical asymptote at $L = 113\,\text{km}$. Given that we require that

$$\|[\kappa_{\text{rel}}(p;p_{\text{in}}), \kappa_{\text{rel}}(p;\lambda)]^T\|_\infty \le 2,$$

it can be concluded for these concrete data that the algebraic model can only be used safely for pipelines up to 60 km length.

For the computation of the temperature

$$T(\boldsymbol{d}) = (T_{\text{in}} - T_w)e^{-\frac{k_w}{Dc_v\rho v}(x-x_0)} + T_w, \tag{3.68}$$

we apply Algorithm 3.2. Due to rounding errors in finite precision arithmetic, a

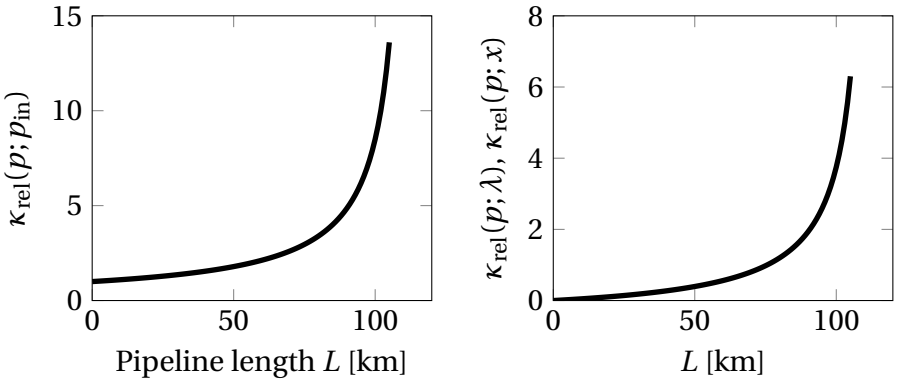

Figure 3.5: The individual relative condition numbers $\kappa_{\mathrm{rel}}(p;p_{\mathrm{in}}), \kappa_{\mathrm{rel}}(p;\lambda)$, $\kappa_{\mathrm{rel}}(p;x)$ in (3.65) considered as a function of the pipeline length $L = x - x_0$, with the nominal values in (3.67). The curve $\kappa_{\mathrm{rel}}(p;x)$ is behind the curve $\kappa_{\mathrm{rel}}(p;\lambda)$.

relative error ε is committed in every step of the algorithm. Using Taylor series expansion, we obtain

$$\begin{aligned}\tilde{T}(\boldsymbol{d}) = &\Big(T_{\mathrm{in}}\big(1+\varepsilon_{11}-T_w(\varepsilon_{11}-\varepsilon_{10})/T_{\mathrm{in}}\big)-T_w(1+\varepsilon_{10})\Big)e^{-\frac{k_w(1+\varepsilon_{12})}{Dc_v\rho v}(x-x_0)}\\ &+T_w(1+\varepsilon_{10}),\end{aligned}$$

where

$$|\varepsilon_{10}| \le \mathbf{u}, \tag{3.69a}$$

$$|\varepsilon_{11}| = |\varepsilon_1+\varepsilon_8+\varepsilon_9+\varepsilon_{10}+O(\varepsilon^2)| \le 4\mathbf{u}+O(\mathbf{u}^2), \tag{3.69b}$$

$$|\varepsilon_{12}| = |\varepsilon_2+\varepsilon_3+\varepsilon_4+\varepsilon_5+\varepsilon_6+\varepsilon_7+O(\varepsilon^2)| \le 6\mathbf{u}+O(\mathbf{u}^2). \tag{3.69c}$$

Algorithm 3.2 Computing the temperature T in (3.68)

Input: T_{in}, T_w, k_w, D, c_v, ρ, v, x, x_0

1: $z_1 \leftarrow T_{\mathrm{in}} - T_w$
2: $z_2 \leftarrow D \cdot c_v$
3: $z_3 \leftarrow z_2 \cdot \rho$
4: $z_4 \leftarrow z_3 \cdot v$
5: $z_5 \leftarrow k_w / z_4$
6: $z_6 \leftarrow x - x_0$
7: $z_7 \leftarrow z_5 \cdot z_6$
8: $z_8 \leftarrow e^{-z_7}$
9: $z_9 \leftarrow z_1 \cdot z_8$
10: $z_{10} \leftarrow z_9 + T_w$
11: $T(\boldsymbol{d}) \leftarrow z_{10}$

Output: T

Including data errors for the input parameters gives

$$\tilde{T}(\boldsymbol{d}) = \big(T_{\text{in}}(1+\varepsilon_{13}) - T_w(1+\varepsilon_{14})\big)e^{-\frac{k_w(1+\varepsilon_{15})}{Dc_v\rho v}\left(x(1+\varepsilon_x)-x_0(1+\varepsilon_{x_0})\right)} + T_w(1+\varepsilon_{14}),$$

with

$$\begin{aligned}
1+\varepsilon_{13} &= 1+\varepsilon_{T_{\text{in}}}+\varepsilon_{11}-T_w(\varepsilon_{11}-\varepsilon_{10})/T_{\text{in}}+O(\varepsilon^2),\\
1+\varepsilon_{14} &= (1+\varepsilon_{T_w})(1+\varepsilon_{10}) = 1+\varepsilon_{T_w}+\varepsilon_{10}+O(\varepsilon^2),\\
1+\varepsilon_{15} &= 1+\varepsilon_{k_w}+\varepsilon_{12}+\varepsilon_D+\varepsilon_{c_v}+\varepsilon_\rho+\varepsilon_v+O(\varepsilon^2).
\end{aligned}$$

This results in the backward error

$$\begin{aligned}
&\tilde{T}(T_{\text{in}}, T_w, k_w, x, x_0)\\
&\quad = T\big(T_{\text{in}}(1+\varepsilon_{13}), T_w(1+\varepsilon_{14}), k_w(1+\varepsilon_{15}), x(1+\varepsilon_x), x_0(1+\varepsilon_{x_0})\big).
\end{aligned} \tag{3.70}$$

The effect of rounding errors in the computation of the temperature, given by $\mathbf{u}$, $4\mathbf{u}$, $6\mathbf{u}$ in (3.69), can in general be neglected again as compared to the measurement errors. Thus, for the backward errors it holds that $\varepsilon_{13} \approx \varepsilon_{T_{\text{in}}}$, $\varepsilon_{14} \approx \varepsilon_{T_w}$, $\varepsilon_{15} \approx \varepsilon_{k_w} + \varepsilon_D + \varepsilon_{c_v} + \varepsilon_\rho + \varepsilon_v$. From (3.70) it follows that an upper bound for the relative error in the temperature $T(\boldsymbol{d})$ due to finite precision arithmetic and data errors is given by

$$\begin{aligned}
\frac{|\Delta T|}{T(\boldsymbol{d})} \le{}& \underbrace{\frac{T_{\text{in}}}{\left|T_{\text{in}} + \left(e^{\frac{k_w(x-x_0)}{Dc_v\rho v}} - 1\right)T_w\right|}}_{\kappa_{\text{rel}}(T;T_{\text{in}})}|\varepsilon_{13}| + \underbrace{\left|\frac{T_w - T_w e^{-\frac{k_w(x-x_0)}{Dc_v\rho v}}}{(T_{\text{in}}-T_w)e^{-\frac{k_w(x-x_0)}{Dc_v\rho v}} + T_w}\right|}_{\kappa_{\text{rel}}(T;T_w)}|\varepsilon_{14}|\\
&+ \underbrace{\left|\frac{(T_{\text{in}}-T_w)(x-x_0)k_w}{Dc_v\rho v\big(T_{\text{in}} + (e^{\frac{k_w(x-x_0)}{Dc_v\rho v}} - 1)T_w\big)}\right|}_{\kappa_{\text{rel}}(T;k_w)}|\varepsilon_{15}|\\
&+ \underbrace{\left|\frac{(T_{\text{in}}-T_w)k_w x}{Dc_v\rho v T(\boldsymbol{d})}\right|e^{-\frac{k_w(x-x_0)}{Dc_v\rho v}}}_{\kappa_{\text{rel}}(T;x)}|\varepsilon_x|\\
&+ \underbrace{\left|\frac{(T_{\text{in}}-T_w)k_w x_0}{Dc_v\rho v T(\boldsymbol{d})}\right|e^{-\frac{k_w(x-x_0)}{Dc_v\rho v}}}_{\kappa_{\text{rel}}(T;x_0)}|\varepsilon_{x_0}| + O\big((\Delta\boldsymbol{d})^2\big),
\end{aligned} \tag{3.71}$$

with $\Delta T = T(\boldsymbol{d}) - T(\boldsymbol{d}+\Delta\boldsymbol{d})$. To see whether the relative backward errors $|\varepsilon_{13}|$, $|\varepsilon_{14}|$, $|\varepsilon_{15}|$, $|\varepsilon_x|$, $|\varepsilon_{x_0}|$ are amplified in the relative error for the temperature, we consider e.g. the concrete nominal values

$$D_{\text{nom}} = 1\,\text{m}, \quad \rho_{\text{nom}} = 1\,\text{kg}\,\text{m}^{-3}, \quad v_{\text{nom}} = 10\,\text{m}\,\text{s}^{-1}, \quad T_{\text{in}_{\text{nom}}} = 293\,\text{K}, \tag{3.72a}$$

$$T_{w_{\text{nom}}} = 283\,\text{K}, \quad k_{w_{\text{nom}}} = 0.0341\,\text{W}\,\text{m}^{-1}\,\text{K}^{-1}, \tag{3.72b}$$

$$c_{v_{\text{nom}}} = 1700\,\text{J}\,\text{kg}^{-1}\,\text{K}^{-1}, \quad x_{0_{\text{nom}}} = 0\,\text{m}, \tag{3.72c}$$

in the individual relative condition numbers in (3.71). With $x_{0_{\text{nom}}} = 0$, then $\kappa_{\text{rel}}(T; x_0) = 0$. The four remaining relative condition numbers are depicted in Figure 3.6 as a function of the pipeline length $L = x - x_0$. The figure shows that all condition numbers remain below one, which means that the relative errors in the input parameters are not amplified. The relative condition numbers $\kappa_{\text{rel}}(T; k_w), \kappa_{\text{rel}}(T; x)$ are so small as compared to $\kappa_{\text{rel}}(T; T_{\text{in}}), \kappa_{\text{rel}}(T; T_w)$ that they can be neglected. Again, we note that the relative condition number $\kappa_{\text{rel}}(T; \boldsymbol{d})$ of T with respect to $\boldsymbol{d} = [T_{\text{in}}, T_w, k_w, x, x_0]^T$ is given by the sum of the four individual condition numbers.

Our backward error analysis and the computation of the associated condition numbers show that the values for the pressure are most affected by data and rounding errors and present restrictions to the pipeline length that can be safely considered. This theoretical analysis presents a first order worst case error analysis. From a practical point of view the worst case analysis is important to obtain warnings, but in view of the large uncertainty that the data will have a statistical analysis, which results in average perturbation estimates, seems more adequate. Such an analysis is performed in the next section.

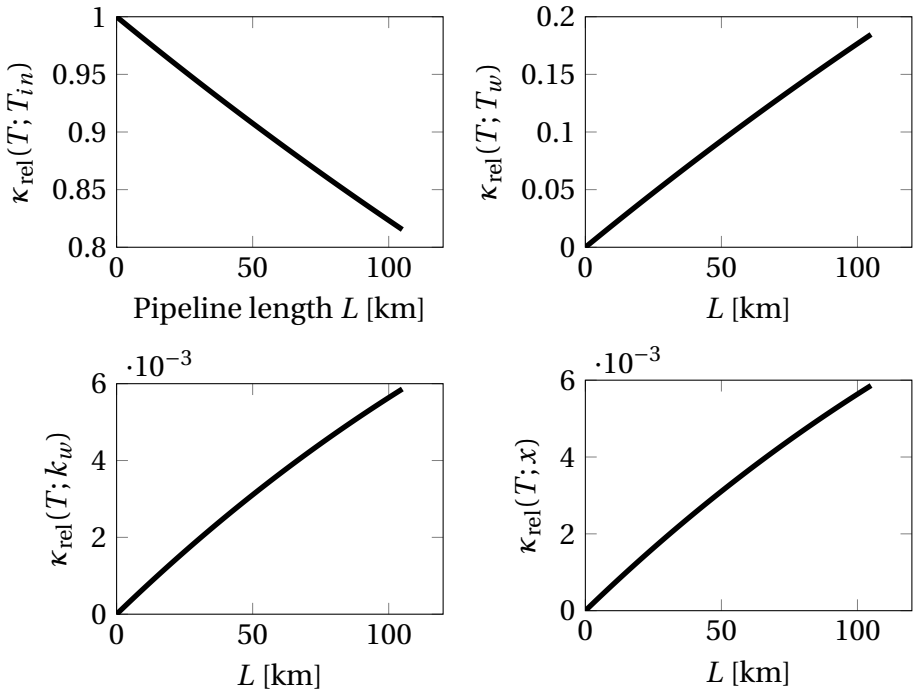

Figure 3.6: The individual relative condition numbers $\kappa_{\text{rel}}(T; T_{\text{in}})$, $\kappa_{\text{rel}}(T; T_w)$, $\kappa_{\text{rel}}(T; k_w)$, $\kappa_{\text{rel}}(T; x)$ in (3.71) considered as a function of the pipeline length $L = x - x_0$ for the concrete values in (3.72).

3.5.2 Statistical Perturbation Analysis

In this section we compute average perturbation amplification estimates for the algebraic model (3.10) using a statistical analysis. It complements the theoretical worst case analysis carried out in the previous section.

The efficient URQ method, see Section 3.3.2, enables us to calculate the relative standard deviation of the pressure p and the temperature T for many different pipeline lengths L. The mean of the remaining input parameters is set to the nominal values in (3.67), (3.72). The relative standard deviation σ_{d_i}/μ_{d_i} is set to 0.5 % for every input parameter d_i of $\boldsymbol{d}$. Subsequently, the mean perturbation amplification factors $\phi(p;\boldsymbol{d})$, $\phi(T;\boldsymbol{d})$, see (3.32), are computed as a function of L. The average perturbation amplification results of the URQ simulation for p and T are depicted in Figure 3.7. A similar behavior as in the worst case analysis in Section 3.5.1 is observed; the uncertainty in the pressure grows quickly for increasing pipeline length and the uncertainty in the temperature decreases slightly for increasing L. As expected, the average uncertainty amplification factors $\phi(p;\boldsymbol{d})$, $\phi(T;\boldsymbol{d})$ in Figure 3.7 are smaller than the first order upper bounds $\kappa_{\text{rel}}(p;\boldsymbol{d})$, $\kappa_{\text{rel}}(T;\boldsymbol{d})$, which are obtained by taking the sum of the individual condition numbers in Figures 3.5 and 3.6, see (3.12). The mass flux $\hat{q}$ is not considered here, because it is constant with respect to L.

Concluding, the backward errors due to rounding and data uncertainty have been presented in the previous section. Multiplying these backward errors with the condition numbers from Section 3.5.1 results in first order worst case error bounds. On the other hand, multiplying the backward errors with the average amplification factors given in this section, yields mean error estimates. The worst case bounds and the mean estimates together provide a useful description of the error in the pressure and the temperature due to rounding and data uncertainty.

Having performed the analysis for the algebraic model including temperature and having observed that the temperature dependence is rather

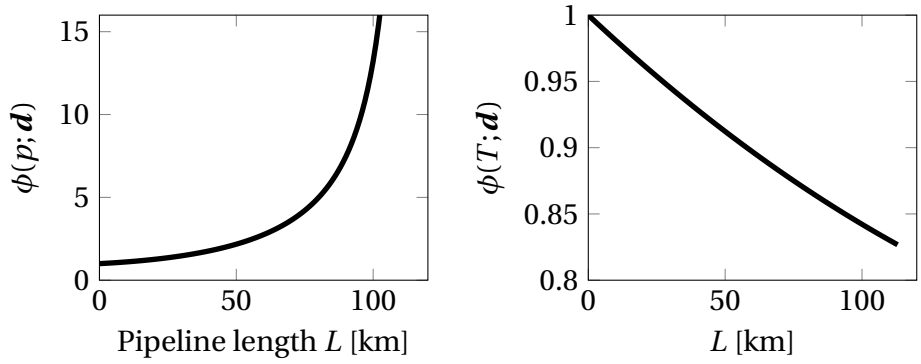

Figure 3.7: The mean uncertainty amplification factors ϕ, see (3.32), for the pressure p (left) and the temperature T (right) as a function of the pipeline length L, computed with the URQ method. The relative standard deviation of the input parameters is set to 0.5 % with mean values in (3.67), (3.72).

insensitive, we can also extend the simplification of the algebraic model to the isothermal version by assuming the temperature T to be constant. The error inflicted by this simplification is analyzed in the following section.

3.5.3 Error between Temperature Dependent and Isothermal Algebraic Model

In this section we analyze the error that is committed when the temperature dependent algebraic model in (3.10) is simplified to the isothermal algebraic model in (3.10a), (3.10b), see the lower level of the model hierarchy in Figure 3.2.

Suppose that the temperature in the algebraic model is set constant and that the value $T(\boldsymbol{d})$, for certain parameter values $\boldsymbol{d}$, is taken for this constant temperature, whereas the actual parameter values are given by $\tilde{\boldsymbol{d}}$. Then, using Taylor series expansion and the triangle inequality, a first order upper bound for the relative error in T is given by

$$\frac{|T(\boldsymbol{d}) - T(\tilde{\boldsymbol{d}})|}{|T(\boldsymbol{d})|} \dot{\leq} \sum_{i=1}^{n} \left| \frac{\partial T(\boldsymbol{d})}{\partial d_i} \frac{d_i}{T(\boldsymbol{d})} \right| \frac{|d_i - \tilde{d}_i|}{|d_i|}.$$

Inserting the nominal values $\boldsymbol{d}_{\text{nom}}$ in (3.72) together with $x_{\text{nom}} = 70\,\text{km}$, the individual relative condition numbers for T with respect to the parameter vector $\boldsymbol{d}$ are given by

$$\begin{aligned}
&\left| \frac{\partial T(\boldsymbol{d})}{\partial \rho} \frac{\rho}{T(\boldsymbol{d})} \right| = \left| \frac{\partial T(\boldsymbol{d})}{\partial \nu} \frac{\nu}{T(\boldsymbol{d})} \right| = \left| \frac{\partial T(\boldsymbol{d})}{\partial D} \frac{D}{T(\boldsymbol{d})} \right| = \left| \frac{\partial T(\boldsymbol{d})}{\partial x} \frac{x}{T(\boldsymbol{d})} \right| \\
&= \left| \frac{\partial T(\boldsymbol{d})}{\partial k_w} \frac{k_w}{T(\boldsymbol{d})} \right| = \left| \frac{\partial T(\boldsymbol{d})}{\partial c_\nu} \frac{c_\nu}{T(\boldsymbol{d})} \right| = 4.18 \cdot 10^{-3}, \\
&\left| \frac{\partial T(\boldsymbol{d})}{\partial x_0} \frac{x_0}{T(\boldsymbol{d})} \right| = 0, \quad \left| \frac{\partial T(\boldsymbol{d})}{\partial T_{\text{in}}} \frac{T_{\text{in}}}{T(\boldsymbol{d})} \right| = 8.73 \cdot 10^{-1}, \\
&\left| \frac{\partial T(\boldsymbol{d})}{\partial T_w} \frac{T_w}{T(\boldsymbol{d})} \right| = 1.27 \cdot 10^{-1}.
\end{aligned}$$

It follows that only perturbations in the parameter T_{in} create an equivalent relative perturbation in the temperature T. Perturbations in the other input parameters only cause a small relative error in T. This means that if the input temperature T_{in} is not subject to change, then the temperature can safely be set constant. If, however, the input temperature changes, for example for different pipelines, then the temperature cannot be set constant and the temperature dependent algebraic model should be chosen.

3.6 Summary of Chapter 3

This chapter presents an error and perturbation analysis for the Euler equations in semilinear and algebraic form. The main focus is on the effect of

rounding and data uncertainty errors on the solution of these two models. However, also the modeling error that is committed in the different simplifications, the discretization error for the semilinear model, and the iteration error due to a preliminary stopping of the Newton method are analyzed.

The partial differential equations of the semilinear model are discretized by applying two simple schemes which are used in natural gas network optimization problems. It is shown that the normwise relative condition number of the resulting nonlinear systems leads to a considerable overestimation of the sensitivity of the problems. The novel componentwise relative condition number constitutes a more accurate measure for the sensitivity. Furthermore, it is shown that the mass flow rate has higher condition numbers with respect to the uncertain parameters than the pressure and we can determine stepsizes for which well-conditioned problems are obtained. Moreover, it is shown that the rounding and iteration errors can be neglected compared to the data uncertainty error and we find that the modeling error between the semilinear and the algebraic model is approximately 1 % for certain concrete parameter values.

The error analysis for the pressure in the algebraic model results in a rounding and data uncertainty error that grows quickly with increasing pipeline length, such that the algebraic model can only be used safely for short pipelines (for certain parameter values up to 60 km length). The error in the temperature decreases slightly with increasing pipeline length. These results are obtained both via a deterministic first order worst case and via a statistical mean perturbation analysis. Finally, it is shown that only if the pipeline input temperature is not subject to change, then the temperature can safely be set constant and the isothermal algebraic model can be used.

In Chapters 5 and 6, we implement the derived error estimators into several error controllers, which allow to adaptively switch between different simulation models and discretization grids within the gas pipeline network in order to achieve a prescribed accuracy while keeping the computational cost low.

Chapter 4

Sensitivity Analysis using Three Transient Models: A Case Study for a Y-Shaped Network

4.1 Introduction

In this chapter, we apply our approach to perform a componentwise sensitivity analysis, as described in Section 3.3.1. To obtain concrete values, we use an exemplary Y-shaped gas network. For this network, besides the equations describing the gas flow through the pipes, we also need appropriate coupling conditions in the junction. Since the coupling conditions also hold in additional junctions, the analysis can easily be extended to larger pipe networks. We analyze the sensitivity of the network state, i.e., the mass flow rate, the pressure, and, if applicable, the temperature distribution along the network, with respect to changes or perturbations in the boundary conditions. In Sections 4.2, 4.3, and 4.4, three different transient models are used to describe the gas flow through the pipes. All models are discretized both in space and in time, where the temporal discretization is implicit. For every model, this yields a nonlinear system of equations for every time integration step. The sensitivity of the three nonlinear systems is analyzed using the componentwise relative condition number in (3.29). Furthermore, the results for the three different models are compared with each other.

4.2 The Isothermal Euler Equations with Constant Compressibility Factor

4.2.1 The Model

The boundaries of a gas pipeline network consist of entry and exit nodes. At entries the gas is inserted into the network and at exits it is ejected. Usually,

the boundary conditions vary in time. We examine the influence of changing boundary conditions on the gas flow in the pipeline network.

As an example, we consider the small Y-shaped network with one entry and two exits depicted in Figure 4.1. As boundary conditions, the pressure of the gas is prescribed at the entry and the mass flow rate is given at the two exits. Our goal is to determine the sensitivity of the pressure and mass flow rate distribution in the network w.r.t. perturbations in the boundary conditions.

The gas flow through the pipe network is modeled by the system of PDEs with boundary and initial conditions

$$\begin{aligned}
&\frac{\partial p_j}{\partial t} + \frac{c^2}{A}\frac{\partial q_j}{\partial x} = 0, \\
&\frac{\partial q_j}{\partial t} + A\frac{\partial p_j}{\partial x} = -\frac{\lambda c^2}{2DA}\frac{q_j|q_j|}{p_j}, \qquad \text{in } (0,L_j)\times(0,t_f], \\
&\begin{bmatrix} p_1(0,t) \\ q_2(L_2,t) \\ q_3(L_3,t) \end{bmatrix} = \begin{bmatrix} p_{\mathrm{En}}(t) \\ q_{\mathrm{Ex1}}(t) \\ q_{\mathrm{Ex2}}(t) \end{bmatrix}, \qquad \begin{bmatrix} q_j(x,0) \\ p_j(x,0) \end{bmatrix} = \begin{bmatrix} q_j^0(x) \\ p_j^0(x) \end{bmatrix},
\end{aligned} \tag{4.1}$$

for the three pipes $j = 1,2,3$. This system has been derived from the isothermal Euler equations of fluid dynamics in [93] and in section 3.2.1. In the inner node the first Kirchhof law

$$q_1(L_1,t) = q_2(0,t) + q_3(0,t), \quad \text{for all } t \in (0,t_f], \tag{4.2}$$

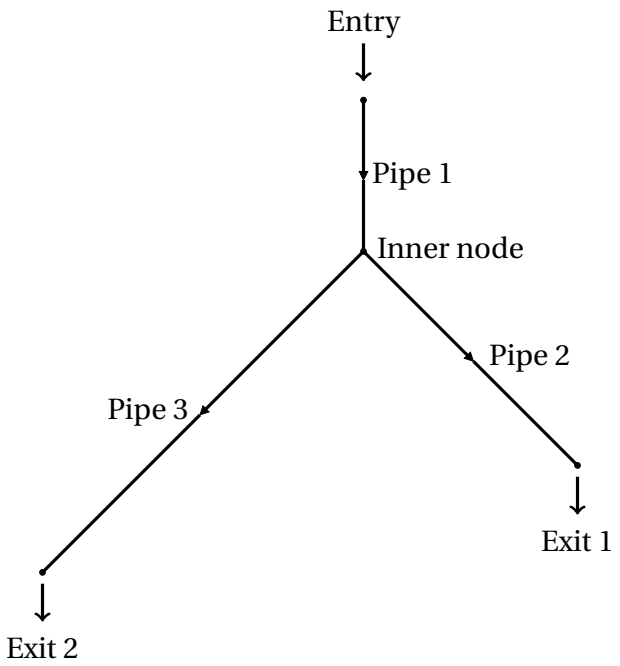

Figure 4.1: Small gas network with one entry and two exit nodes. Pipe 1 is 10 km, Pipe 2 is 20 km and Pipe 3 is 30 km long.

and the pressure equality

$$p_1(L_1,t) = p_2(0,t) = p_3(0,t), \quad \text{for all } t \in (0,t_f], \tag{4.3}$$

hold, which are in the following referred to as the *coupling conditions*. To discretize system (4.1) in space, we apply a first order finite difference scheme, which results in the system of ODEs with boundary and initial conditions

$$\begin{aligned}
&\frac{dp_j(x_{i+1},t)}{dt} + \frac{c^2}{A}\frac{q_j(x_{i+1},t) - q_j(x_i,t)}{h} = 0,\\
&\frac{dq_j(x_i,t)}{dt} + A\frac{p_j(x_{i+1},t) - p_j(x_i,t)}{h} = -\frac{\lambda c^2}{2DA}\frac{q_j(x_i,t)|q_j(x_i,t)|}{p_j(x_{i+1},t)},\\
&\begin{bmatrix} p_1(x_0,t)\\ q_2(x_N,t)\\ q_3(x_N,t)\end{bmatrix} = \begin{bmatrix} p_{\mathrm{En}}(t)\\ q_{\mathrm{Ex1}}(t)\\ q_{\mathrm{Ex2}}(t)\end{bmatrix}, \quad \begin{bmatrix} q_j(x_i,0)\\ p_j(x_{i+1},0)\end{bmatrix} = \begin{bmatrix} q_j^0(x_i)\\ p_j^0(x_{i+1})\end{bmatrix},
\end{aligned} \tag{4.4}$$

for pipes $j = 1,2,3$, time $t \in (0,t_f]$, equidistant spatial gridpoints $x_i = ih$, $i = 0,1,\ldots,N_j$, and the number of spatial intervals $N_j = L_j/h$. The ODEs in (4.4) are equivalent to system (3.34). We now consider the temporal discretization of system (4.4). Let the temporal gridpoints be denoted by t_k, $k = 0,1,\ldots,M$, with uniform stepsize $\tau = t_f/M$. Furthermore, we define $q_{j,i}^k := q_j(x_i,t_k)$ and $p_{j,i}^k := p_j(x_i,t_k)$. There are several possibilities to discretise system (4.4) in time. Implicit temporal discretization schemes are frequently used because of their favourable stability properties. After implicitly discretizing system (4.4) in time, a nonlinear system of equations has to be solved in every time integration step.

4.2.2 Sensitivity Analysis

In this section the sensitivity of the gas flow in the network with respect to changes in the boundary conditions is determined.

Using the implicit Euler method to discretize system (4.4) in time results in the nonlinear systems of equations $F^k = 0$, $k = 1,\ldots,M$, where $F^k = [F_1^k,\ldots,F_{3+2\sum_{\ell=1}^3 N_\ell}^k]^T$ is given by

$$F_{i+\sum_{\ell=1}^{j-1}N_\ell}^k = \frac{p_{j,i}^k - p_{j,i}^{k-1}}{\tau} + \frac{c^2}{A}\frac{q_{j,i}^k - q_{j,i-1}^k}{h}, \tag{4.5a}$$

$$F_{i+\sum_{\ell=1}^{j-1}N_\ell+\sum_{\ell=1}^{3}N_\ell}^k = \frac{q_{j,i-1}^k - q_{j,i-1}^{k-1}}{\tau} + A\frac{p_{j,i}^k - p_{j,i-1}^k}{h} + \frac{\lambda c^2 q_{j,i-1}^k|q_{j,i-1}^k|}{2DAp_{j,i}^k}, \tag{4.5b}$$

$$F_{1+2\sum_{\ell=1}^3 N_\ell}^k = q_{1,N_1}^k - q_{2,0}^k - q_{3,0}^k, \tag{4.5c}$$

$$F_{2+2\sum_{\ell=1}^3 N_\ell}^k = p_{1,N_1}^k - p_{2,0}^k, \tag{4.5d}$$

$$F_{3+2\sum_{\ell=1}^3 N_\ell}^k = p_{1,N_1}^k - p_{3,0}^k, \tag{4.5e}$$

for $j = 1,2,3$ and $i = 1,\dots,N_j$. Equations (4.5c)–(4.5e) are the discrete versions of the coupling conditions (4.2) and (4.3). As an example, we consider the first time integration step and we set $F := F^1$. In [93, p. 9] the first order approximation

$$D_{u^1}^{-1}\Delta u^1 \doteq -D_{u^1}^{-1}\left(F'_{u^1}\right)^{-1} F'_d\, d\Delta d/d, \quad \text{with} \quad u^1 := \begin{bmatrix} q^1 \\ p^1 \end{bmatrix}, \tag{4.6}$$

for the componentwise relative perturbation in the state variables u^1 w.r.t. datum $d \in \mathbb{R}$ is derived. Here, matrix D_z is a diagonal matrix with z on the diagonal, $\Delta z := z - \tilde{z}$, $\doteq$ denotes a first order approximation in Δu^1 and Δd, F'_z is the Jacobian matrix of F w.r.t. z,

$$\begin{aligned} q^1 &:= [q^1_{1,0},\dots,q^1_{1,N_1},q^1_{2,0},\dots,q^1_{2,N_2-1},q^1_{3,0},\dots,q^1_{3,N_3-1}]^T \quad \text{and} \\ p^1 &:= [p^1_{1,1},\dots,p^1_{1,N_1},p^1_{2,0},\dots,p^1_{2,N_2},p^1_{3,0},\dots,p^1_{3,N_3}]^T. \end{aligned} \tag{4.7}$$

We define $|x| := [\,|x_1|,\dots,|x_n|\,]^T$ to be the *componentwise absolute value* of the vector $x \in \mathbb{R}^n$ and

$$k(u^1;d) := |D_{u^1}^{-1}\left(F'_{u^1}\right)^{-1} F'_d\, d| \tag{4.8}$$

to be the *componentwise relative amplification vector* for the perturbation in u^1 w.r.t. a perturbation in d. Then, taking the componentwise absolute value in (4.6) yields

$$|D_{u^1}^{-1}\Delta u^1| \doteq k(u^1;d)\,|\Delta d/d|. \tag{4.9}$$

Dividing amplification vector $k(u^1;d)$ into

$$\begin{aligned} k(q^1;d) &:= [k(u^1;d)]_{1:1+\sum_{\ell=1}^3 N_\ell}, \\ k(p^1;d) &:= [k(u^1;d)]_{2+\sum_{\ell=1}^3 N_\ell:3+2\sum_{\ell=1}^3 N_\ell}, \end{aligned} \tag{4.10}$$

where $z_{1:n}$ denotes the first n components of vector z, approximation (4.9) can be rewritten as

$$\begin{aligned} |D_{q^1}^{-1}\Delta q^1| &\doteq k(q^1;d)\,|\Delta d/d|, \\ |D_{p^1}^{-1}\Delta p^1| &\doteq k(p^1;d)\,|\Delta d/d|. \end{aligned}$$

Taking the infinity-norm gives

$$\begin{aligned} \|D_{q^1}^{-1}\Delta q^1\|_\infty &\doteq \kappa(q^1;d)\,|\Delta d/d|, \\ \|D_{p^1}^{-1}\Delta p^1\|_\infty &\doteq \kappa(p^1;d)\,|\Delta d/d|, \end{aligned}$$

with the *componentwise relative condition numbers* given by $\kappa(q^1;d) = \|k(q^1;d)\|_\infty$ and $\kappa(p^1;d) = \|k(p^1;d)\|_\infty$. In summary, we obtain the condition numbers of q^1 and p^1 w.r.t. d given by

$$\begin{aligned} \kappa(q^1;d) &= \left\| \left[D_{u^1}^{-1}(F'_{u^1})^{-1}F'_d\, d\right]_{1:1+\sum_{\ell=1}^3 N_\ell} \right\|_\infty, \\ \kappa(p^1;d) &= \left\| \left[D_{u^1}^{-1}(F'_{u^1})^{-1}F'_d\, d\right]_{2+\sum_{\ell=1}^3 N_\ell:3+2\sum_{\ell=1}^3 N_\ell} \right\|_\infty, \end{aligned} \tag{4.11}$$

respectively, cf. [93, Eq. (28)]. We examine the influence of changing boundary conditions on the solution. In nonlinear system (4.5), with $k = 1$, the boundary values are given by $p^1_{\mathrm{En}} = p^1_{1,0}$, $q^1_{\mathrm{Ex1}} = q^1_{2,N_2}$ and $q^1_{\mathrm{Ex2}} = q^1_{3,N_3}$. Thus, we consecutively insert $d = p^1_{\mathrm{En}}$, $d = q^1_{\mathrm{Ex1}}$ and $d = q^1_{\mathrm{Ex2}}$ into the condition numbers (4.11). We choose, e.g., the concrete parameter values

$$\begin{aligned} &D = 0.8\,\mathrm{m}, \quad A = 0.503\,\mathrm{m}^2, \quad \lambda = 0.06, \quad c = 372\,\mathrm{m\,s^{-1}}, \quad h = 500\,\mathrm{m}, \\ &\tau = 15\,\mathrm{s}, \quad L_1 = 10\,\mathrm{km}, \quad L_2 = 20\,\mathrm{km}, \quad L_3 = 30\,\mathrm{km}, \quad p^1_{\mathrm{En}} = 60\,\mathrm{bar}, \\ &q^1_{\mathrm{Ex1}} = q^1_{\mathrm{Ex2}} = 150\,\mathrm{kg\,s^{-1}}, \quad q^0_1 = \mathbb{1} \cdot 300\,\mathrm{kg\,s^{-1}}, \\ &q^0_2 = q^0_3 = \mathbb{1} \cdot 150\,\mathrm{kg\,s^{-1}}, \quad p^0_1 = p^0_2 = p^0_3 = \mathbb{1} \cdot 60\,\mathrm{bar}, \end{aligned} \tag{4.12}$$

where $z^0_1 := [z^0_{1,0}, z^0_{1,1}, \ldots, z^0_{1,N}]^T$ and $\mathbb{1}$ is the one vector of appropriate length. The Newton method, see, e.g., [63], is used to find an approximate solution of the nonlinear system (4.5). The results of the sensitivity analysis are contained in section 4.2.3.

4.2.3 Results

Inserting the concrete parameter values (4.12) into the componentwise relative condition numbers (4.11) for the Y-shaped network in Figure 4.1 results in the values given in Table 4.1. We observe that all condition numbers are smaller than one except for $\kappa(q^1; p^1_{\mathrm{En}})$. Therefore, we depict the componentwise relative amplification vectors $k(q^1; p^1_{\mathrm{En}})$ and $k(p^1; p^1_{\mathrm{En}})$, given in (4.10), in Figure 4.2. Here, we observe both that a perturbation in p^1_{En} has the largest effect on $q^1_{1,0}$ and that the amplification vectors decrease along the pipe network.

As a comparison, in [93] the PDEs (4.1) are reduced to a purely algebraic model using simplifying assumptions. Here, it is obtained that the condition number $\kappa(p; p_{\mathrm{En}})$ increases significantly w.r.t. x, see [93, Figure 5, left]. Hence, the pressure distribution in system (4.5) is much less sensitive to perturbations in the boundary value p_{En} and thus has better numerical stability properties than the pressure distribution in the algebraic model.

We conclude that changes in the boundary value p^1_{En} have a large influence on the mass flow rate q^1_1 in Pipe 1 and a small influence on q^1_2, q^1_3 and p^1, whereas perturbations in the boundary values q^1_{Ex1} and q^1_{Ex2} have a small influence on both q^1 and p^1 along the entire Y-shaped network.

Table 4.1: The condition numbers (4.11) into which the concrete parameter values (4.12) are inserted.

d	$\kappa(q^1; d)$	$\kappa(p^1; d)$
p^1_{En}	34.0	0.809
q^1_{Ex1}	0.889	0.0451
q^1_{Ex2}	0.889	0.0451

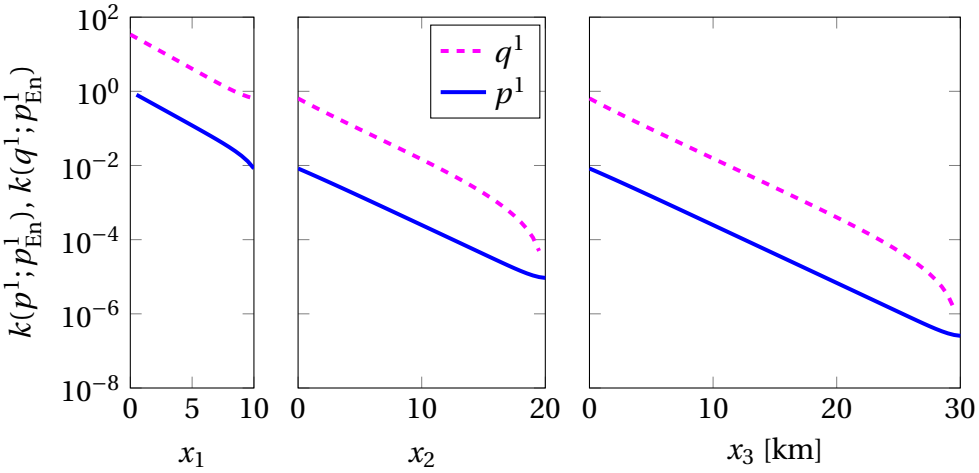

Figure 4.2: The componentwise relative amplification vectors $k(q^1;p^1_{\mathrm{En}})$ and $k(p^1;p^1_{\mathrm{En}})$ in (4.10) for system (4.5) and the small pipe network in Figure 4.1. Here, q^1 and p^1 are defined in (4.7) and x_1, x_2 and x_3 correspond to pipes 1, 2 and 3, respectively.

4.3 The Isothermal Euler Equations with Variable Compressibility Factor

4.3.1 The Model

In this chapter, the temperature $T = \bar{T}$ is again assumed to be constant. Using the mass flow rate $q = A\rho v$, keeping the friction coefficient $\lambda = \lambda(|q|)$ variable and inserting the state equation for real gases $\rho = p/(R\bar{T}z(p))$, where the compressibility factor $z(p)$ is given in (3.4), the isothermal Euler equations (3.1a), (3.1b) can be rewritten in the form

$$\begin{aligned} &\frac{\partial}{\partial t}\left(\frac{p}{R\bar{T}z(p)}\right)+\frac{1}{A}\frac{\partial q}{\partial x}=0,\\ &\frac{1}{A}\frac{\partial q}{\partial t}+\frac{\partial p}{\partial x}+\frac{1}{A^2}\frac{\partial}{\partial x}\left(\frac{q^2}{\rho}\right)=-\frac{gh'}{R\bar{T}}\frac{p}{z(p)}-\frac{R\bar{T}}{2DA^2}\frac{z(p)q|q|\lambda(|q|)}{p}. \end{aligned} \tag{4.13}$$

Here, the friction factor $\lambda(|q|)$ is implicitly given by the Prandtl-Colebrook law, see, e.g., [35],

$$\frac{1}{\sqrt{\lambda}}=-2\log_{10}\left(\frac{2.51}{\mathrm{Re}\sqrt{\lambda}}+\frac{k}{3.71D}\right)$$

with the roughness k of the pipe and the Reynolds number $\mathrm{Re} = D\rho|v|/\eta = D|q|/(A\eta)$, where η is the dynamic viscosity of the gas. We use a close approximation of the Prandtl-Colebrook law given in [26]

$$\frac{1}{\sqrt{\lambda}}=-2\log_{10}\left(\frac{k}{3.7065D}-\frac{5.0425}{\mathrm{Re}}\log_{10}\left[\frac{(k/D)^{1.1098}}{2.8257}+\frac{5.8506}{\mathrm{Re}^{0.8981}}\right]\right), \tag{4.14}$$

which is an explicit formula for the friction factor. Eliminating the density ρ and introducing $P = p/z(p)$ and the constant $C = R\bar{T}/A$, system (4.13) can be written shortly as

$$\begin{aligned} \frac{\partial P}{\partial t} + C\frac{\partial q}{\partial x} &= 0, \\ \frac{\partial q}{\partial t} + A\frac{\partial p}{\partial x} + C\frac{\partial}{\partial x}\left(\frac{q^2}{P}\right) &= -\frac{gh'}{C}P - \frac{C}{2D}\frac{q|q|\lambda(|q|)}{P}. \end{aligned} \tag{4.15}$$

In order to be able to choose a suitable discretization scheme, it is important to study the flow characteristics of the gas. In [35] it is derived that the characteristic curves of system (4.15) are given by $\frac{dx}{dt} = v \pm c$, with speed of sound c. Since in practical gas flow applications it holds that $|v| \ll c$, the characteristics do not change sign, i.e., there is always one negative and one positive characteristic. For this type of systems, box schemes, which are introduced in [99], have been shown to be effective discretization schemes. In this chapter we use the implicit box scheme, which is conservative and stable under mild conditions [35]. For the scalar balance law

$$\frac{\partial u}{\partial t} + \frac{\partial f(u)}{\partial x} = g(u),$$

with initial conditions $u(x,0) = u_0(x)$, this box scheme is given by

$$\frac{u_{i-1}^k + u_i^k}{2} = \frac{u_{i-1}^{k-1} + u_i^{k-1}}{2} - \frac{\Delta t}{\Delta x}(f_i^k - f_{i-1}^k) + \Delta t\frac{g_{i-1}^k + g_i^k}{2}. \tag{4.16}$$

The main properties and advantages of the implicit box scheme have been described in [66].

4.3.2 Sensitivity Analysis

We again consider the Y-shaped network in Figure 4.1. The gas flow within this network is now modeled using the PDE system (4.15) with coupling conditions (4.2) and (4.3). We use the notation introduced in Section 4.2.1 and discretise the PDE system in space and time using the implicit box scheme. This results in the nonlinear systems of equations $F^k = 0$, $k = 1, \dots, M$, where F^k is given by

$$F^k_{i+\sum_{\ell=1}^{j-1} N_\ell} = \frac{P_{j,i-1}^k + P_{j,i}^k}{2\tau} - \frac{P_{j,i-1}^{k-1} + P_{j,i}^{k-1}}{2\tau} + C\frac{q_{j,i}^k - q_{j,i-1}^k}{h}, \tag{4.17a}$$

$$\begin{aligned} F^k_{i+\sum_{\ell=1}^{j-1} N_\ell + \sum_{\ell=1}^{3} N_\ell} = {} & \frac{q_{j,i-1}^k + q_{j,i}^k}{2\tau} - \frac{q_{j,i-1}^{k-1} + q_{j,i}^{k-1}}{2\tau} + A\frac{p_{j,i}^k - p_{j,i-1}^k}{h} \\ & + \frac{C}{h}\left(\frac{(q_{j,i}^k)^2}{P_{j,i}^k} - \frac{(q_{j,i-1}^k)^2}{P_{j,i-1}^k}\right) + \frac{gh'}{C}\frac{P_{j,i-1}^k + P_{j,i}^k}{2} \\ & + \frac{C}{4D}\left(\frac{q_{j,i-1}^k|q_{j,i-1}^k|\lambda(|q_{j,i-1}^k|)}{P_{j,i-1}^k} + \frac{q_{j,i}^k|q_{j,i}^k|\lambda(|q_{j,i}^k|)}{P_{j,i}^k}\right), \end{aligned} \tag{4.17b}$$

$$F^k_{1+2\sum_{\ell=1}^3 N_\ell} = q^k_{1,N_1} - q^k_{2,0} - q^k_{3,0}, \tag{4.17c}$$

$$F^k_{2+2\sum_{\ell=1}^3 N_\ell} = p^k_{1,N_1} - p^k_{2,0}, \tag{4.17d}$$

$$F^k_{3+2\sum_{\ell=1}^3 N_\ell} = p^k_{1,N_1} - p^k_{3,0}, \tag{4.17e}$$

for $j = 1,2,3$ and $i = 1,\dots,N_j$, with N_j the number of spatial intervals of pipe j. Moreover, the initial conditions p^0, q^0 and boundary conditions $p^k_{1,0}, q^k_{2,N_2}, q^k_{3,N_3}$ have to be prescribed. In (4.17b), $\lambda(|q^k_{j,i}|)$ is given in (4.14). We perform the same sensitivity analysis as in Section 4.2.2 for system (4.17). We choose, e.g., the concrete parameter values

$$\begin{aligned}
&D = 0.8\,\mathrm{m}, \quad c = 372\,\mathrm{m\,s^{-1}}, \quad k = 0.12\,\mathrm{mm}, \quad \eta = 10^{-5}\,\mathrm{Pa\,s}, \quad \bar{T} = 288\,\mathrm{K},\\
&R = 518\,\mathrm{m^2\,s^{-2}\,K^{-1}}, \quad p_c = 46.4\,\mathrm{bar}, \quad T_c = 191\,\mathrm{K}, \quad h' = 0.05, \quad g = 9.81\,\mathrm{m\,s^{-2}},\\
&h = 500\,\mathrm{m}, \quad \tau = 7.5\,\mathrm{s}, \quad L_1 = 10\,\mathrm{km}, \quad L_2 = 20\,\mathrm{km}, \quad L_3 = 30\,\mathrm{km},\\
&p^1_{\mathrm{En}} = 60\,\mathrm{bar}, \quad q^1_{\mathrm{Ex1}} = q^1_{\mathrm{Ex2}} = 150\,\mathrm{kg\,s^{-1}}, \quad q^0_1 = \mathbb{1}\cdot 300\,\mathrm{kg\,s^{-1}},\\
&q^0_2 = q^0_3 = \mathbb{1}\cdot 150\,\mathrm{kg\,s^{-1}}, \quad p^0_1 = p^0_2 = p^0_3 = \mathbb{1}\cdot 60\,\mathrm{bar}
\end{aligned} \tag{4.18}$$

and again use the Newton method to find an approximate solution of the nonlinear system (4.17). Parameter values (4.18) are inserted in the componentwise relative condition numbers (4.11) with F given in (4.17).

4.3.3 Results

The results are given in Table 4.2. We observe that the values are similar to the ones in Table 4.1. Again, only $\kappa(q^1; p^1_{\mathrm{En}})$ is larger than one. The componentwise relative amplification vectors $k(q^1; p^1_{\mathrm{En}})$ and $k(p^1; p^1_{\mathrm{En}})$ in (4.10) are depicted in Figure 4.3. Again, we observe that a perturbation in the pressure at the entry has the largest effect on the mass flow rate at the entry. This means that if one is interested in the mass flow rate in Pipe 1, then the pressure at the entry should be determined accurately. However, if the mass flow rate in Pipe 1 is of lower interest, then a larger uncertainty in the input pressure can be permitted.

Table 4.2: The condition numbers (4.11), where F is given by (4.17), into which the concrete parameter values (4.18) are inserted.

d	$\kappa(q^1; d)$	$\kappa(p^1; d)$
p^1_{En}	38.7	0.780
q^1_{Ex1}	0.903	0.0208
q^1_{Ex2}	0.903	0.0208

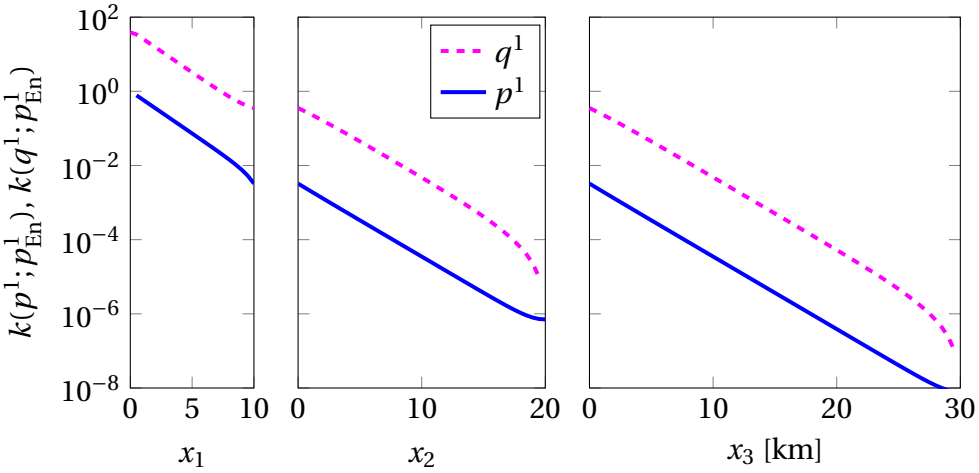

Figure 4.3: The componentwise relative amplification vectors $k(q^1; p^1_{\mathrm{En}})$ and $k(p^1; p^1_{\mathrm{En}})$ in (4.10) for system (4.17) and the small pipe network in Figure 4.1. Here, q^1 and p^1 are defined in (4.7) and x_1, x_2 and x_3 correspond to pipes 1, 2 and 3, respectively.

4.4 The Temperature Dependent Euler Equations

4.4.1 The Model

With mass flow rate $q = A\rho v$ and energy $E = \rho(\frac{1}{2}v^2 + e)$, the full Euler equations (3.1)–(3.3) may be rewritten into the form $u_t + f(u)_x = g(u)$, given by

$$\begin{pmatrix} \rho \\ q \\ E \end{pmatrix}_t + \begin{pmatrix} \frac{q}{A} \\ Ap + \frac{q^2}{A\rho} \\ \frac{q}{A\rho}(E+p) \end{pmatrix}_x = \begin{pmatrix} 0 \\ -\frac{\lambda}{2D\rho A} q|q| - Ag\rho h' \\ -\frac{k_w}{D}(T - T_w) \end{pmatrix}, \tag{4.19}$$

together with the algebraic equations

$$E = \frac{q^2}{2A^2\rho} + c_v \rho T + \rho g h, \tag{4.20a}$$

$$p = RT\rho\big(1 + 0.257\frac{p}{p_c} - 0.533\frac{pT_c}{p_c T}\big). \tag{4.20b}$$

4.4.2 Sensitivity Analysis

We again consider the Y-shaped network in Figure 4.1. As boundary conditions the pressure $p_1(0,t)$ and the temperature $T_1(0,t)$ are prescribed at the entry and the mass flow rates $q_2(L_2,t), q_3(L_3,t)$ are prescribed at the two exits. The coupling conditions are given by (4.2), (4.3) together with the temperature at the inner node, cf. [64, Eq. (2.10)],

$$T_1(L_1,t) = T_2(0,t) = T_3(0,t), \quad \text{for all } t \in (0, t_f].$$

For the initial conditions, we use the solution of the temperature-dependent algebraic model, i.e.,

$$
\begin{aligned}
&q_1(x,0) = q_2(L_2,0) + q_3(L_3,0), \quad q_2(x,0) = q_2(L_2,0), \quad q_3(x,0) = q_3(L_3,0),\\
&p_j(x,0) = \sqrt{p_j(0,0)^2 - \frac{\lambda_j(x,0)c^2 x}{A^2 D} q|q|},\\
&T_j(x,0) = (T_j(0,0) - T_w)e^{-\frac{k_w A}{Dc_v q}x} + T_w,\\
&\rho_j(x,0) = p_j(x,0)/\Big(RT_j(x,0)\big(1 + 0.257\frac{p_j(x,0)}{p_c} - 0.533\frac{p_j(x,0)T_c}{p_c T_j(x,0)}\big)\Big),\\
&E_j(x,0) = \frac{q_j^2(x,0)}{2A^2\rho_j(x,0)} + c_v\rho_j(x,0)T_j(x,0) + \rho_j(x,0)gh,
\end{aligned}
$$

where $\lambda_j(x,0)$ is given in (4.14). Applying the implicit box scheme, see (4.16), to system (4.19)–(4.20) results in the nonlinear system of equations $F^k = 0$, $k = 1,\dots,M$, where F^k is given by

$$
F^k_{i+\sum_{\ell=1}^{j-1} N_\ell} = \frac{1}{2\tau}(\rho^k_{j,i-1} + \rho^k_{j,i} - \rho^{k-1}_{j,i-1} - \rho^{k-1}_{j,i}) + \frac{1}{Ah}(q^k_{j,i} - q^k_{j,i-1}), \tag{4.21a}
$$

$$
\begin{aligned}
F^k_{\sum_{\ell=1}^{3} N_\ell + \sum_{\ell=1}^{j-1} N_\ell + i} = {}& \frac{1}{2\tau}(q^k_{j,i-1} + q^k_{j,i} - q^{k-1}_{j,i-1} - q^{k-1}_{j,i})\\
&+ \frac{1}{h}\Big(Ap^k_{j,i} + \frac{(q^k_{j,i})^2}{A\rho^k_{j,i}} - Ap^k_{j,i-1} - \frac{(q^k_{j,i-1})^2}{A\rho^k_{j,i-1}}\Big)\\
&+ \frac{1}{2}\Big(\frac{\lambda(|q^k_{j,i-1}|)}{2D\rho^k_{j,i-1}A} q^k_{j,i-1}|q^k_{j,i-1}| + Ag\rho^k_{j,i-1}h'\\
&+ \frac{\lambda(|q^k_{j,i}|)}{2D\rho^k_{j,i}A} q^k_{j,i}|q^k_{j,i}| + Ag\rho^k_{j,i}h'\Big),
\end{aligned} \tag{4.21b}
$$

$$
\begin{aligned}
F^k_{2\sum_{\ell=1}^{3} N_\ell + \sum_{\ell=1}^{j-1} N_\ell + i} = {}& \frac{1}{2\tau}(E^k_{j,i-1} + E^k_{j,i} - E^{k-1}_{j,i-1} - E^{k-1}_{j,i})\\
&+ \frac{1}{Ah}\Big(\frac{q^k_{j,i}}{\rho^k_{j,i}}(E^k_{j,i} + p^k_{j,i}) - \frac{q^k_{j,i-1}}{\rho^k_{j,i-1}}(E^k_{j,i-1} + p^k_{j,i-1})\Big)\\
&+ \frac{k_w}{2D}(T^k_{j,i-1} + T^k_{j,i} - 2T_w),
\end{aligned} \tag{4.21c}
$$

$$
F^k_{3\sum_{\ell=1}^{3} N_\ell + \sum_{\ell=1}^{j-1} N_\ell + j} = E^k_{j,0} - \frac{(q^k_{j,0})^2}{2A^2\rho^k_{j,0}} - c_v\rho^k_{j,0}T^k_{j,0} - \rho^k_{j,0}gh, \tag{4.21d}
$$

$$
F^k_{3\sum_{\ell=1}^{3} N_\ell + \sum_{\ell=1}^{j-1} N_\ell + j + i} = E^k_{j,i} - \frac{(q^k_{j,i})^2}{2A^2\rho^k_{j,i}} - c_v\rho^k_{j,i}T^k_{j,i} - \rho^k_{j,i}gh, \tag{4.21e}
$$

$$F^k_{4\sum_{\ell=1}^3 N_\ell+\sum_{\ell=1}^{j-1} N_\ell+3+j} = p^k_{j,0} - RT^k_{j,0}\rho^k_{j,0}\big(1+0.257\frac{p^k_{j,0}}{p_c} - 0.533\frac{p^k_{j,0}T_c}{p_c T^k_{j,0}}\big), \tag{4.21f}$$

$$F^k_{4\sum_{\ell=1}^3 N_\ell+\sum_{\ell=1}^{j-1} N_\ell+3+j+i} = p^k_{j,i} - RT^k_{j,i}\rho^k_{j,i}\big(1+0.257\frac{p^k_{j,i}}{p_c} - 0.533\frac{p^k_{j,i}T_c}{p_c T^k_{j,i}}\big), \tag{4.21g}$$

$$F^k_{5\sum_{\ell=1}^3 N_\ell+7} = q^k_{1,N_1} - q^k_{2,0} - q^k_{3,0}, \tag{4.21h}$$

$$F^k_{5\sum_{\ell=1}^3 N_\ell+8} = p^k_{1,N_1} - p^k_{2,0}, \tag{4.21i}$$

$$F^k_{5\sum_{\ell=1}^3 N_\ell+9} = p^k_{1,N_1} - p^k_{3,0}, \tag{4.21j}$$

$$F^k_{5\sum_{\ell=1}^3 N_\ell+10} = T^k_{1,N_1} - T^k_{2,0}, \tag{4.21k}$$

$$F^k_{5\sum_{\ell=1}^3 N_\ell+11} = T^k_{1,N_1} - T^k_{3,0}, \tag{4.21l}$$

for $j = 1,2,3$ and $i = 1,\dots,N_j$, with N_j again the number of spatial intervals of pipe j. Again, the Newton method is used to find an approximate solution of this nonlinear system after the first time integration step. We define $u^1 := [(q^1)^T,(p^1)^T,(\rho^1)^T,(E^1)^T,(T^1)^T]^T$ to be the solution of the nonlinear system. Then, from the first order approximation

$$D^{-1}_{u^1}\Delta u^1 \doteq -D^{-1}_{u^1}\left(F'_{u^1}\right)^{-1}F'_d\, d\Delta d/d \tag{4.22}$$

it follows that the componentwise relative condition numbers and the componentwise relative amplification vectors for the mass flow rate, the pressure, and the temperature are given by

$$\kappa(q^1;d) = \|k(q^1;d)\|_\infty, \quad k(q^1;d) = |D^{-1}_{u^1}\left(F'_{u^1}\right)^{-1}F'_d\, d|_{1:1+\sum_{\ell=1}^3 N_\ell}, \tag{4.23a}$$

$$\kappa(p^1;d) = \|k(p^1;d)\|_\infty, \quad k(p^1;d) = |D^{-1}_{u^1}\left(F'_{u^1}\right)^{-1}F'_d\, d|_{2+\sum_{\ell=1}^3 N_\ell:3+2\sum_{\ell=1}^3 N_\ell}, \tag{4.23b}$$

$$\kappa(T^1;d) = \|k(T^1;d)\|_\infty, \quad k(T^1;d) = |D^{-1}_{u^1}\left(F'_{u^1}\right)^{-1}F'_d\, d|_{10+4\sum_{\ell=1}^3 N_\ell:11+5\sum_{\ell=1}^3 N_\ell}, \tag{4.23c}$$

cf. the derivation in Section 4.2.2.

4.4.3 Results

We choose, e.g., the concrete parameter values in (4.18) and $T^1_{1,0} = 293\,\mathrm{K}$, $T_w = 283\,\mathrm{K}$, $k_w = 0.0341\,\mathrm{W\,m^{-1}\,K^{-1}}$, $c_v = 1850\,\mathrm{J\,kg^{-1}\,K^{-1}}$. The corresponding values for the condition numbers are given in Table 4.3. Again, we observe that the largest condition number is $\kappa(q^1;p^1_{\mathrm{En}}) = 18.1$. Thus, perturbations in the inlet pressure cause large deviations in the mass flow rate. In order to investigate this further, the componentwise relative amplification vectors

$k(q^1; p^1_{\mathrm{En}}), k(p^1; p^1_{\mathrm{En}}), k(T^1; p^1_{\mathrm{En}})$ w.r.t. p^1_{En} are depicted in Figure 4.4 as a function of the spatial coordinate x. Again, we observe that perturbations in the inlet pressure have the largest influence on the mass flow rate in Pipe 1.

4.5 Summary of Chapter 4

In this chapter, for a simple example of a network we have carried out a case study and we have determined the sensitivity of the state of the gas network with respect to changes or perturbations in the boundary conditions. We have used three different transient models for the gas flow through the pipes and discretized them both in space and in time with an implicit discretization scheme. In all three models we find that the largest condition number is $\kappa(q^1; p^1_{\mathrm{En}})$ and that all other condition numbers are around or smaller than 1. The computation of the componentwise relative amplification vectors shows, for all models, that perturbations in the inlet pressure have the largest effect on the mass flow rate in pipe 1.

Table 4.3: The condition numbers in (4.23), where F is given by (4.21), into which concrete parameter values are inserted.

d	$\kappa(q^1; d)$	$\kappa(p^1; d)$	$\kappa(T^1; d)$
p^1_{En}	18.1	0.780	0.261
T^1_{En}	1.48	$2.11 \cdot 10^{-3}$	0.470
q^1_{Ex1}	0.839	0.0338	$6.87 \cdot 10^{-3}$
q^1_{Ex2}	0.834	0.0359	$7.32 \cdot 10^{-3}$

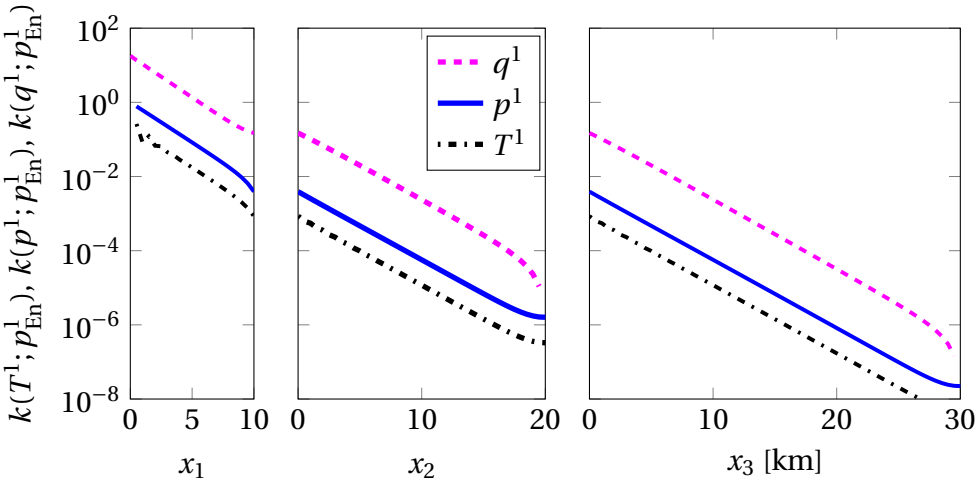

Figure 4.4: The componentwise relative amplification vectors $k(q^1; p^1_{\mathrm{En}})$, $k(p^1; p^1_{\mathrm{En}})$, $k(T^1; p^1_{\mathrm{En}})$ in (4.23) for system (4.21) and the small pipe network in Figure 4.1. Here, x_1, x_2, x_3 correspond to pipes 1, 2 and 3, respectively.

Chapter 5

Adaptive Refinement Strategies for the Simulation of Gas Flow in Networks using a Model Hierarchy

5.1 Introduction

Studies in control and optimization of natural gas supply in a dynamic supply-demand environment strongly depend on large scale simulations of pipeline networks. Depending upon requirement, there exist multiple models, based on the Euler equations of fluid dynamics, to predict the system behavior with varying levels of accuracy. Generally, more accurate models are computationally more expensive. Hence, in order to make real-time decisions, an appropriate trade-off between accuracy and computational complexity should be made. This can be achieved by using a hierarchy of models, where the models can be adaptively switched during the simulation process. Beside the models, the discretization mesh may be varied in space and time, which places the demand for an adaptive strategy to automatically steer the simulation by changing the models and the discretization meshes.

Since simulations are the basis for decisions in the optimization and control of the gas flow, the reliability of the simulation is of prime importance. The simulation is to be carried out such that the relative error in the state or in a functional of interest is below a specified tolerance. In this chapter, starting with a coarse simulation, an adaptive strategy is used to bring the error below the tolerance by refining the discretization in time and space or refining models, i.e., shifting to a model of higher accuracy. Hence, we have three different refinement possibilities for each pipe $j \in \mathcal{J}_p$ of the pipeline network, where $\mathcal{J}_p$ denotes the set of pipes in the network. These refinement possibilities are indexed by $i = 1, \ldots, 3N_p$, where $N_p := |\mathcal{J}_p|$ is the number of pipes. Refinements are to be chosen such that the computational costs are kept low. We define an optimal refinement strategy as a strategy which returns

the solution of the constrained optimization problem

$$\begin{aligned} \min_{r_i} \; & c + \sum_{i=1}^{3N_p} \sum_{k=1}^{r_i} \Delta c_{ik} \\ \text{s.t.} \; & |\eta| - \sum_{i=1}^{3N_p} \sum_{k=1}^{r_i} \Delta \eta_{ik} \leq tol. \end{aligned} \tag{5.1}$$

Here, the constants c and η denote the cost and relative error of the starting simulation, respectively. For each refinement possibility i, r_i is the number of refinements, $\Delta\eta_{ik}$ the relative error reduction due to the kth subsequent refinement, and Δc_{ik} the corresponding cost addition. We note that if Δc_{ik}, $\Delta\eta_{ik}$ are constant for all k, then this problem is equivalent to the unbounded knapsack problem, which is NP-hard; see, e.g., [62]. We aim to find a good approximation to the solution of this generalization of the knapsack problem. For this, we examine three adaptive refinement strategies which return approximate solutions of (5.1). We call these strategies *individual tolerances* (S1), *maximal error refinement* (S2), and *maximal error-to-cost refinement* (S3). The ideas of the first two strategies are frequently used in practice for the adaptation of the computational mesh; cf. the overview given in [7, Section 5.2]. An effective adaptive mesh refinement strategy for hyperbolic partial differential equations (PDEs) on a rectangular domain has been developed in [8–11]. Based on the ideas of this strategy, a mesh and model adaptation strategy for hyperbolic PDEs on a pipe network has been presented in [33, 37–40, 65]. The latter strategy is almost identical to strategy S1. The idea of strategy S2 is similar to the technique that is used in the adaptive finite element method; see, e.g., [17, 22, 23, 41, 42]. Strategy S2 also bears similarities to the adaptive strategy in a general multiscale setting that is discussed in [79]. Strategy S3 is based on the idea of the greedy approximation algorithm for solving the unbounded knapsack problem; see [29]. The aim of this chapter is to compare the performance of the three mesh and model refinement strategies S1–S3 on a gas pipeline network with respect to their computational cost incurred. The ideas presented here are for the example of pipe networks. By generalizing pipes to functional sub-domains, the described principles of adaptive refinement can be extended to simulations for other applications which use a model hierarchy, e.g., power grids and water supply networks.

This chapter is organized as follows. Section 5.2 introduces a model hierarchy for the simulation of gas flow through a single pipe as well as the aim of the adaptive refinement strategies. Section 5.3 describes the three proposed refinement strategies and Section 5.4 introduces both a synthetic experiment on an abstract gas network and an application of the refinement strategies to a realistic network simulation. Finally, a summary of this chapter is given in Section 5.5.

5.2 Simulation of Gas Flow

In this section, we present a framework for the simulation of gas flow in a pipe network. We give a description of a gas network in Section 5.2.1, including a model hierarchy for the pipes and the fuel gas consumption of a compressor. Model and discretization error estimators w.r.t. a user-defined functional are derived in Section 5.2.2. We then outline a framework for the adaptive simulation of pipe networks using the given model hierarchy in Section 5.2.3. Finally, we highlight the aims of the refinement strategies within the simulation framework in Section 5.2.4.

5.2.1 Gas Network

We follow the framework given in [33, 40] to describe the gas network. The network is modeled as a directed graph $\mathcal{G} = (\mathcal{J}, \mathcal{V})$ with edges $\mathcal{J}$ and vertices $\mathcal{V}$. The set of edges $\mathcal{J}$ consists of pipes $j \in \mathcal{J}_p$, compressor stations $c \in \mathcal{J}_c$, and valves $\mathcal{J}_v$. Each pipe $j \in \mathcal{J}_p$ is defined as an interval $[x_j^a, x_j^b]$ with a direction from x_j^a to x_j^b. In each pipe, one of the models described in Section 5.2.1 holds and adequate initial and coupling as well as boundary conditions have to be specified. Valves and compressors are described by algebraic equations.

Model Hierarchy

As an example, we take a three-model hierarchy for the gas flow simulations, discussed in detail in [37]. The *isothermal Euler equations* [69] consist of the continuity and the momentum equation together with the equation of state for real gases. We simplify these equations by assuming the pipe to be horizontal and the speed of sound to be constant, yielding a *nonlinear model*

$$\begin{aligned} p_t + \frac{\rho_0 c^2}{A} q_x &= 0, \\ q_t + \frac{A}{\rho_0} p_x + \frac{\rho_0 c^2}{A} \left(\frac{q^2}{p} \right)_x &= -\frac{\lambda \rho_0 c^2}{2DA} \frac{|q|q}{p}. \end{aligned} \tag{M1}$$

Here, $q = A\rho v/\rho_0$ denotes the mass flow rate under standard conditions (1 atm air pressure, temperature of 0 °C), p denotes the pressure, $c = \sqrt{p/\rho}$ the speed of sound, A the cross-sectional area of the pipe, $\lambda > 0$ the Darcy friction coefficient, D the pipe diameter, ρ the gas density, v the gas velocity, and ρ_0 the density under standard conditions. If the gas velocity is much smaller than the speed of sound, i.e., if $|v| \ll c$, then we can neglect the nonlinear term in the spatial derivative of the momentum equation in M1. This results in a *semilinear model* [33, 80]

$$\begin{aligned} p_t + \frac{\rho_0 c^2}{A} q_x &= 0, \\ q_t + \frac{A}{\rho_0} p_x &= -\frac{\lambda \rho_0 c^2}{2DA} \frac{|q|q}{p}. \end{aligned} \tag{M2}$$

A further simplification of assuming a stationary state, i.e., setting the time derivatives to zero, yields a system of two ordinary differential equations, which can be solved analytically and are referred to as the *algebraic model*

$$\begin{aligned} q &= \text{const.}, \\ p(x) &= \sqrt{p_{\text{in}}^2 - \frac{\lambda \rho_0^2 c^2 |q| q}{DA^2} x}. \end{aligned} \tag{M3}$$

Here, $p_{\text{in}} = p(0)$ denotes the pressure at the inbound of the pipe. The three models are shown in hierarchical form in Figure 5.1. The model hierarchy is set in the decreasing order of accuracy for our purpose of gas flows. In general, models M1 and M2 can not be solved analytically. Therefore, a discretization method has to be applied in order to obtain an approximate discrete solution. In practical gas flow applications, box schemes, which are introduced in [99], have been shown to be effective discretization schemes for these two systems of hyperbolic PDEs. We apply the implicit box scheme, which is conservative and stable under mild conditions [35]. For the scalar balance law

$$u_t + f(u)_x = g(u),$$

with initial conditions $u(x,0) = u_0(x)$, this box scheme is given by

$$\frac{u_{i-1}^{\ell} + u_i^{\ell}}{2} = \frac{u_{i-1}^{\ell-1} + u_i^{\ell-1}}{2} - \frac{\Delta t}{\Delta x}(f_i^{\ell} - f_{i-1}^{\ell}) + \Delta t \frac{g_{i-1}^{\ell} + g_i^{\ell}}{2}, \tag{5.2}$$

where $u_i^{\ell} = u(x_i, t_{\ell})$ and $f_i^{\ell} = f(u(x_i, t_{\ell}))$. The implicit box scheme is convergent of order 2 in space and order 1 in time [66]. Each pipe in the network is simulated using one of the three models and varying discretization stepsizes in space and time.

Compressor Station

The pressure of the gas is increased using a compressor station, which consists of several compressors. A compressor consumes some of the gas during its operation. The equation for the fuel gas consumption of a compressor $c \in \mathscr{J}_c$ is given by [55]

$$G_c(t) = c_F q_{\text{in}}(t) \left(\left(\frac{p_{\text{out}}(t)}{p_{\text{in}}(t)} \right)^{\frac{\gamma-1}{\gamma}} - 1 \right), \tag{5.3}$$

with in- and outgoing pressure p_{in}, p_{out}, and ingoing flow rate q_{in}. The parameter c_F is a compressor specific constant and γ the isentropic coefficient of the gas.

5.2.2 Error Estimators

Using the solution of adjoint equations as done in [7, 12, 16, 33, 40], we derive a model and a discretization error estimator which measure the influence

of the model and the discretization on a user-defined output functional M. The functional M can be of any form, for example measuring the fuel gas consumption of the compressor stations via

$$M(p,q) = \sum_{c \in \mathscr{J}_c} \int_0^T G_c(t)\,\mathrm{d}t$$

with $G_c(t)$ being the fuel gas consumption of the individual compressor $c \in \mathscr{J}_c$ as given in (5.3). In the following, we consider the arbitrary cost functional

$$\begin{aligned} M(p,q) = &\int_0^T \int_\Omega N(p,q)\,\mathrm{d}x\,\mathrm{d}t + \int_\Omega N_T(p,q)\,\mathrm{d}x \\ &+ \sum_{v \in \mathscr{V}} \int_0^T N_v(p,q)\,\mathrm{d}t + \sum_{i \in \mathscr{J}_{\mathrm{ALG}}} \int_0^T N_i(\boldsymbol{p}_i, \boldsymbol{q}_i)\,\mathrm{d}t, \end{aligned}$$

where $\Omega = \sum_{j \in \mathscr{J}_{\mathrm{PDE}}} [x_j^a, x_j^b]$, $\boldsymbol{p}_i = [p(x_i^a,t), p(x_i^b,t)]^T$, and $\boldsymbol{q}_i = [q(x_i^a,t), q(x_i^b,t)]^T$. The sets $\mathscr{J}_{\mathrm{ALG}}$ and $\mathscr{J}_{\mathrm{PDE}}$ contain the arcs that are modeled by algebraic equations (i.e., pipes using model M3 or other network components like valves or compressor stations) and arcs that are modeled by PDEs (i.e., pipes using models M1 or M2), respectively. The components $N(p,q)$, $N_v(p,q)$, and $N_i(\boldsymbol{p}_i, \boldsymbol{q}_i)$ define tracking-type costs on the respective sets (Ω, specific nodes, or algebraic arcs) in the whole time interval $(0,T)$ and the component $N_T(p,q)$ defines costs on Ω at the final time T. The adjoint equations of model M2 with respect to $M(p,q)$ are given by

$$\begin{aligned} \xi_{1_t} + \frac{A}{\rho_0}\xi_{2_x} &= -\frac{\lambda \rho_0 c^2}{2DA}\frac{|q|q}{p^2}\xi_2 - \frac{\partial N(p,q)}{\partial p}, \\ \xi_{2_t} + \frac{\rho_0 c^2}{A}\xi_{1_x} &= \frac{\lambda \rho_0 c^2}{DA}\frac{|q|}{p}\xi_2 - \frac{\partial N(p,q)}{\partial q}, \end{aligned} \tag{5.4}$$

together with appropriate "initial", coupling, and node conditions. Note that in the adjoint equation (5.4) only the tracking-type component $N(p,q)$ appears. The remaining components occur in the "initial", coupling, and node

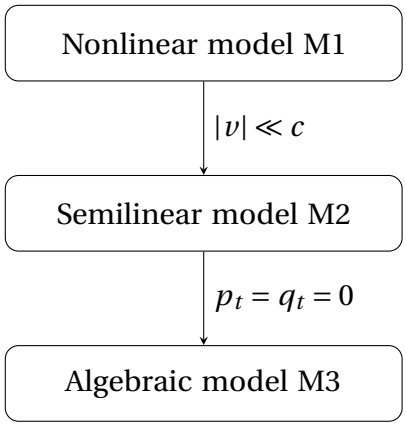

Figure 5.1: The model hierarchy for the simulation of gas flow that is considered in this chapter.

conditions, cf. [33, Eq. (3.33)] or [39, Eq. (20)]. The solution $\boldsymbol{\xi} = [\xi_1, \xi_2]^T$ of the adjoint equations consists of the adjoint pressure and mass flow rate of the semilinear model M2 with respect to the functional $M(p,q)$. Let $\boldsymbol{u} = [p,q]^T$ be the solution of the nonlinear model M1 and $\boldsymbol{u}^h = [p^h, q^h]^T$ the discretized solution of the semilinear model M2. For the discretization of M2 we apply the implicit box scheme in (5.2). Then, the difference between the output functional $M(\boldsymbol{u})$ and $M(\boldsymbol{u}^h)$ can be approximated using Taylor expansion. Inserting the solution $\boldsymbol{\xi}$ of the adjoint system (5.4), we get a first order error estimator for the model and the discretization error given by [33, 39, 40]

$$
\begin{aligned}
M(\boldsymbol{u}) - M(\boldsymbol{u}^h) &\approx \eta_m^{\text{LIN-NL}} + \eta_h^{\text{LIN}}, \\
\eta_m^{\text{LIN-NL}} &= \int_0^T \int_\Omega -\boldsymbol{\xi}^T \begin{bmatrix} 0 \\ \frac{\rho_0 c^2 (q^h)^2}{A p^h} \end{bmatrix}_x \mathrm{d}x\,\mathrm{d}t, \\
\eta_h^{\text{LIN}} &= \int_0^T \int_\Omega -\boldsymbol{\xi}^T \begin{bmatrix} p_t^h + \frac{\rho_0 c^2}{A} q_x^h \\ q_t^h + \frac{A}{\rho_0} p_x^h + \frac{\lambda \rho_0 c^2 |q^h| q^h}{2DAp^h} \end{bmatrix} \mathrm{d}x\,\mathrm{d}t.
\end{aligned}
$$

The discretization error estimator η_h^{LIN} may be split up into a temporal and spatial discretization error estimator as follows. Let $\boldsymbol{u}$ be the exact and $\boldsymbol{u}^h$ be the discretized solution of the semilinear model M2. We use a short notation of M2, i.e., $\boldsymbol{u}_t + f(\boldsymbol{u})_x = g(\boldsymbol{u})$, which yields

$$
\begin{aligned}
\eta_h^{\text{LIN}} &= \int_0^T \int_\Omega -\boldsymbol{\xi}^T \left(\boldsymbol{u}_t^h + f(\boldsymbol{u}^h)_x - g(\boldsymbol{u}^h) \right) \mathrm{d}x\,\mathrm{d}t \\
&= \int_0^T \int_\Omega -\boldsymbol{\xi}^T \left((\boldsymbol{u}_t^h - \boldsymbol{u}_t) + (f(\boldsymbol{u}^h)_x - f(\boldsymbol{u})_x) - (g(\boldsymbol{u}^h) - g(\boldsymbol{u})) \right) \mathrm{d}x\,\mathrm{d}t \\
&= \underbrace{\int_0^T \int_\Omega -\boldsymbol{\xi}^T (\boldsymbol{u}_t^h - \boldsymbol{u}_t)\,\mathrm{d}x\,\mathrm{d}t}_{=:\eta_t^{\text{LIN}}} \\
&\quad + \underbrace{\int_0^T \int_\Omega -\boldsymbol{\xi}^T \left((f(\boldsymbol{u}^h)_x - f(\boldsymbol{u})_x) - (g(\boldsymbol{u}^h) - g(\boldsymbol{u})) \right) \mathrm{d}x\,\mathrm{d}t}_{=:\eta_x^{\text{LIN}}},
\end{aligned}
$$

since $\boldsymbol{u}$ is the exact solution of M2. The temporal discretization error estimator can be split up into error estimators for the individual pipes via

$$
\eta_t^{\text{LIN}} = \int_0^T \sum_{j \in \mathcal{J}_p} \int_{x_j^a}^{x_j^b} -\boldsymbol{\xi}^T (\boldsymbol{u}_t^h - \boldsymbol{u}_t)\,\mathrm{d}x\,\mathrm{d}t = \sum_{j \in \mathcal{J}_p} \eta_{t,j}^{\text{LIN}}, \tag{5.5}
$$

analogously for the spatial discretization and model error estimator. For the computation of the discretization error estimators, the exact solution is approximated by a higher order reconstruction using neighboring points. We use a polynomial reconstruction of order 2 for the time derivative and denote it by $\boldsymbol{u}_t \approx R_t(\boldsymbol{u}^h)$. The spatial derivative of f and the value of g are reconstructed with order 4, giving $f(\boldsymbol{u})_x \approx R_x(f(\boldsymbol{u}^h))$ and $g(\boldsymbol{u}) \approx R(g(\boldsymbol{u}^h))$. Thus, the

computed estimators are given by

$$\eta_{t,j}^{\mathrm{LIN}} \approx \int_0^T \int_{x_j^a}^{x_j^b} -\boldsymbol{\xi}^T \left(\boldsymbol{u}_t^h - R_t(\boldsymbol{u}^h)\right) \mathrm{d}x\,\mathrm{d}t, \tag{5.6a}$$

$$\eta_{x,j}^{\mathrm{LIN}} \approx \int_0^T \int_{x_j^a}^{x_j^b} -\boldsymbol{\xi}^T \Big(\big(f(\boldsymbol{u}^h)_x - R_x(f(\boldsymbol{u}^h))\big) - \big(g(\boldsymbol{u}^h) - R(g(\boldsymbol{u}^h))\big)\Big) \mathrm{d}x\,\mathrm{d}t, \tag{5.6b}$$

$$\eta_{m,j}^{\text{LIN-NL}} = \int_0^T \int_{x_j^a}^{x_j^b} -\boldsymbol{\xi}^T \begin{bmatrix} 0 \\ \frac{\rho_0 c^2 (q^h)^2}{A p^h} \end{bmatrix}_x \mathrm{d}x\,\mathrm{d}t, \tag{5.6c}$$

for all $j \in \mathscr{J}_p$. The model error estimator $\eta_{m,j}^{\text{ALG-LIN}}$ between the algebraic and the semilinear model and the discretization error estimators $\eta_{t,j}^{\mathrm{NL}}$ and $\eta_{x,j}^{\mathrm{NL}}$ for the nonlinear model are derived analogously for every pipe $j \in \mathscr{J}_p$; see [38].

5.2.3 Adaptive Gas Network Simulation

We consider a gas flow simulation over a pipeline network $\mathscr{J}_p$. The simulation time $[0,T]$ is divided into time intervals of equal size $[t_k, t_{k+1}]$, $k = 0,1,\ldots,N-1$ and $t_N = T$. Given a starting model distribution over the network $\boldsymbol{m}_0 = [m_{0,1}, m_{0,2}, \ldots, m_{0,N_p}]^T$, with $m_{0,j} \in \{1,2,3\}$, and a corresponding discretization in space $\boldsymbol{n}_{x,0}$ and in time $\boldsymbol{n}_{t,0}$, a simulation is run for $[t_0, t_1]$. We obtain error distributions along the network using the *a posteriori* error estimators in Section 5.2.2: $\boldsymbol{\eta}_m = [\eta_{m,1}, \eta_{m,2}, \ldots, \eta_{m,N_p}]^T$ for the model errors and $\boldsymbol{\eta}_x = [\eta_{x,1}, \eta_{x,2}, \ldots, \eta_{x,N_p}]^T$ and $\boldsymbol{\eta}_t = [\eta_{t,1}, \eta_{t,2}, \ldots, \eta_{t,N_p}]^T$ for the spatial and temporal discretization errors, respectively. The simulation error for a single pipe is the sum of all three errors. For the simulation to be valid, the relative error in M must be below a given tolerance *tol*. Hence, we require that

$$\frac{|M(\boldsymbol{u}) - M(\boldsymbol{u}^h)|}{|M(\boldsymbol{u}^h)|} \approx \frac{|\sum_{j \in \mathscr{J}_p} (\eta_{m,j} + \eta_{x,j} + \eta_{t,j})|}{|M(\boldsymbol{u}^h)|} < tol. \tag{5.7}$$

If the tolerance is not achieved, models and discretization meshes are refined. The task of deciding the required refinements is made by an adaptive strategy. A switch to a higher model in the hierarchy is called a *model refinement* and a refinement of the mesh is called a *discretization refinement*. With the new models and discretizations we re-simulate for the time interval and continue the cycle. Once the solution meets the tolerance requirements, the models and discretizations are coarsened if appropriate, the simulation progresses to the next time interval, and the cycle repeats. This simulation flow is shown in Figure 5.2 for an interval $[t_k, t_{k+1}]$.

5.2.4 Structure and Aim of Adaptive Strategies

Our focus lies on comparing adaptive strategies that control the errors and drive the simulation. For the time interval $[t_k, t_{k+1}]$ an adaptive strategy takes

as input the error distributions $\boldsymbol{\eta}_{m,k}, \boldsymbol{\eta}_{x,k}, \boldsymbol{\eta}_{t,k}$, the model distribution $\boldsymbol{m}_k$, and the number of (equidistant) nodes in the spatial and temporal discretizations $\boldsymbol{n}_{x,k}, \boldsymbol{n}_{t,k}$. For notational convenience we drop the dependence on k in the following. The strategy returns a refinement scheme $\boldsymbol{r}_m = [r_{m,1}, \ldots, r_{m,N_p}]^T$, $\boldsymbol{r}_x = [r_{x,1}, \ldots, r_{x,N_p}]^T$, $\boldsymbol{r}_t = [r_{t,1}, \ldots, r_{t,N_p}]^T$, where $r_{m,j} \in \{0,1,2\}$, $r_{x,j}, r_{t,j} \in \mathbb{N}$ denote the number of refinements to be made in the models and in the discretizations for all pipes $j \in \mathscr{J}_p$ such that constraint (5.7) is satisfied. The aim of the adaptive strategies is to achieve this constraint while keeping the computational costs that are incurred in the simulation low.

5.3 Refinement Strategies

In this section, we discuss three strategies for the adaptive refinements in the network simulation. The first strategy assigns individual error tolerances to each pipe and executes multiple discretization refinements simultaneously. The second and third strategy use the overall error tolerance and iteratively refine only the best option(s) in the network.

We first provide some general remarks which hold for every strategy. Relations between the initial numbers of discretization intervals $n-1$ and the

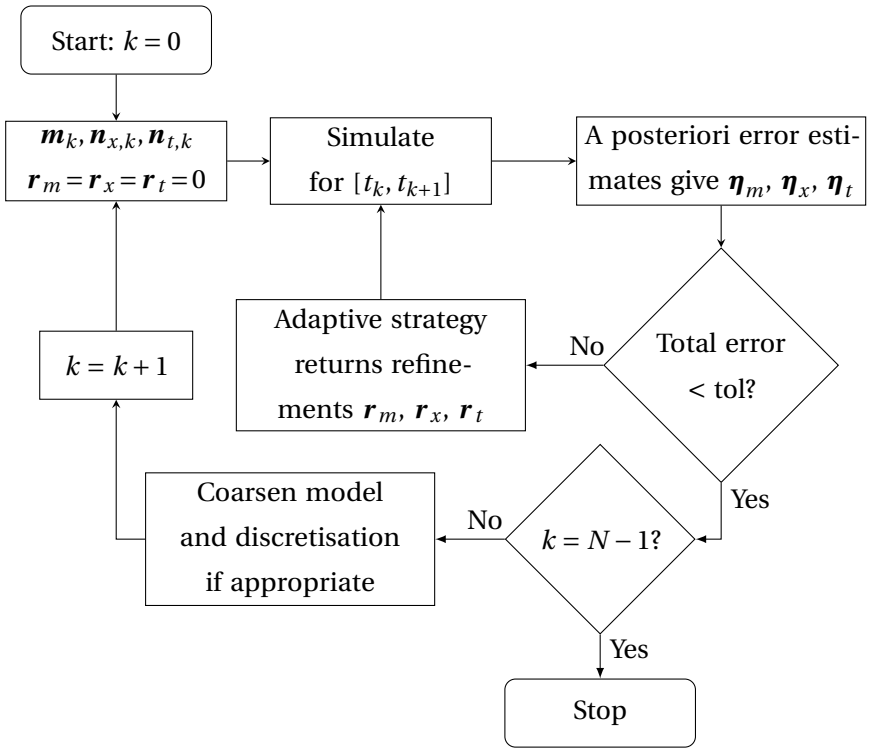

Figure 5.2: Gas flow adaptive simulation process using an adaptive refinement strategy which returns a set of refinements $\boldsymbol{r}_m, \boldsymbol{r}_x, \boldsymbol{r}_t$.

numbers of intervals after r refinements $n(r)-1$ are given by

$$\begin{aligned} n_{x,j}\left(r_{x,j}\right)-1 &= 2^{r_{x,j}}\left(n_{x,j}-1\right), \\ n_{t,j}\left(r_{t,j}\right)-1 &= 2^{r_{t,j}}\left(n_{t,j}-1\right), \qquad \forall\, j \in \mathscr{J}_p, \end{aligned} \tag{5.8}$$

where n is the number of nodes. Thus, the number of intervals is doubled for a single refinement. We choose this factor 2 such that, given a conservative initialization for the implicit box scheme (5.2) on the coarser grid, it is possible to obtain a conservative initialization on the refined grid. Namely, the pointwise values of corresponding grid points are copied from the coarser grid and the intermediate grid points are assigned the arithmetic mean of the two neighboring grid points [39, 65]. From (5.8) it follows that approximate relations between the initial discretization error estimators η and the estimators after r refinements $\eta(r)$ are given by

$$\eta_{x,j}\left(r_{x,j}\right) \approx \frac{\eta_{x,j}}{2^{s_x r_{x,j}}}, \quad \eta_{t,j}\left(r_{t,j}\right) \approx \frac{\eta_{t,j}}{2^{s_t r_{t,j}}}, \quad \forall\, j \in \mathscr{J}_p,$$

where s_x and s_t are the convergence orders of the spatial and temporal discretization schemes, respectively. The reduction for the error is only an approximation. Therefore, to have a safe upper bound for the estimated error after refinement, we multiply these approximated errors by a *safety factor of refinement* $f_r > 1$ in each of the pipes that require refinements to be made. This ensures that it is very unlikely that the actual error overshoots its estimated value after the refinement. In the model hierarchy presented in Figure 5.1, discretization errors feature only in the models M1 and M2. The algebraic model M3 has no discretization errors. Thus, when models are switched from M3 to M2, discretization errors are introduced. For pipe j simulated with the most detailed model M1, we set the model error to $\eta_{m,j} = 0$.

Strategy 1 - Individual tolerances (S1)

In order to meet the tolerance of the network error, we derive fixed individual error tolerances for the individual pipes for each of the three error types. The simulation is then carried out such that for each pipe the error is below the individual tolerance for all three errors. The pseudocode for *individual tolerances* is given in Algorithm 5.1. We set the tolerance for the model errors as

$$tol_m = \kappa \cdot tol, \quad \kappa \in (0,1).$$

The remaining tolerance $tol - tol_m = (1-\kappa)\,tol$ is equally divided between the spatial and temporal discretizations, i.e.,

$$tol_x = tol_t = (1-\kappa)/2 \cdot tol$$

are the tolerances for both error types for the entire network. To get the tolerances for individual pipes, we uniformly distribute these tolerances over the entire network, i.e., we divide them by the number of pipes N_p. For the

refinements, first the number of discretization refinements are computed that bring the discretization errors below the respective tolerances for every pipe. That is, for every pipe j for which

$$|\eta_{x,j}| > \frac{tol_x}{N_p}|M(\boldsymbol{u}^h)| \tag{5.9}$$

holds, we require for the spatial discretization error after $r_{x,j}$ refinements that

$$f_r|\eta_{x,j}(r_{x,j})| = f_r\frac{|\eta_{x,j}|}{2^{s_x r_{x,j}}} \leq \frac{tol_x}{N_p}|M(\boldsymbol{u}^h)|.$$

Solving this inequality for the number of refinements $r_{x,j}$ yields

$$r_{x,j} = \text{ceil}\left(\log\left(\frac{f_r|\eta_{x,j}|N_p}{tol_x|M(\boldsymbol{u}^h)|}\right)\frac{1}{\log(2^{s_x})}\right),$$

where ceil is the ceiling function, i.e., ceil(α) is the smallest integer greater than or equal to α. The mesh size is then refined $r_{x,j}$ times for every pipe j for which (5.9) holds, see Alg. 5.1, lines 4, 5. The procedure for the computation of

Algorithm 5.1 : Individual tolerances

Input: $\boldsymbol{\eta}_m, \boldsymbol{\eta}_x, \boldsymbol{\eta}_t, tol, s_x, s_t, f_r$

1: $\boldsymbol{r}_m \leftarrow \boldsymbol{0}$
2: **while** $|\sum_{j\in\mathcal{J}_p}(\eta_{m,j}+\eta_{x,j}+\eta_{t,j})| > tol|M(\boldsymbol{u}^h)|$ **do**
3: **for** $j = 1,\ldots,N_p$ **do**
4: **if** $|\eta_{x,j}| > tol_x|M(\boldsymbol{u}^h)|/N_p$ **then**
5: $r_{x,j} \leftarrow \text{ceil}\left(\log\left(\frac{f_r|\eta_{x,j}|N_p}{tol_x|M(\boldsymbol{u}^h)|}\right)\frac{1}{\log(2^{s_x})}\right)$
6: **end if**
7: **if** $|\eta_{t,j}| > tol_t|M(\boldsymbol{u}^h)|/N_p$ **then**
8: $r_{t,j} \leftarrow \text{ceil}\left(\log\left(\frac{f_r|\eta_{t,j}|N_p}{tol_t|M(\boldsymbol{u}^h)|}\right)\frac{1}{\log(2^{s_t})}\right)$
9: **end if**
10: **end for**
11: **update** $\boldsymbol{\eta}_m, \boldsymbol{\eta}_x, \boldsymbol{\eta}_t$
12: **if** $|\sum_{j\in\mathcal{J}_p}(\eta_{m,j}+\eta_{x,j}+\eta_{t,j})| > tol|M(\boldsymbol{u}^h)|$ **then**
13: **for** $j = 1,\ldots,N_p$ **do**
14: **if** $|\eta_{m,j}| > tol_m|M(\boldsymbol{u}^h)|/N_p$ **then**
15: $r_{m,j} \leftarrow r_{m,j}+1$
16: **end if**
17: **end for**
18: **end if**
19: **update** $\boldsymbol{\eta}_m, \boldsymbol{\eta}_x, \boldsymbol{\eta}_t$
20: **end while**

Output: $\boldsymbol{r}_m, \boldsymbol{r}_x, \boldsymbol{r}_t$

the number of temporal discretization refinements is analogous, see Alg. 5.1, lines 7, 8. The gas network is simulated again with the refined spatial and temporal stepsizes and the new error distributions $\boldsymbol{\eta}_m, \boldsymbol{\eta}_x, \boldsymbol{\eta}_t$ are computed (Alg. 5.1, line 11). Subsequently, if the relative network error still exceeds the tolerance, i.e., if (5.7) is not satisfied, then the model of every pipe j for which

$$|\eta_{m,j}| > \frac{tol_m}{N_p} |M(\boldsymbol{u}^h)|$$

holds is refined to the next model higher up in the hierarchy (Alg. 5.1, lines 12, 14, 15). The simulation errors are then re-evaluated again and this cycle is repeated until (5.7) is satisfied (Alg. 5.1, lines 19, 2). This strategy is very similar to the one discussed in [33, Section 3.3]. The only differences are that the temporal error and tolerance are there considered for the entire network instead of the individual pipes.

Strategy 2 - Maximal error refinement (S2)

Since strategy 1 assigns individual tolerances, it loses the view of the network as a whole. However, the contribution of different errors to the overall network can balance each other without overshooting the total network tolerance. This is accounted for in the following strategy where we seek to make only those refinements which result in the maximal error reduction. This results in an iterative procedure, which we split in a network controller, see Algorithm 5.2a, and pipe level computations, see Algorithm 5.2b. For every pipe j, the estimated error reductions due to a single refinement in the model $\Delta\eta_{m,j}$ and in the space and time discretizations $\Delta\eta_{x,j}$, $\Delta\eta_{t,j}$ are given by

$$\begin{aligned}
\Delta\eta_{m,j} &= F_m(m_{c,j}, m_{c,j}-1)\,|\eta_{m,j}| + |\eta_{x,j}(m_{c,j}, r_{x,j})| - |\eta_{x,j}(m_{c,j}-1, r_{x,j})| \\
&\quad + |\eta_{t,j}(m_{c,j}, r_{t,j})| - |\eta_{t,j}(m_{c,j}-1, r_{t,j})| \\
&= F_m(m_{c,j}, m_{c,j}-1)\,|\eta_{m,j}| \\
&\quad + \big(F_x(m_{c,j}) - F_x(m_{c,j}-1)\big)\big(1 + (f_r - 1)\operatorname{sign}(r_{x,j})\big)\frac{|\eta_{x,j}|}{2^{s_x r_{x,j}}} \\
&\quad + \big(F_t(m_{c,j}) - F_t(m_{c,j}-1)\big)\big(1 + (f_r - 1)\operatorname{sign}(r_{t,j})\big)\frac{|\eta_{t,j}|}{2^{s_t r_{t,j}}}, \qquad (5.10a) \\
\Delta\eta_{x,j} &= |\eta_{x,j}(m_{c,j}, r_{x,j})| - |\eta_{x,j}(m_{c,j}, r_{x,j}+1)| \\
&= F_x(m_{c,j})\big(1 + (f_r - 1)\operatorname{sign}(r_{x,j}) - 2^{-s_x} f_r\big)\frac{|\eta_{x,j}|}{2^{s_x r_{x,j}}}, \qquad (5.10b) \\
\Delta\eta_{t,j} &= |\eta_{t,j}(m_{c,j}, r_{t,j})| - |\eta_{t,j}(m_{c,j}, r_{t,j}+1)| \\
&= F_t(m_{c,j})\big(1 + (f_r - 1)\operatorname{sign}(r_{t,j}) - 2^{-s_t} f_r\big)\frac{|\eta_{t,j}|}{2^{s_t r_{t,j}}}, \qquad (5.10c)
\end{aligned}$$

where $\eta_{x,j}, \eta_{t,j}, \eta_{m,j}$ denote the error estimators for the initial discretization stepsizes and model distribution and the functions

$$\eta_{x,j}(m_{c,j}, r_{x,j}) = F_x(m_{c,j})\big(1 + (f_r - 1)\,\mathrm{sign}(r_{x,j})\big)\frac{\eta_{x,j}}{2^{s_x r_{x,j}}},$$
$$\eta_{t,j}(m_{c,j}, r_{t,j}) = F_t(m_{c,j})\big(1 + (f_r - 1)\,\mathrm{sign}(r_{t,j})\big)\frac{\eta_{t,j}}{2^{s_t r_{t,j}}},$$

estimate the new discretization errors after model and/or grid refinements. Here, the factor $F_m(a,b)$ denotes an error reduction factor for the model error when models are shifted from a to b. The spatial and temporal discretization errors also depend on the simulation model. The factors $F_x(m_{c,j}), F_t(m_{c,j})$ denote error amplification factors for the discretization errors which account for this model dependency, where $m_{c,j} = 1,2,3$ denotes the current model of

Algorithm 5.2a : Maximal error refinement

Input: $\boldsymbol{m}, \boldsymbol{\eta}_m, \boldsymbol{\eta}_x, \boldsymbol{\eta}_t, tol, s_x, s_t, \phi$
for $j = 1, \ldots, N_p$ **do**
  $b_j, z_j \leftarrow$ MAXERRORRED$(m_j, r_{m,j}, r_{x,j}, r_{t,j}, \eta_{m,j}, \eta_{x,j}, \eta_{t,j}, s_x, s_t)$
end for
while networkError $> tol|M(\boldsymbol{u}^h)|$ **do**
  bound $\leftarrow \phi \cdot \max_j b_j$
  for $j = 1, \ldots, N_p$ **do**
    if $b_j >$ bound **then**
      $r_{z_j,j} \leftarrow r_{z_j,j} + 1$
      $b_j, z_j \leftarrow$ MAXERRORRED$(m_j, r_{m,j}, r_{x,j}, r_{t,j}, \eta_{m,j}, \eta_{x,j}, \eta_{t,j}, s_x, s_t)$
    end if
  end for
  update networkError
end while
Output: $\boldsymbol{r}_m, \boldsymbol{r}_x, \boldsymbol{r}_t$

Algorithm 5.2b : Maximal pipe error reduction

function MAXERRORRED$(m, r_m, r_x, r_t, \eta_m, \eta_x, \eta_t, s_x, s_t)$
  $m_c \leftarrow m - r_m$
  if $m_c \neq 1$ **then**
    Compute $\Delta\eta_m$ as in (5.10a)
  else
    $\Delta\eta_m \leftarrow 0$
  end if
  Compute $\Delta\eta_x$ as in (5.10b)
  Compute $\Delta\eta_t$ as in (5.10c)
  $[b, z] = \mathtt{max}\{\Delta\eta_m, \Delta\eta_x, \Delta\eta_t\}$
  return b, z
end function

pipe j and refers to models M1, M2, M3, respectively. Since the discretization error is absent for $m_c = 3$, we set $F_x(3) = F_t(3) = 0$. Furthermore, we set $F_x(2) = F_t(2) = 1$. For model M1, the amplification factor for the discretization errors is set with respect to the benchmark model M2. Note that in determining $\Delta\eta_{m,j}$ in (5.10a) we also consider changes in the spatial and temporal discretization errors, since the central idea is to account for net error reduction. The approximate error reductions $\Delta\eta_{m,j}, \Delta\eta_{x,j}, \Delta\eta_{t,j}$ are computed in Algorithm 5.2b, lines 4, 8, 9. Then, the best option

$$b_j = \max_{j \in \mathscr{J}_p} \{\Delta\eta_{m,j}, \Delta\eta_{x,j}, \Delta\eta_{t,j}\}$$

is passed to the network, see Alg. 5.2b, line 10. There, the notation $[b, z] = \texttt{max}\{\cdot\}$ is similar to MATLAB notation where b denotes the maximal element and z is the corresponding index. On the network level, we mark those pipes for refinement for which the error reductions are larger than $\phi \cdot \max_j b_j$, with $\phi \leq 1$ (Alg. 5.2a, lines 5, 7). The numbers of refinements of the selected pipes are increased by one and the best options of these pipes are updated (Alg. 5.2a, lines 8, 9). Then, the total network error is updated (Alg. 5.2a, line 12). This can be done either by simulating the gas network again with the refined models and discretizations and computing the new error estimates in (5.6) or by using the error reduction estimates $\Delta\eta$ in (5.10) to update the error estimators via

$$\eta(r+1) = \eta(r) - \text{sign}(\eta(r))\Delta\eta, \tag{5.11}$$

with r the number of refinements. This iteration is repeated until the relative absolute network error is brought below the tolerance (Alg. 5.2a, line 4).

Strategy 3 - Maximal error-to-cost refinement (S3)

The adaptive refinements are made with an objective of reducing the computational cost without compromising on the simulation error. However, the previous two strategies do not address the computational costs explicitly. They address the error tolerance which is merely a constraint to the adaptive strategies, viewed in the optimization setting (5.1). In this strategy we also take into account the computational costs that are incurred by the refinements. Strategy 3, given in Algorithm 5.3a for the network level and Algorithm 5.3b for the pipe level, is identical to strategy 2 on the network level. On the pipe level, however, we also compute the cost additions $\Delta c_{m,j}, \Delta c_{x,j}, \Delta c_{t,j}$ using a cost functional $F_c(m_c, r_x, r_t)$, for each of the corresponding error reductions $\Delta\eta_{m,j}, \Delta\eta_{x,j}, \Delta\eta_{t,j}$, see Alg. 5.3b, lines 11, 13, 14. The error controller on the pipe level passes the best option

$$b_j = \max\left\{\frac{\Delta\eta_{m,j}}{\Delta c_{m,j}}, \frac{\Delta\eta_{x,j}}{\Delta c_{x,j}}, \frac{\Delta\eta_{t,j}}{\Delta c_{t,j}}\right\},$$

i.e., the maximal error-to-cost ratio, to the network (Alg. 5.3b, line 15). The idea of this strategy is similar to the greedy approximation algorithm for solving the unbounded knapsack problem, see [29].

For the experiments and simulations performed in this chapter we compute the computational cost per pipe in CPU seconds using a cost functional of the form

$$F(m, n_x, n_t) = C_m \, n_x^{\alpha_m} \, n_t^{\beta_m}, \tag{5.12}$$

where n_x, n_t denote the number of nodes in space and time, $m \in \{1,2,3\}$ denotes the model, and C_m, α_m, β_m are model-dependent constants. These constants are determined by a least squares fit to experimental data. For this, gas flow simulations through a single pipe are performed using the software *ANACONDA* (cf. [65, 66]) with many different values of n_x and n_t, which return the corresponding computational cost values F. The constants are given in Table 5.1. We note that although no discretization is required for the algebraic model M3, still a mesh is used in this model to determine the evaluation points. These evaluation points are used for the computation of the model error estimator $\eta_{m,j}^{\text{ALG-LIN}}$; cf. Section 5.2.2. We can rewrite the functional (5.12) in terms of refinements, which is needed in Algorithm 5.3b, assuming that the initial number of nodes $n_{x,0}$, $n_{t,0}$ are known. Then we get the cost functional

$$F_c(m, r_x, r_t) = C_m (2^{r_x} \, n_{x,0})^{\alpha_m} (2^{r_t} \, n_{t,0})^{\beta_m}. \tag{5.13}$$

Having defined two new greedy-like refinement strategies S2 and S3, in the next section we compare the performance of these strategies with the existing strategy S1.

Algorithm 5.3a : Maximal error-to-cost refinement

Input: $\boldsymbol{m}, \boldsymbol{\eta}_m, \boldsymbol{\eta}_x, \boldsymbol{\eta}_t, tol, s_x, s_t, \phi$

Same as Algorithm 5.2a, replacing lines 2, 9 with

$b_j, z_j \leftarrow$ MAXERRORTOCOSTRATIO$(m, r_{m,j}, r_{x,j}, r_{t,j}, \eta_{m,j}, \eta_{x,j}, \eta_{t,j}, s_x, s_t)$

Output: $\boldsymbol{r}_m, \boldsymbol{r}_x, \boldsymbol{r}_t$

Algorithm 5.3b : Maximal pipe error-to-cost ratio

1: **function** MAXERRORTOCOSTRATIO$(m, r_m, r_x, r_t, \eta_m, \eta_x, \eta_t, s_x, s_t)$

Lines 2-9 same as Algorithm 5.2b

10: **if** $m_c \neq 1$ **then**

11: $\Delta c_m \leftarrow F_c(m_c - 1, r_x, r_t) - F_c(m_c, r_x, r_t)$

12: **end if**

13: $\Delta c_x \leftarrow F_c(m_c, r_x + 1, r_t) - F_c(m_c, r_x, r_t)$

14: $\Delta c_t \leftarrow F_c(m_c, r_x, r_t + 1) - F_c(m_c, r_x, r_t)$

15: $[b, z] = \texttt{max}\{\Delta\eta_m/\Delta c_m, \Delta\eta_x/\Delta c_x, \Delta\eta_t/\Delta c_t\}$

16: **return** b, z

17: **end function**

Table 5.1: Cost functional constants in (5.12), (5.13).

m	C_m	α_m	β_m
1	$8.45 \cdot 10^{-5}$	0.952	0.937
2	$1.06 \cdot 10^{-4}$	0.908	0.925
3	$5.49 \cdot 10^{-5}$	0.694	0.857

5.4 Numerical Results

In this section we numerically test the performance of the three refinement strategies given in Section 5.3. A synthetic experiment on an abstract gas network is conducted in Section 5.4.1 and an application of the algorithms to the numerical simulation of a realistic gas network is presented in Section 5.4.2.

5.4.1 Synthetic Experiment

Let us consider an abstract gas network that is given by its number of pipes N_p. On this network we perform a synthetic experiment in order to test and compare the three refinement strategies given in Section 5.3. The experiment is conducted by first drawing random samples of initial discretization and model errors $\boldsymbol{\eta}_m, \boldsymbol{\eta}_x, \boldsymbol{\eta}_t \in \mathbb{R}^{N_p}$ and initial numbers of discretization nodes $\boldsymbol{n}_x, \boldsymbol{n}_t \in \mathbb{N}^{N_p}$ from probability distributions. Then, for every sample, the three algorithms are executed using the approximate error reductions in (5.10) to update the errors. The computational simulation cost after applying the resulting refinement scheme is computed using the functional in (5.13) for every sample and strategy. Finally, the mean of the computational cost values over all samples is computed for every strategy. Each error sample represents the evaluation of the error estimators in (5.6) on a specific but unknown network configuration of N_p pipes. Thus, the abstract network setting enables us to consider many possible pipe network configurations by drawing a large number of error samples. It also enables us to execute the three algorithms a large number of times with a low computational cost, since the need for actual gas flow simulations within the network is circumvented.

We test the performance of the three refinement strategies on 10^4 random samples of error distributions $\boldsymbol{\eta}_m, \boldsymbol{\eta}_x, \boldsymbol{\eta}_t \in \mathbb{R}^{12}$ in a network of $N_p = 12$ pipes. The initial number of space and time discretization nodes $n_{x,j}$, $n_{t,j}$ are randomly chosen from the interval $[100, 200]$ for every pipe j. All models are set to the most simple model M3 in the beginning. The error reduction upon model refinement also takes into account the introduction or increase of the spatial and temporal errors; see (5.10a). This requires that the spatial and temporal errors are small when compared to the model error. Hence, for the experiment, the initial model errors are drawn from the distribution $\mathcal{U}[0,1]$, where $\mathcal{U}[a,b]$ denotes a uniform probability distribution on the interval $[a,b]$. The initial spatial and temporal discretization errors are drawn from the distribution

$\mathscr{U}[0,0.2]$. The model and discretization error estimators η after increasing the number of refinements r by one are given in (5.11), where $\Delta\eta$ is given in (5.10) with $F_m(3,2)=3/4$, $F_m(2,1)=1/4$. We choose $s_x=2, s_t=1$, since these are the convergence orders of the implicit box scheme in (5.2). The parameter $\kappa=1/3$ for strategy 1 is chosen such that all three error types have an equal fraction of the network tolerance. Strategies 2 and 3 are tested for a fraction $\phi\in\{0.8,0.9,1\}$ of the maximal best option. The strategies work with a relative error tolerance of $tol=10^{-1}$ with a target functional value $M(\boldsymbol{u}^h)=2.5\cdot N_p=30$. Hence, we require for the total network simulation error that

$$\Big|\sum_{j\in\mathscr{J}_p}(\eta_{m,j}+\eta_{x,j}+\eta_{t,j})\Big| < tol|M(\boldsymbol{u}^h)|=3.$$

Each strategy returns a refinement scheme which brings the simulation error below the network tolerance. The goal is to have a low computational cost. The mean of the total computational cost values in CPU seconds over 10^4 samples is shown in Table 5.2 for every refinement strategy. We also show the percentage savings in mean total computational cost of the strategies with respect to strategy 1. We denote the strategies as S1–S3. The subscripts $1,2,3$ refer to $\phi=0.8,0.9,1$, respectively. We observe that strategies S2 and S3 have a percentage saving of over 77% with respect to S1 for all values of $\phi\in\{0.8,0.9,1\}$. Among the different values, $\phi=1$ performs best for both S2 and S3.

In this experiment we find that by working with a greedy-like strategy for error control, an adaptive process can reduce the computational cost significantly. Furthermore, accounting for the computational cost explicitly in our estimates, we find even better refinement schemes that result in lower computational costs.

Table 5.2: Mean total computational cost values in CPU seconds for strategies S1–S3 and savings with respect to S1. The subscripts $1,2,3$ denote the different values of $\phi=0.8,0.9,1$, respectively.

Strategy	Mean CPU time [s]	Savings
S1	36.1	-
$S2_1$	8.30	77.0 %
$S2_2$	8.04	77.7 %
$S2_3$	7.72	78.6 %
$S3_1$	7.64	78.8 %
$S3_2$	7.39	79.5 %
$S3_3$	7.12	80.3 %

5.4.2 Application to a Realistic Network Simulation

We now apply the three different strategies to a simulation of a gas supply network, which is shown in Figure 5.3. The considered network consists of

twelve pipes (P01–P12, with lengths between 30 km and 100 km), two sources (S01–S02), four consumers (C01–C04), three compressor stations (Comp01–Comp03) and one control valve (CV01). Starting with stationary initial data, the boundary conditions and the control for the compressor stations and the control valve are time-dependent. The simulation time is 4 hours. The target functional $M(\boldsymbol{u})$ is given by the total fuel gas consumption of the three compressors and the error estimators are evaluated using a dual weighted residual method; see Section 5.2.2. The simulation is performed using the software *ANACONDA*; cf. [65, 66].

Remark. For the strategies proposed in Section 5.3, the temporal error

$$\eta_t = \sum_{j \in \mathscr{J}_p} \eta_{t,j},$$

cf. (5.5), is considered individually for each pipe. In the implementation of *ANACONDA*, however, it is only computed globally. In order to get a local temporal error and hence to fit into the setting, we distribute the temporal error uniformly among the pipes. If the time stepsize has to be refined in a single pipe following one of the strategies above, then it will be refined globally and the temporal error estimators of all pipes are updated.

A reference solution was computed using model M1 and a very fine spatial-temporal discretization with approximately 24 million degrees of freedom in space and time (DOF-ST). The simulation was performed using the strategies from Section 5.3 with a relative tolerance of $tol = 10^{-4}$ and with a conventional modeling using the most accurate model and a uniform space and time discretization with 360 000 DOF-ST. Note that with the conventional modeling, we did not estimate any model or discretization errors and hence did not gain any information about the accuracy of the solution. Table 5.3 shows the relative errors of the simulations compared to the reference solution, the total CPU

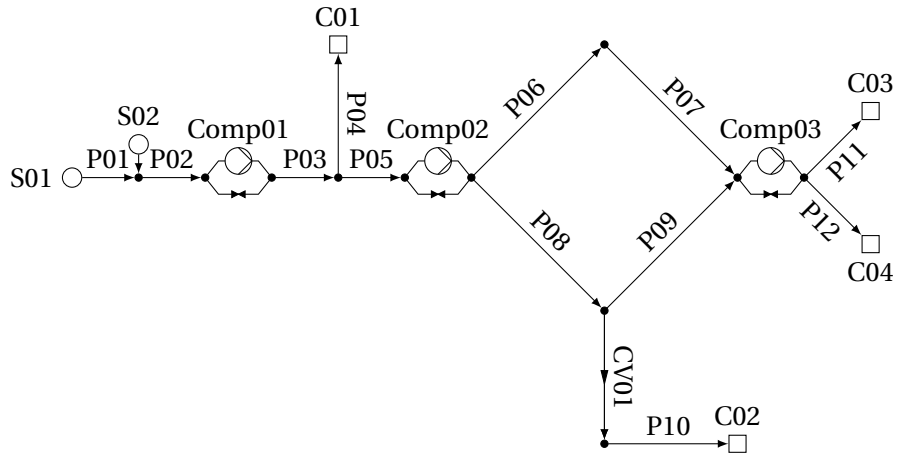

Figure 5.3: Gas supply network with compressor stations and a control valve.

Table 5.3: Relative error ($tol = 10^{-4}$) and computational cost (in s) of a network simulation using strategies S1–S3 and savings with respect to a conventional modeling. The subscripts $1,2,3$ denote the different values of $\phi = 0.8, 0.9, 1$, respectively.

Strategy	Rel. error	CPU time	DOF-ST	M1/M2/M3 [%]	Savings
S1	$1.38 \cdot 10^{-5}$	7.53	49 700	100 / 0 / 0	73.3 %
$S2_1$	$3.73 \cdot 10^{-5}$	2.42	11 300	92 / 0 / 8	91.4 %
$S2_2$	$3.09 \cdot 10^{-5}$	2.27	10 500	92 / 0 / 8	92.0 %
$S2_3$	$3.09 \cdot 10^{-5}$	2.29	10 500	92 / 0 / 8	91.9 %
$S3_1$	$5.08 \cdot 10^{-5}$	3.12	11 700	83 / 17 / 0	88.9 %
$S3_2$	$5.19 \cdot 10^{-5}$	2.83	12 900	100 / 0 / 0	90.0 %
$S3_3$	$5.10 \cdot 10^{-5}$	2.83	11 700	92 / 8 / 0	90.0 %
conventional	$4.57 \cdot 10^{-5}$	28.2	359 000	100 / 0 / 0	-
reference	-	1013	23 900 000		

time, the degrees of freedom in space and time (DOF-ST), the models used (in percent), and the percentage savings of the strategies S1 to S3 in relation to the conventional modeling.

We see that the relative error of the Strategies S1 to S3 are in a similar range as of the simulation using the conventional modeling. However, due to the adaptive error control, the DOF-ST are reduced significantly. We see that the results of Strategies S2 and S3 are in a similar range and that these strategies gain an additional saving of 15 % to 20 % as compared to strategy S1. Regarding the synthetic experiment in Section 5.4.1, this means that the savings with respect to S1 are in the range of 60 % to 70 %. The choice of the parameter $\phi \in \{0.8, 0.9, 1.0\}$, however, does not seem to have a significant influence on the saving. Moreover, the *maximal error-to-cost* strategy S3 does not result in a larger saving of CPU time. What is noticeable is that the relative errors of the strategies S2 and S3 are closer to the proposed relative tolerance, which shows that they are not as restrictive as the *individual tolerances* strategy S1.

5.5 Summary of Chapter 5

In this chapter we address the problem of automatic error control for large scale gas flow simulations that use a model hierarchy. The simulation needs to be reliable, i.e., keeping the total relative error below a specified tolerance, while retaining low computational costs. The problem of finding an optimal refinement strategy is a generalization of the knapsack problem. We present three strategies for adaptive simulation error control via spatial and temporal discretization and model refinements. The strategy *individual tolerances*, which is currently implemented in *ANACONDA*, sets a uniform tolerance for each error type and each pipe, *maximal error refinement* iteratively chooses those refinements that result in the largest error reduction and has a network

overview, and *maximal error-to-cost refinement* also accounts for the increase in computational cost inflicted by the refinement.

We constructed a synthetic experiment to test the three strategies on many different network configurations. From this experiment we find that the two greedy-like strategies significantly reduce the computational cost as compared to the *individual tolerances* strategy. This result is largely reflected in an actual gas flow simulation using *ANACONDA* for a 12 pipe network including compressor stations and a control valve. Especially when the simulation process is a key component in a gas flow optimization problem, the greedy-like refinement strategies lead to considerable computational savings without compromising on the simulation accuracy.

Chapter 6

Model and Discretization Error Adaptivity within Stationary Gas Transport Optimization

6.1 Introduction

In this chapter we discuss the minimization of operation costs for natural gas transport networks based on a model hierarchy, see [36, 54], which ranges from detailed models based on instationary partial differential equations with temperature dependence to highly simplified algebraic equations. The detailed models are necessary to achieve a good understanding of the system state, but in many practical optimization applications only the stationary algebraic equations—or even further simplifications like piecewise linearizations as in [47, 48, 87]—are used in order to reduce the high computational effort of evaluating the state of the system with the more sophisticated models. However, it is then unclear how good the true state is approximated by these simplified models and error bounds are typically not available in this context; see the chapter [60] in [64] for a more detailed discussion of this issue. Recently, in [93], a detailed error and perturbation analysis has been developed for several components in the model hierarchy and it has been shown how the more detailed model components can be used to estimate the error obtained in the simplified models.

Here, we use these error estimates from the model hierarchy together with classical error estimate grid adaptation techniques for the space discretization within an optimization method to control the error adaptively by switching to more detailed models or finer discretizations if necessary. Moreover, our adaptive method also allows to locally switch back to coarser models or to coarser discretizations if they are sufficiently accurate with respect to the local flow situation. Our new approach can, in general, be used for the entire model hierarchy by also using space-time grid adaptation. However, to keep things simple and to illustrate the functionality of the new adaptive approach, we will use three stationary isothermal models from the hierarchy in [36].

Using adaptive techniques to achieve a trade-off between computational efficiency and accuracy by using adaptive discretization methods in the context of optimization and optimal control problems is an important research topic, in particular in the context of real-time optimal control of constrained dynamical systems, see, e.g., [14, 31, 32, 78], or in the context of optimal control of problems constrained by partial differential equations; see, e.g., [6, 68, 70, 71]. We extend these ideas and combine adaptive grid refinement and model selection in a model hierarchy in the context of nonlinear optimization problems. We also theoretically analyze the new algorithm. First promising numerical results for such an approach were presented in [89, 90].

The chapter is structured as follows. The models used in this chapter are described in Sect. 6.2 together with a simple first-order Euler method for the space discretization. In Sect. 6.3 we introduce model and discretization error estimators, which are used in Sect. 6.4 to derive an adaptive model and discretization control algorithm for the nonlinear optimization of gas transport networks that, in the end, delivers solutions that satisfy prescribed error tolerances. Numerical results are presented in Sect. 6.5 and a summary of the chapter is given in Sect. 6.6.

6.2 Problem Description, Modeling Hierarchy, and Discretizations

In this section we introduce the problem of operation cost minimization for natural gas transport networks. We present our overall model of a gas transport network involving continuous nonlinear models describing a stationary flow for all the considered network elements. Since the majority of the elements are pipes, our focus lies on the precise and physically accurate modeling of these pipes. The typical models for the pipe flow are nonlinear instationary partial differential equations (PDEs) on a graph and their appropriate space-time discretizations. To address the fact that the behavior of the flow and the accuracy of the model may vary significantly in different regions of the network, we discuss a small part of the complete model hierarchy of instationary models, see [36], where the lower level models in the hierarchy are simplifications of the higher level models. Which model is most appropriate to obtain a computationally tractable, adequately accurate, and finite-dimensional approximation depends on the task that needs to be performed with the model.

Our modeling approach is based on the following physical assumptions. First, we only consider a stationary gas flow, i.e., we neglect all time effects of gas dynamics, so that we have ordinary differential equations (ODEs) in space instead of systems of PDEs on a graph. Second, we assume an isothermal regime, i.e., we neglect all effects arising from changes in the gas temperature.

These assumptions are taken carefully such that we still obtain physically meaningful solutions and such that we are still able to derive and analyze an adaptive model and discretization control algorithm—without unnecessarily

overloading the models with all technical details of the application that may distract us from the main mathematical ideas.

6.2.1 The Network

We model the gas transport network by a directed and connected graph $G = (V, A)$. The node set is made up of entry nodes V_+, where gas is supplied, of exit nodes V_-, where gas is discharged, and of inner nodes V_0, i.e., we have $V = V_+ \cup V_- \cup V_0$. The set of arcs in our models comprises pipes A_{pi} and compressor machines A_{cm}, i.e., we have $A = A_{\mathrm{pi}} \cup A_{\mathrm{cm}}$.

Real-world gas transport networks contain many other element types like (control) valves, short cuts, or resistors. For detailed information on modeling these devices, see [46] in general or [89, 90] for a focus on nonlinear programming (NLP) type models. However, we restrict ourselves to models with pipes and compressors in order to streamline the presentation of our basic ideas and methods, and to show in a prototypical way that our approach of space discretization and model adaptivity leads to major accuracy and efficiency improvements.

As basic quantities we introduce gas pressure variables p_u at all nodes $u \in V$ and mass flow variables q_a at all arcs $a \in A$ of the network. Both types of variables are bounded due to technical constraints on the pipes, i.e.,

$$p_u \in [\underline{p}_u, \overline{p}_u] \quad \text{for all } u \in V, \tag{6.1a}$$

$$q_a \in [\underline{q}_a, \overline{q}_a] \quad \text{for all } a \in A. \tag{6.1b}$$

All other required quantities are introduced where they are used first.

6.2.2 Nodes

In stationary gas network models, the nodes $u \in V$ are modeled by a mass balance equation, i.e., we have the constraint

$$\sum_{a \in \delta^{\mathrm{in}}(u)} q_a - \sum_{a \in \delta^{\mathrm{out}}(u)} q_a = q_u \quad \text{for all } u \in V, \tag{6.2}$$

where for ingoing arcs we use the notation

$$\delta^{\mathrm{in}}(u) := \{a \in A : \text{there exists } w \in V \text{ and } a = (w, u)\}$$

and for outgoing arcs

$$\delta^{\mathrm{out}}(u) := \{a \in A : \text{there exists } w \in V \text{ and } a = (u, w)\}.$$

Moreover, q_u models the supplied or discharged mass flow at the corresponding node, i.e., we have

$$q_u \begin{cases} \geq 0 & \text{for all } u \in V_-, \\ \leq 0 & \text{for all } u \in V_+, \\ = 0 & \text{for all } u \in V_0. \end{cases}$$

6.2.3 Pipes

Isothermal gas flow through cylindrical pipes is described by the Euler equations for compressible fluids,

$$\frac{\partial \rho}{\partial t} + \frac{1}{A}\frac{\partial q}{\partial x} = 0, \tag{6.3a}$$

$$\frac{1}{A}\frac{\partial q}{\partial t} + \frac{\partial p}{\partial x} + \frac{1}{A}\frac{\partial (q v)}{\partial x} = -\lambda(q)\frac{|v|v}{2D}\rho - g\rho h', \tag{6.3b}$$

see, e.g., [45, 72] for a detailed discussion. Here and in what follows, ρ is the gas density, v is its velocity, $\lambda = \lambda(q)$ is the friction term, A denotes the cross-sectional area of the pipe, h' is its slope, and D is the diameter of the pipe. Furthermore, g is the acceleration due to gravity, t is the temporal coordinate, and $x \in [0, L]$ is the spatial coordinate with L being the length of the pipe. Equation (6.3a) is called the continuity equation and (6.3b) the momentum equation. Since we only consider the stationary case, all partial derivatives with respect to time vanish and we obtain the simplified stationary model

$$\frac{1}{A}\frac{\partial q}{\partial x} = 0, \tag{6.4a}$$

$$\frac{\partial p}{\partial x} + \frac{1}{A}\frac{\partial (q v)}{\partial x} = -\lambda(q)\frac{|v|v}{2D}\rho - g\rho h'. \tag{6.4b}$$

Thus, the continuity equation in its stationary variant simply states that the mass flow along the pipe is constant, i.e., $q(x) \equiv q = \text{const}$ for all $x \in [0, L]$.

To simplify the stationary momentum equation (6.4b), we consider two more model equations. First, the equation of state

$$p = \rho c^2 \quad \text{with} \quad c = \sqrt{R_s T z},$$

where c is the speed of sound, R_s is the specific gas constant, and z is the compressibility factor. The second model is the relation of gas mass flow, density, and velocity given by

$$q = A\rho v.$$

Substituting both these models into (6.4b), we obtain

$$\frac{\partial p}{\partial x}\left(1 - \frac{q^2}{A^2}\frac{c^2}{p^2}\right) = -\frac{\lambda c^2}{2A^2 D p}|q|q - \frac{g h'}{c^2}p, \tag{M_1}$$

i.e., the stationary momentum equation written in dependence of the gas pressure $p = p(x)$, $x \in [0, L]$, and the mass flow q.

A simplified version of the latter equation can be obtained by ignoring the ram pressure term

$$\frac{1}{A}\frac{\partial (q v)}{\partial x},$$

in (6.4b), i.e., the total pressure exerted on the gas by the pipe wall, or, equivalently, the term

$$-\frac{q^2}{A^2}\frac{c^2}{p^2}\frac{\partial p}{\partial x} \tag{6.5}$$

in (M_1). For a discussion of this simplification step, see [100]. Neglecting the ram pressure term (6.5) yields

$$\frac{\partial p}{\partial x} = -\frac{\lambda c^2}{2A^2 D p}|q|q - \frac{g h'}{c^2} p. \tag{M_2}$$

Finally, one may also neglect gravitational forces, i.e., set the term $g h' p/c^2$ to 0 and obtain

$$\frac{\partial p}{\partial x} = -\frac{\lambda c^2}{2A^2 D p}|q|q. \tag{M_3}$$

Analytical solutions for the models (M_1)–(M_3) are only rarely known; see, e.g., [51, 52, 89]. Thus, in order to obtain finite-dimensional nonlinear optimization models, we discretize these differential equations in space. Applying, e.g., the implicit Euler method we obtain

$$\frac{p_k - p_{k-1}}{h}\left(1 - \frac{q^2}{A^2}\frac{c^2}{p_k^2}\right) = -\frac{\lambda c^2}{2A^2 D p_k}|q|q - \frac{g h'}{c^2} p_k, \qquad k = 1, \dots, n, \tag{D_1}$$

$$\frac{p_k - p_{k-1}}{h} = -\frac{\lambda c^2}{2A^2 D p_k}|q|q - \frac{g h'}{c^2} p_k, \qquad k = 1, \dots, n, \tag{D_2}$$

$$\frac{p_k - p_{k-1}}{h} = -\frac{\lambda c^2}{2A^2 D p_k}|q|q, \qquad k = 1, \dots, n, \tag{D_3}$$

where $p_k = p(x_k)$ and $\Gamma = \{x_0, x_1, \dots, x_n\}$ is an equidistant spatial discretization of the pipe with constant stepsize $h = x_k - x_{k-1}$ and $x_0 = 0, x_n = L$. Of course, one could also apply a higher-order Runge–Kutta method, which would allow a larger stepsize and would thus reduce the computational cost.

These discretizations extend the model hierarchy (M_1)–(M_3) for the Euler equations by infinitely many models that are parameterized by the discretization stepsize h applied in (D_1)–(D_3). In summary, we obtain the pipe model hierarchy of stationary Euler equations depicted in Figure 6.1.

6.2.4 Compressors

Compressor machines $a = (u, w) \in A_{\mathrm{cm}}$ increase the inflow gas pressure to a higher outflow pressure, i.e., they can be described in a simplified way by

$$p_w = p_u + \Delta_a, \quad \Delta_a \in [0, \bar{\Delta}_a] \quad \text{for all } a \in A_{\mathrm{cm}}. \tag{6.6}$$

Moreover, for simplicity, we assume that we are given cost coefficients $\omega_a \geq 0$ for every compressor $a \in A_{\mathrm{cm}}$ that convert pressure increase to compression cost. Of course, this is an extremely coarse approximation of a compressor machine. An alternative would be to use a simple input-output surrogate model obtained from a realization or system identification of an input-output transfer function; see, e.g., [18]. However, our focus is on an accurate modeling of the gas flow in pipes and on deriving an adaptive model and discretization control algorithm. Model (6.6) allows for setting up a reasonable objective function for our NLPs and is thus appropriate in this work. For more details, see [86, 89, 90] or [46].

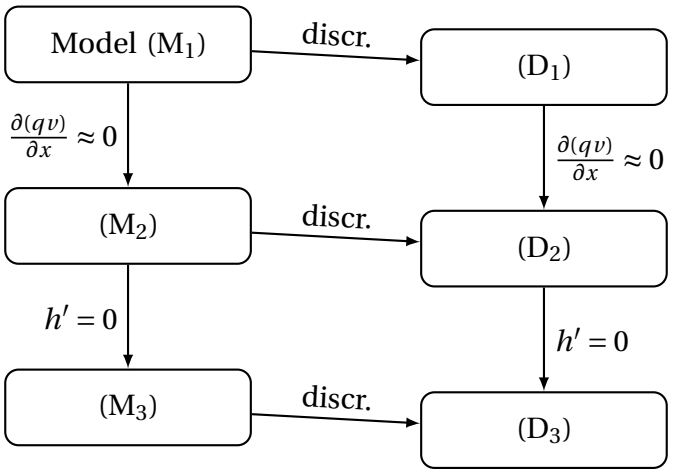

Figure 6.1: Pipe model hierarchy based on the Euler equations. The space continuous models are positioned in the left column and their space discretized counterparts are positioned in the right column.

6.2.5 The Optimization Problem

We will use the adaptive model and discretization control algorithm in the context of the following nonlinear ODE-constrained optimization problem

$$\begin{aligned}
\min \quad & \sum_{a \in A_{\mathrm{cm}}} \omega_a \Delta_a && \text{(6.7a)}\\
\text{s.t.} \quad & \text{variable bounds (6.1)}, && \text{(6.7b)}\\
& \text{mass balance (6.2)}, && \text{(6.7c)}\\
& \text{compressor model (6.6) for all } a \in A_{\mathrm{cm}}, && \text{(6.7d)}\\
& \text{pipe model } (\mathrm{M}_1) \text{ for all } a \in A_{\mathrm{pi}}, && \text{(6.7e)}
\end{aligned}$$

where our objective function models the cost for the compressor activity that is constrained by an infinite-dimensional description of the gas flow in pipes. Problem (6.7) is a classical nonlinear optimal control problem. A typical approach to solve such problems in practice is the first-discretize-then-optimize paradigm; see, e.g., [13]. In this setting, one replaces the ODE constraints by finite sets of nonlinear constraints that arise, e.g., from implicit Euler discretizations like (D_1) for (M_1). Moreover, practical experience suggests that for the evaluation of the constraints, it is often not required to apply the most accurate model like (D_1) with a small stepsize for every pipe in the network. Instead, in many situations it is sufficient to use simplified models like (D_2) and (D_3) with a coarse grid, which then typically yields fast execution times for the evaluation of the constraint functions.

To this end, we define discretized problem variants of Problem (6.7) by specifying the model level $\ell_a \in \{1,2,3\}$ for every arc $a \in A_{\mathrm{pi}}$ (i.e., the discretized model (D_1), (D_2), or (D_3), respectively) together with a stepsize h_a. This yields

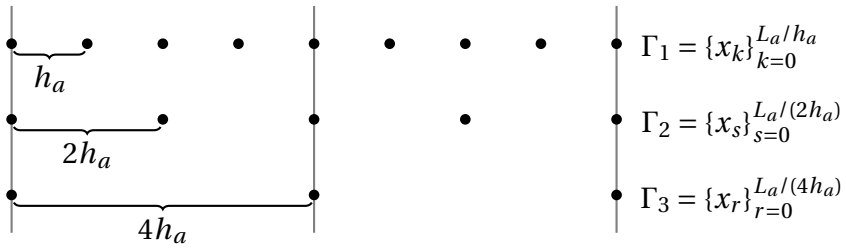

Figure 6.2: Overview of the three considered discretization grids Γ_1, Γ_2, and Γ_3 with gridpoints x_k, x_s, and x_r and stepsizes h_a, $2h_a$, and $4h_a$, respectively. The vertical lines represent the evaluation grid Γ_3 for the error estimators in (6.9) and (6.10).

the family of finite-dimensional NLPs

$$\begin{aligned}
\min \quad & \sum_{a \in A_{\mathrm{cm}}} \omega_a \Delta_a && \text{(6.8a)}\\
\text{s.t.} \quad & \text{variable bounds (6.1)}, && \text{(6.8b)}\\
& \text{mass balance (6.2)}, && \text{(6.8c)}\\
& \text{compressor model (6.6) for all } a \in A_{\mathrm{cm}}, && \text{(6.8d)}\\
& \text{pipe model } (\mathrm{D}_{\ell_a}) \text{ with stepsize } h_a \text{ for all } a \in A_{\mathrm{pi}}. && \text{(6.8e)}
\end{aligned}$$

Note that the constraints (6.7b)–(6.7d) in the infinite-dimensional problem are exactly the same as constraints (6.8b)–(6.8d) in the family of discretized problems.

6.3 Error Estimators

In this section we introduce a first-order estimate for the error between the most detailed infinite-dimensional and an arbitrary space-discretized model. This error estimator is obtained as the sum of a discretization and a model error estimator. Since we consider the stationary case, mass flows in pipes are constant in the spatial dimension. This is why we base our error estimators on the differences of the pressures $p(x)$ for different models and discretizations.

Suppose that for a given pipe $a \in A_{\mathrm{pi}}$, the model level $\ell_a \in \{1,2,3\}$ with discretization stepsize h_a is currently used for the computations. The overall solution of the optimization problem for the entire network, also including pressure increases in compressors etc., is denoted by y and contains the discretized pressure distributions of the separate pipes $a \in A_{\mathrm{pi}}$, which we denote by $p^{\ell_a}(x_k; h_a)$ with discretization grid $\Gamma_1 = \{x_k\}_{k=0}^{L_a/h_a}$ obtained by using the stepsize h_a. We now compute an estimate for the error between the solution of the currently used model (D_{ℓ_a}) and the solution of the reference model (M_1). Let the solution of model (M_1) for pipe $a \in A_{\mathrm{pi}}$ be denoted by $\hat{p}(x)$ with $x \in [0, L_a]$.

Furthermore, let the solutions of Model (D_1) with discretization grids $\Gamma_2 = \{x_s\}_{s=0}^{L_a/(2h_a)}$ and $\Gamma_3 = \{x_r\}_{r=0}^{L_a/(4h_a)}$ using stepsizes $2h_a$ and $4h_a$, be denoted

by $p^1(x_s;2h_a)$ and $p^1(x_r;4h_a)$, respectively. Due to the larger stepsize, the computation of these two solutions is in general less expensive than computing a solution of Model (D_{ℓ_a}) on the grid Γ_1. Since the discretization grid Γ_3 is the coarsest grid and all computed pressure profiles can be evaluated on this grid, Γ_3 is called the evaluation grid. This grid is used in the definitions of the following error estimators. The considered discretization grids and the evaluation grid are depicted in Figure 6.2.

For a pipe $a \in A_{\mathrm{pi}}$, let the discretization error estimator be defined by

$$\eta_{\mathrm{d},a}(y) := \|p^1(x_r;2h_a) - p^1(x_r;4h_a)\|_\infty \tag{6.9}$$

and let the model error estimator be defined by

$$\eta_{\mathrm{m},a}(y) := \|p^1(x_r;2h_a) - p^{\ell_a}(x_r;h_a)\|_\infty. \tag{6.10}$$

Here,

$$p^{\ell_a}(x_r;h_a) = [p^{\ell_a}(x_0;h_a),\dots,p^{\ell_a}(x_n;h_a)]^\top, \quad n = L_a/(4h_a),$$

denotes the solution of Model (D_{ℓ_a}) computed with stepsize h_a that is evaluated at the gridpoints x_r, i.e., on the grid Γ_3. If $\ell_a = 1$, i.e., if the considered solution already corresponds to the most accurate model, then we set the model error to zero, i.e., $\eta_{\mathrm{m},a}(y) = 0$. Furthermore, let the overall error estimator $\eta_a(y)$ for a pipe $a \in A_{\mathrm{pi}}$ be defined to be a first-order upper bound for the maximum error between the solutions of models (M_1) and (D_{ℓ_a}) at gridpoints x_r with stepsize $4h_a$. Thus, we have

$$\begin{aligned} &\|\hat{p}(x_r) - p^{\ell_a}(x_r;h_a)\|_\infty \\ &\le \|\hat{p}(x_r) - p^1(x_r;2h_a)\|_\infty + \|p^1(x_r;2h_a) - p^{\ell_a}(x_r;h_a)\|_\infty \\ &\doteq \eta_{\mathrm{d},a}(y) + \eta_{\mathrm{m},a}(y) =: \eta_a(y), \end{aligned} \tag{6.11}$$

where $\doteq$ denotes a first-order approximation in h_a, see [92, page 420], and we use that the implicit Euler method has convergence order 1. The error estimator $\eta_a(y)$ is the absolute counterpart of the componentwise relative error estimator given in [93]. An overview of the considered models in this section together with the considered stepsizes is depicted in Figure 6.3.

We close this section with a remark on the computation of the discretization error estimator in (6.9). A straightforward way is to solve Model (D_1) once with stepsize $2h_a$ and once again with stepsize $4h_a$ for every $a \in A_{\mathrm{pi}}$. Another possibility would be to use an embedded Runge–Kutta method, see, e.g., [53], which in general saves computational cost due to the reduced number of function evaluations.

6.4 The Grid and Model Adaptation Algorithm

In this section we present and analyze an algorithm that adaptively switches between the model levels in the hierarchy of Figure 6.1 and adapts discretization stepsizes in order to find a convenient trade-off between physical accuracy

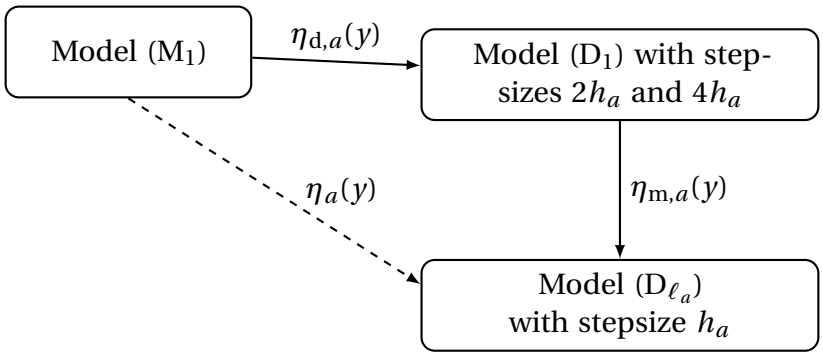

Figure 6.3: Overview of the models and stepsizes used for the computation of the overall error estimator $\eta_a(y)$ between models (M_1) and (D_{ℓ_a}) in (6.11). Here, for a pipe a, $\eta_{\mathrm{d},a}(y)$ is the discretization error estimator and $\eta_{\mathrm{m},a}(y)$ is the model error estimator.

and computational costs. To this end, the algorithm iteratively solves NLPs and initial value problems (IVPs). Solutions of the latter are used to evaluate the error estimators discussed in the last section and to decide on the model levels and the discretization stepsizes for the next NLP.

Consider a single NLP of the sequence of NLPs that are solved during the algorithm and assume that pipe $a \in A_{\mathrm{pi}}$ is modeled using model (D_{ℓ_a}) and stepsize h_a. Let the solution of this NLP be denoted by y. According to the last section, the overall model and discretization error estimator for this pipe is given by $\eta_a(y)$ as defined in (6.11). Thus, it is given by the error estimator between the solutions of the most accurate model (M_1) and the current model (D_{ℓ_a}).

The overall goal of our method is to compute a solution of a member of the family of discretized problems (6.8) for which it is guaranteed that this solution has an estimated average error per pipe with respect to the reference model (M_1), that is less than an a-priorily given tolerance $\varepsilon > 0$. This leads us to the following definition:

Definition 6.1 (ε-feasibility)**.** Let $\varepsilon > 0$ be given. We say that a solution y of problem (6.8) with discretized models (D_{ℓ_a}), $\ell_a \in \{1,2,3\}$, and stepsizes h_a for the pipes $a \in A_{\mathrm{pi}}$ is *ε-feasible* with respect to the reference problem (6.7) if

$$\frac{1}{|A_{\mathrm{pi}}|} \sum_{a \in A_{\mathrm{pi}}} \eta_a(y) \leq \varepsilon.$$

The remainder of this section is organized as follows. Sect. 6.4.1 introduces rules about how the model levels and discretization stepsizes are modified. The strategies for marking pipes for model or grid adaptation are explained in Sect. 6.4.2. The adaptive model and discretization control algorithm is introduced in Sect. 6.4.3, together with a theorem for the finite termination of the algorithm. Finally, some remarks regarding the adaptive control algorithm are given in Sect. 6.4.4.

6.4.1 Model and Discretization Adaptation Rules

Before we present and discuss the overall adaptive model control algorithm we have to

1. describe the mechanisms of switching up or down pipe model levels as well as that of refining and coarsening the discretization grids, and
2. discuss our marking strategy that determines the arcs on which the model or grid should be adapted.

We start with the first issue and follow the standard PDE grid adaptation technique; see, e.g., [22, 23, 42] or [17]. The general strategy is as follows. We switch up one level in the model hierarchy if this yields an error reduction that is larger than ε; otherwise, we switch up to the most accurate discretized model (D_1). Hence, for pipe $a \in A_{\mathrm{pi}}$ we have the rule

$$\ell_a^{\mathrm{new}} = \begin{cases} \ell_a - 1, & \text{if } \eta_{\mathrm{m},a}(y;\ell_a) - \eta_{\mathrm{m},a}(y;\ell_a - 1) > \varepsilon, \\ 1, & \text{otherwise,} \end{cases} \tag{6.12}$$

for switching up levels in the model hierarchy. We apply this rule because it is possible that the effects of neglecting the ram pressure term (which is the difference between model levels $\ell = 1$ and $\ell = 2$) and neglecting gravitational forces for non-horizontal pipes (which is the difference between model levels $\ell = 2$ and $\ell = 3$) balance each other out in the computation of the pressure profile of model (D_3). In this case, switching from model (D_3) to (D_2) would increase the model error, which is why we switch from (D_3) to (D_1) directly.

A discretization grid refinement or coarsening with a factor $\gamma > 1$ is defined by taking the new stepsize as

$$h_a^{\mathrm{new}} := \begin{cases} h_a/\gamma, & \text{for a grid refinement,} \\ \gamma h_a, & \text{for a grid coarsening.} \end{cases} \tag{6.13}$$

For a discretization scheme of order β it is well-known that a first-order approximation for the discretization error in $x \in [0, L_a]$ is given by $e_{\mathrm{d},a}(x) \doteq c(x) h_a^{\beta}$, where $c(x)$ is independent of h_a; see, e.g., [92]. From this, it follows that the new discretization error after a grid refinement or coarsening can be written as

$$e_{\mathrm{d},a}^{\mathrm{new}}(x) \doteq (h_a^{\mathrm{new}}/h_a)^{\beta} e_{\mathrm{d},a}(x).$$

Since the implicit Euler method has convergence order $\beta = 1$, with h_a^{new} in (6.13) and $\gamma = 2$, for the new discretization error estimator after a grid refinement or coarsening, it holds that

$$\eta_{\mathrm{d},a}^{\mathrm{new}}(y) \doteq \begin{cases} \eta_{\mathrm{d},a}(y)/2, & \text{for a grid refinement,} \\ 2\eta_{\mathrm{d},a}(y), & \text{for a grid coarsening.} \end{cases} \tag{6.14}$$

6.4.2 Marking Strategies

We now describe our marking strategies, i.e., how we choose which pipes should be switched up or down in their model level and which pipes should get a refined or coarsened grid. Given marking strategy parameters $\Theta_{\mathrm{d}}, \Theta_{\mathrm{m}} \in [0,1]$, we compute subsets $\mathscr{R}, \mathscr{U} \subseteq A_{\mathrm{pi}}$ such that they are the minimal subsets of arcs that satisfy

$$\Theta_{\mathrm{d}} \sum_{a \in A_{\mathrm{pi}}} \eta_{\mathrm{d},a}(y) \leq \sum_{a \in \mathscr{R}} \eta_{\mathrm{d},a}(y) \tag{6.15}$$

and

$$\Theta_{\mathrm{m}} \sum_{a \in A_{\mathrm{pi}}^{>\varepsilon}} (\eta_{\mathrm{m},a}(y;\ell_a) - \eta_{\mathrm{m},a}(y;\ell_a^{\mathrm{new}})) \leq \sum_{a \in \mathscr{U}} (\eta_{\mathrm{m},a}(y;\ell_a) - \eta_{\mathrm{m},a}(y;\ell_a^{\mathrm{new}})) \tag{6.16}$$

with

$$A_{\mathrm{pi}}^{>\varepsilon} := \{a \in A_{\mathrm{pi}} : \eta_{\mathrm{m},a}(y;\ell_a) - \eta_{\mathrm{m},a}(y;\ell_a^{\mathrm{new}}) > \varepsilon\},$$

where ℓ_a^{new} is given in (6.12). Analogously, given marking strategy parameters $\Phi_{\mathrm{d}}, \Phi_{\mathrm{m}} \in [0,1]$ and $\tau \geq 1$, we compute $\mathscr{C}, \mathscr{D} \subseteq A_{\mathrm{pi}}$ such that they are the maximal subsets of arcs that satisfy

$$\Phi_{\mathrm{d}} \sum_{a \in A_{\mathrm{pi}}} \eta_{\mathrm{d},a}(y) \geq \sum_{a \in \mathscr{C}} \eta_{\mathrm{d},a}(y) \tag{6.17}$$

and

$$\Phi_{\mathrm{m}} \sum_{a \in A_{\mathrm{pi}}^{<\varepsilon}(\tau)} (\eta_{\mathrm{m},a}(y;\ell_a^{\mathrm{new}}) - \eta_{\mathrm{m},a}(y;\ell_a)) \geq \sum_{a \in \mathscr{D}} (\eta_{\mathrm{m},a}(y;\ell_a^{\mathrm{new}}) - \eta_{\mathrm{m},a}(y;\ell_a)) \tag{6.18}$$

with

$$A_{\mathrm{pi}}^{<\varepsilon}(\tau) := \{a \in A_{\mathrm{pi}} : \eta_{\mathrm{m},a}(\ell_a^{\mathrm{new}}) - \eta_{\mathrm{m},a}(\ell_a) \leq \tau\varepsilon\}.$$

In (6.18), ℓ_a^{new} is always set to $\min\{\ell_a + 1, 3\}$. For every arc $a \in \mathscr{R}$ ($a \in \mathscr{C}$) we refine (coarsen) the discretization grid by halving (doubling) the stepsize, i.e., we set $\gamma = 2$ in (6.13). We note that these marking strategies are very similar to the greedy strategies on a network described in [34], where those pipes are marked for a spatial, temporal, or model refinement which yield the largest error reduction.

6.4.3 The Algorithm

With these preliminaries we can now state the overall adaptive model and discretization control algorithm for finding an ε-feasible solution of the reference problem (6.7). The formal listing is given in Alg. 6.1.

The algorithm makes use of the safeguard parameter $\mu \in \mathbb{N}$. This parameter ensures that the algorithm performs grid coarsenings and switches down the model level only after applying μ rounds of grid refinements and switching up model levels. It prevents an alternating switching up and down model levels or

an alternating refining and coarsening of the discretization grid. We note that this technique is similar to the use of hysteresis parameters; see, e.g., [77]. By employing this safeguard, we can prove that Alg. 6.1 terminates after a finite number of iterations with an ε-feasible point of the reference model (M_1).

To improve readability, we split the proof of our main theorem into two parts. The first lemma states finite termination at an ε-feasible point if only discretization grid refinements and coarsenings are applied, whereas the second lemma considers the case of switching levels in the model hierarchy only, i.e., with a fixed stepsize for every pipe.

Lemma 6.1. *Suppose that the model level $\ell_a \in \{1,2,3\}$ is fixed for every pipe $a \in A_{\mathrm{pi}}$. Let the resulting set of model levels be denoted by $\mathscr{M}$. Suppose further that $\eta_a(y) = \eta_{d,a}(y)$ holds in* (6.11) *and that every NLP is solved to local optimality. Consider Alg. 6.1 without applying the model switching steps in Lines 11 and 20. Then, the algorithm terminates after a finite number of refinements in Line 12 and coarsenings in Line 21 with an ε-feasible solution with respect to model*

Algorithm 6.1 Adaptive Model and Discretization Control

Input: A full specification of the gas network $G = (V, A)$, a tolerance $\varepsilon > 0$, initial marking strategy parameters $\Theta_{\mathrm{d}}^0, \Theta_{\mathrm{m}}^0, \Phi_{\mathrm{d}}^0, \Phi_{\mathrm{m}}^0 \in [0,1]$, $\tau^0 \geq 1$, and an initial safeguard parameter $\mu^0 \in \mathbb{N}$.

Output: An ε-feasible solution of the reference problem (6.7).

1: Choose an initial model level ℓ_a^0 and a stepsize h_a^0 for every $a \in A_{\mathrm{pi}}$.
2: Solve Problem (6.8) and let y^0 denote the optimal solution.
3: Compute $\eta_a(y^0)$ for every $a \in A_{\mathrm{pi}}$.
4: **if** y^0 is ε-feasible **then**
5: **return** y^0.
6: **end if**
7: Set $k = 1$ and $\Theta_{\mathrm{d}}^k = \Theta_{\mathrm{d}}^0, \Theta_{\mathrm{m}}^k = \Theta_{\mathrm{m}}^0, \Phi_{\mathrm{d}}^k = \Phi_{\mathrm{d}}^0, \Phi_{\mathrm{m}}^k = \Phi_{\mathrm{m}}^0, \mu^k = \mu^0, \tau^k = \tau^0$.
8: **for** $k = 1, 2, \ldots$ **do**
9: **for** $j = 1, \ldots, \mu^k$ **do**
10: Compute the sets $\mathscr{U}_{k,j}, \mathscr{R}_{k,j} \subseteq A_{\mathrm{pi}}$ according to (6.15) and (6.16).
11: Switch up the model level for every pipe $a \in \mathscr{U}_{k,j}$.
12: Refine the discretization grid for every pipe $a \in \mathscr{R}_{k,j}$.
13: Solve Problem (6.8) and let $y^{k,j}$ denote the solution.
14: Compute $\eta_a(y^{k,j})$ for every $a \in A_{\mathrm{pi}}$.
15: **if** $y^{k,j}$ is ε-feasible **then**
16: **return** $y^{k,j}$.
17: **end if**
18: **end for**
19: Compute the sets $\mathscr{D}_k, \mathscr{C}_k \subseteq A_{\mathrm{pi}}$ according to (6.17) and (6.18).
20: Switch down the model level for every pipe $a \in \mathscr{D}_k$.
21: Coarsen the discretization grid for every pipe $a \in \mathscr{C}_k$.
22: Increase $k \leftarrow k+1$ and update parameters $\Theta_{\mathrm{d}}^k, \Theta_{\mathrm{m}}^k, \Phi_{\mathrm{d}}^k, \Phi_{\mathrm{m}}^k, \mu^k, \tau^k$.
23: **end for**

level set $\mathscr{M}$ if there exists a constant $C > 0$ such that

$$\frac{1}{2}\Theta_d^k \mu^k > \Phi_d^k + C \tag{6.19}$$

holds for all k.

Proof. We consider the total discretization error

$$\eta_{\mathrm{d}}(y) = \sum_{a \in A_{\mathrm{pi}}} \eta_{\mathrm{d},a}(y)$$

and show that for every iteration k the difference between the decrease obtained in the inner for-loop and the increase obtained due to the coarsenings applied in Line 21 is positive and uniformly bounded away from zero. In what follows, we only consider a single iteration and drop its index k for better readability.

First, we consider one refinement step in Line 12. Let $\eta_{\mathrm{d},a}^{j-1}$ denote the discretization error before the jth inner iteration and let $\eta_{\mathrm{d},a}^{j}$ denote the discretization error after the jth inner iteration. With this, we have

$$\begin{aligned}
&\sum_{a \in A_{\mathrm{pi}}} \eta_{\mathrm{d},a}^{j-1} - \sum_{a \in A_{\mathrm{pi}}} \eta_{\mathrm{d},a}^{j} \\
&= \sum_{a \in \mathscr{R}_j} \eta_{\mathrm{d},a}^{j-1} + \sum_{a \in A_{\mathrm{pi}} \setminus \mathscr{R}_j} \eta_{\mathrm{d},a}^{j-1} - \sum_{a \in \mathscr{R}_j} \eta_{\mathrm{d},a}^{j} - \sum_{a \in A_{\mathrm{pi}} \setminus \mathscr{R}_j} \eta_{\mathrm{d},a}^{j} \\
&= \sum_{a \in \mathscr{R}_j} \eta_{\mathrm{d},a}^{j-1} - \sum_{a \in \mathscr{R}_j} \eta_{\mathrm{d},a}^{j} \\
&= \sum_{a \in \mathscr{R}_j} \frac{1}{2} \eta_{\mathrm{d},a}^{j-1}
\end{aligned}$$

for every $j = 1, \ldots, \mu$. For the last equality we have used that the implicit Euler method has convergence order 1, which (for small stepsizes h_a) implies $\eta_{\mathrm{d},a}^{j} = \frac{1}{2}\eta_{\mathrm{d},a}^{j-1}$ when we take the new stepsize as half the current stepsize; see (6.14). Summing up over all μ inner iterations we obtain a telescopic sum and finally get an error decrease of

$$\sum_{j=1}^{\mu} \left(\sum_{a \in A_{\mathrm{pi}}} \eta_{\mathrm{d},a}^{j-1} - \sum_{a \in A_{\mathrm{pi}}} \eta_{\mathrm{d},a}^{j} \right) = \sum_{a \in A_{\mathrm{pi}}} \eta_{\mathrm{d},a}^{0} - \sum_{a \in A_{\mathrm{pi}}} \eta_{\mathrm{d},a}^{\mu} = \frac{1}{2} \sum_{j=1}^{\mu} \sum_{a \in \mathscr{R}_j} \eta_{\mathrm{d},a}^{j-1}.$$

We now consider the coarsening step. For this, let $\eta_{\mathrm{d},a}^{\mu}$ denote the discretization error before and $\eta_{\mathrm{d},a}^{\mu+1}$ the discretization error after the coarsening

step in Line 21. Using similar ideas like above we obtain

$$\begin{aligned}
&\sum_{a\in A_{\mathrm{pi}}} \eta_{\mathrm{d},a}^{\mu+1} - \sum_{a\in A_{\mathrm{pi}}} \eta_{\mathrm{d},a}^{\mu} \\
&= \sum_{a\in A_{\mathrm{pi}}\setminus\mathscr{C}} \eta_{\mathrm{d},a}^{\mu+1} + \sum_{a\in\mathscr{C}} \eta_{\mathrm{d},a}^{\mu+1} - \sum_{a\in A_{\mathrm{pi}}\setminus\mathscr{C}} \eta_{\mathrm{d},a}^{\mu} - \sum_{a\in\mathscr{C}} \eta_{\mathrm{d},a}^{\mu} \\
&= \sum_{a\in\mathscr{C}} \eta_{\mathrm{d},a}^{\mu+1} - \sum_{a\in\mathscr{C}} \eta_{\mathrm{d},a}^{\mu} \\
&= 2\sum_{a\in\mathscr{C}} \eta_{\mathrm{d},a}^{\mu} - \sum_{a\in\mathscr{C}} \eta_{\mathrm{d},a}^{\mu} \\
&= \sum_{a\in\mathscr{C}} \eta_{\mathrm{d},a}^{\mu}.
\end{aligned}$$

Thus, we are finished if we prove that

$$\frac{1}{2}\sum_{j=1}^{\mu}\sum_{a\in\mathscr{R}_j} \eta_{\mathrm{d},a}^{j-1} - \sum_{a\in\mathscr{C}} \eta_{\mathrm{d},a}^{\mu}$$

is positive and uniformly bounded away from zero. Using

$$\eta_{\mathrm{d},a}^{j-1} \geq \eta_{\mathrm{d},a}^{\mu}, \quad \text{for all } j = 1,\dots,\mu,$$

(6.15), (6.17), and (6.19), we obtain

$$\begin{aligned}
&\frac{1}{2}\sum_{j=1}^{\mu}\sum_{a\in\mathscr{R}_j} \eta_{\mathrm{d},a}^{j-1} \geq \frac{1}{2}\Theta_{\mathrm{d}}\sum_{j=1}^{\mu}\sum_{a\in A_{\mathrm{pi}}} \eta_{\mathrm{d},a}^{j-1} \geq \frac{1}{2}\Theta_{\mathrm{d}}\sum_{j=1}^{\mu}\sum_{a\in A_{\mathrm{pi}}} \eta_{\mathrm{d},a}^{\mu} \\
&= \frac{1}{2}\Theta_{\mathrm{d}}\mu\sum_{a\in A_{\mathrm{pi}}} \eta_{\mathrm{d},a}^{\mu} > (\Phi_{\mathrm{d}} + C)\sum_{a\in A_{\mathrm{pi}}} \eta_{\mathrm{d},a}^{\mu} > \sum_{a\in\mathscr{C}} \eta_{\mathrm{d},a}^{\mu} + C\left|A_{\mathrm{pi}}\right|\varepsilon,
\end{aligned}$$

which completes the proof. □

Next, we prove an analogous lemma for the case that we fix the stepsize of every arc $a \in A_{\mathrm{pi}}$ and only allow for model switching.

Lemma 6.2. *Suppose that the discretization stepsize h_a is fixed for every pipe $a \in A_{\mathrm{pi}}$. Suppose further that $\eta_a(y) = \eta_{m,a}(y)$ holds in* (6.11) *and that every NLP is solved to local optimality. Consider Alg. 6.1 without applying the discretization refinements in Line 12 and the coarsenings in Line 21. Then, Algorithm 6.1 terminates after a finite number of model switches in Lines 11 and 20 with an ε-feasible solution with respect to the stepsizes h_a, $a \in A_{\mathrm{pi}}$, if there exists a constant $C > 0$ such that*

$$\Theta_m^k \mu^k > \tau^k \Phi_m^k \left|A_{\mathrm{pi}}\right| + C \tag{6.20}$$

holds for all k.

Proof. We consider the total model error

$$\eta_{\mathrm{m}}(y) = \sum_{a \in A_{\mathrm{pi}}} \eta_{\mathrm{m},a}(y)$$

and show that the difference between the decrease obtained in the inner loop and the increase obtained due to switching model levels down in Line 20 is positive and uniformly bounded away from zero for every iteration k. We again consider only a single iteration and drop the corresponding index.

First, we consider a single step of switching up the model level in Line 11. Let $\eta_{\mathrm{m},a}^{j-1}$ denote the model error before the jth inner iteration and $\eta_{\mathrm{m},a}^{j}$ the model error after the jth inner iteration. We then have

$$\begin{aligned}
&\sum_{a \in A_{\mathrm{pi}}} \eta_{\mathrm{m},a}^{j-1} - \sum_{a \in A_{\mathrm{pi}}} \eta_{\mathrm{m},a}^{j} \\
&= \sum_{a \in \mathscr{U}_j} \eta_{\mathrm{m},a}^{j-1} + \sum_{a \in A_{\mathrm{pi}} \setminus \mathscr{U}_j} \eta_{\mathrm{m},a}^{j-1} - \sum_{a \in \mathscr{U}_j} \eta_{\mathrm{m},a}^{j} - \sum_{a \in A_{\mathrm{pi}} \setminus \mathscr{U}_j} \eta_{\mathrm{m},a}^{j} \\
&= \sum_{a \in \mathscr{U}_j} \eta_{\mathrm{m},a}^{j-1} - \sum_{a \in \mathscr{U}_j} \eta_{\mathrm{m},a}^{j}
\end{aligned}$$

for every $j = 1, \dots, \mu$. Summing up over all j yields the overall model error decrease after μ for-loop iterations of

$$\sum_{j=1}^{\mu} \left(\sum_{a \in A_{\mathrm{pi}}} \eta_{\mathrm{m},a}^{j-1} - \sum_{a \in A_{\mathrm{pi}}} \eta_{\mathrm{m},a}^{j} \right) = \sum_{a \in A_{\mathrm{pi}}} \eta_{\mathrm{m},a}^{0} - \sum_{a \in A_{\mathrm{pi}}} \eta_{\mathrm{m},a}^{\mu} = \sum_{j=1}^{\mu} \sum_{a \in \mathscr{U}_j} (\eta_{\mathrm{m},a}^{j-1} - \eta_{\mathrm{m},a}^{j}).$$

We now consider the step of switching down the model level in Line 20. Let $\eta_{\mathrm{m},a}^{\mu}$ denote the model error before and $\eta_{\mathrm{m},a}^{\mu+1}$ the model error after this step. It holds that

$$\begin{aligned}
&\sum_{a \in A_{\mathrm{pi}}} \eta_{\mathrm{m},a}^{\mu+1} - \sum_{a \in A_{\mathrm{pi}}} \eta_{\mathrm{m},a}^{\mu} \\
&= \sum_{a \in \mathscr{D}} \eta_{\mathrm{m},a}^{\mu+1} + \sum_{a \in A_{\mathrm{pi}} \setminus \mathscr{D}} \eta_{\mathrm{m},a}^{\mu+1} - \sum_{a \in \mathscr{D}} \eta_{\mathrm{m},a}^{\mu} - \sum_{a \in A_{\mathrm{pi}} \setminus \mathscr{D}} \eta_{\mathrm{m},a}^{\mu} \\
&= \sum_{a \in \mathscr{D}} (\eta_{\mathrm{m},a}^{\mu+1} - \eta_{\mathrm{m},a}^{\mu}).
\end{aligned}$$

Thus, the proof is finished if we show that

$$\sum_{j=1}^{\mu} \sum_{a \in \mathscr{U}_j} (\eta_{\mathrm{m},a}^{j-1} - \eta_{\mathrm{m},a}^{j}) - \sum_{a \in \mathscr{D}} (\eta_{\mathrm{m},a}^{\mu+1} - \eta_{\mathrm{m},a}^{\mu})$$

is positive and uniformly bounded away from zero. With similar ideas as in

the proof of Lemma 6.1 and using (6.16), (6.18), and (6.20), we obtain

$$\sum_{j=1}^{\mu}\sum_{a\in\mathscr{U}_j}(\eta_{\mathrm{m},a}^{j-1}-\eta_{\mathrm{m},a}^{j}) \geq \Theta_{\mathrm{m}}\sum_{j=1}^{\mu}\sum_{a\in A_{\mathrm{pi}}^{>\varepsilon}}(\eta_{\mathrm{m},a}^{j-1}-\eta_{\mathrm{m},a}^{j}) > \Theta_{\mathrm{m}}\sum_{j=1}^{\mu}\sum_{a\in A_{\mathrm{pi}}^{>\varepsilon}}\varepsilon$$

$$= \Theta_{\mathrm{m}}\mu\left|A_{\mathrm{pi}}^{>\varepsilon}\right|\varepsilon \geq \Theta_{\mathrm{m}}\mu\varepsilon > \tau\Phi_{\mathrm{m}}\left|A_{\mathrm{pi}}\right|\varepsilon + C\varepsilon \geq \Phi_{\mathrm{m}}\sum_{a\in A_{\mathrm{pi}}^{<\varepsilon}(\tau)}\varepsilon\tau + C\varepsilon$$

$$\geq \Phi_{\mathrm{m}}\sum_{a\in A_{\mathrm{pi}}^{<\varepsilon}(\tau)}(\eta_{\mathrm{m},a}^{\mu+1}-\eta_{\mathrm{m},a}^{\mu}) + C\varepsilon \geq \sum_{a\in\mathscr{D}}(\eta_{\mathrm{m},a}^{\mu+1}-\eta_{\mathrm{m},a}^{\mu}) + C\varepsilon,$$

where we used that $|A_{\mathrm{pi}}^{>\varepsilon}| \geq 1$. This completes the proof. □

Let $\eta_{\mathrm{m},a}^{\mathrm{new}}(y)$ denote the new model error estimator after a grid refinement or coarsening. In order to prove our main theorem we need to assume that, for every pipe $a \in A_{\mathrm{pi}}$, the change in the model error estimator after a grid refinement or coarsening can be neglected as compared to $\eta_{\mathrm{m},a}(y)$, i.e., $|\eta_{\mathrm{m},a}(y) - \eta_{\mathrm{m},a}^{\mathrm{new}}(y)| \ll \eta_{\mathrm{m},a}(y)$, such that we may write $\eta_{\mathrm{m},a}^{\mathrm{new}}(y) = \eta_{\mathrm{m},a}(y)$. A sufficient condition for this assumption to hold is given by $\eta_{\mathrm{d},a}(y) \ll \eta_{\mathrm{m},a}(y)$ for every $a \in A_{\mathrm{pi}}$. This condition also implies that $\eta_{\mathrm{m},a}(y)$ is a first-order approximation of the exact model error $e_{\mathrm{m},a}(y)$ and is thus reliable for small stepsizes h_a.

Lemma 6.3. *Let the discretization and model error estimator $\eta_{d,a}(y)$ and $\eta_{m,a}(y)$ as defined in* (6.9) *and* (6.10) *be given for every $a \in A_{\mathrm{pi}}$. Let further $e_{m,a}(y)$ be the exact error between models* (M_1) *and (M_{ℓ_a}) and let $\eta_{m,a}^{new}(y)$ be the new model error estimator after a grid refinement or coarsening. Then, the implications*

1. $\eta_{d,a}(y) \ll \eta_{m,a}(y) \implies \eta_{m,a}(y) \doteq e_{m,a}(y)$,
2. $\eta_{d,a}(y) \ll \eta_{m,a}(y) \implies \eta_{m,a}^{new}(y) = \eta_{m,a}(y)$

hold for every $a \in A_{\mathrm{pi}}$.

Proof. Let pipe $a \in A_{\mathrm{pi}}$ be arbitrary. To improve readability, in the following we drop the dependencies of the exact errors and the error estimators on a and y. Without loss of generality, we consider only one arbitrary spatial gridpoint x_k.

Let us first introduce some notation. The exact model error is given by $e_{\mathrm{m}}(x_k) = \hat{p}(x_k) - p^{\mathrm{M}_{\ell_a}}(x_k)$ for the current model level ℓ_a, the exact discretization error for model (D_1) is given by $e_{\mathrm{d}}^1(x_k) = \hat{p}(x_k) - p^1(x_k;2h_a)$ and the exact discretization error for model (D_{ℓ_a}) is denoted by $e_{\mathrm{d}}^{\ell_a}(x_k) = p^{\mathrm{M}_{\ell_a}}(x_k) - p^{\ell_a}(x_k;2h_a)$. Furthermore, the model error estimator is given by $\eta_{\mathrm{m}}(x_k) = p^1(x_k;2h_a) - p^{\ell_a}(x_k;2h_a)$, see (6.10), and we define the discretization error estimators $\eta_{\mathrm{d}}^1(x_k) := p^1(x_k;2h_a) - p^1(x_k;4h_a)$ and $\eta_{\mathrm{d}}^{\ell_a}(x_k) := p^{\ell_a}(x_k;2h_a) - p^{\ell_a}(x_k;4h_a)$ as in (6.9). Then, we have $\eta_{\mathrm{d}}^1(x_k) \doteq e_{\mathrm{d}}^1(x_k)$ and $\eta_{\mathrm{d}}^{\ell_a}(x_k) \doteq e_{\mathrm{d}}^{\ell_a}(x_k)$; see [92, page 420]. Further, it holds that

$$|\eta_{\mathrm{d}}^1(x_k)| \ll |\eta_{\mathrm{m}}(x_k)| \iff |\eta_{\mathrm{d}}^{\ell_a}(x_k)| \ll |\eta_{\mathrm{m}}(x_k)|, \tag{6.21}$$

because $\eta_{\mathrm{d}}^{1}(x_k)$ and $\eta_{\mathrm{d}}^{\ell_a}(x_k)$ use the same stepsizes $2h_a$ and $4h_a$ to compute the discrete pressure distributions.

We now prove implication 1. Using the previously defined notation it holds that

$$\begin{aligned} e_{\mathrm{m}}(x_k) &= \hat{p}(x_k) - p^{\mathrm{M}_{\ell_a}}(x_k) \\ &= e_{\mathrm{d}}^{1}(x_k) + p^{1}(x_k;2h_a) - e_{\mathrm{d}}^{\ell_a}(x_k) - p^{\ell_a}(x_k;2h_a) \\ &\doteq \eta_{\mathrm{d}}^{1}(x_k) + p^{1}(x_k;2h_a) - \eta_{\mathrm{d}}^{\ell_a}(x_k) - p^{\ell_a}(x_k;2h_a) \\ &= \eta_{\mathrm{d}}^{1}(x_k) - \eta_{\mathrm{d}}^{\ell_a}(x_k) + \eta_{\mathrm{m}}(x_k). \end{aligned}$$

Thus, if $|\eta_{\mathrm{d}}^{1}(x_k)|$ and $|\eta_{\mathrm{d}}^{\ell_a}(x_k)|$ may be neglected as compared to $|\eta_{\mathrm{m}}(x_k)|$, then we have $e_{\mathrm{m}}(x_k) \doteq \eta_{\mathrm{m}}(x_k)$, i.e.,

$$|\eta_{\mathrm{d}}^{1}(x_k)| \ll |\eta_{\mathrm{m}}(x_k)| \wedge |\eta_{\mathrm{d}}^{\ell_a}(x_k)| \ll |\eta_{\mathrm{m}}(x_k)| \implies e_{\mathrm{m}}(x_k) \doteq \eta_{\mathrm{m}}(x_k).$$

Considering also the equivalence relation (6.21) it follows that

$$|\eta_{\mathrm{d}}^{1}(x_k)| \ll |\eta_{\mathrm{m}}(x_k)| \implies e_{\mathrm{m}}(x_k) \doteq \eta_{\mathrm{m}}(x_k),$$

from which implication 1 follows directly.

Finally, we prove implication 2. We show that this implication holds for the case that $\eta_{\mathrm{m}}^{\mathrm{new}}(x_k)$ is the new model error estimator after a grid coarsening. The case for a grid refinement can be shown analogously. It holds that

$$\begin{aligned} \eta_{\mathrm{m}}^{\mathrm{new}}(x_k) &= p^{1}(x_k;4h_a) - p^{\ell_a}(x_k;4h_a) \\ &= -\eta_{\mathrm{d}}^{1}(x_k) + p^{1}(x_k;2h_a) + \eta_{\mathrm{d}}^{\ell_a}(x_k) - p^{\ell_a}(x_k;2h_a) \\ &= -\eta_{\mathrm{d}}^{1}(x_k) + \eta_{\mathrm{d}}^{\ell_a}(x_k) + \eta_{\mathrm{m}}(x_k). \end{aligned}$$

This yields

$$|\eta_{\mathrm{d}}^{1}(x_k)| \ll |\eta_{\mathrm{m}}(x_k)| \wedge |\eta_{\mathrm{d}}^{\ell_a}(x_k)| \ll |\eta_{\mathrm{m}}(x_k)| \implies \eta_{\mathrm{m}}^{\mathrm{new}}(x_k) = \eta_{\mathrm{m}}(x_k). \tag{6.22}$$

Again, considering (6.21) and (6.22) results in

$$|\eta_{\mathrm{d}}^{1}(x_k)| \ll |\eta_{\mathrm{m}}(x_k)| \implies \eta_{\mathrm{m}}^{\mathrm{new}}(x_k) = \eta_{\mathrm{m}}(x_k),$$

from which implication 2 follows immediately. □

With the three preceding lemmas at hand, we are now ready to state and prove our main theorem about finite termination of Alg. 6.1.

Theorem 6.4 (Finite termination)**.** *Suppose that $\eta_{d,a} \ll \eta_{m,a}$ for every $a \in A_{\mathrm{pi}}$ and that every NLP is solved to local optimality. Then, Algorithm 6.1 terminates after a finite number of refinements, coarsenings and model switches in Lines 11, 12, 20, and 21 with an ε-feasible solution with respect to the reference problem* (6.7) *if there exist constants $C_1, C_2 > 0$ such that*

$$\frac{1}{2}\Theta_d^k \mu^k > \Phi_d^k + C_1, \quad \Theta_m^k \mu^k > \tau^k \Phi_m^k \left|A_{\mathrm{pi}}\right| + C_2$$

hold for all k.

Proof. We consider the total error $\sum_{a\in A_{\mathrm{pi}}} \eta_a$ and show that the difference between the decrease obtained in the inner loop and the increase obtained due to switching down the model level and coarsening the grid is positive and uniformly bounded away from zero for every iteration k. Again, we consider only a single iteration and drop the corresponding index. We first consider Lines 11 and 12 for fixed j. It holds that

$$
\begin{aligned}
&\sum_{a\in A_{\mathrm{pi}}} \eta_a^{j-1} - \sum_{a\in A_{\mathrm{pi}}} \eta_a^{j} \\
&= \sum_{a\in A_{\mathrm{pi}}} \eta_{\mathrm{m},a}^{j-1} + \sum_{a\in A_{\mathrm{pi}}} \eta_{\mathrm{d},a}^{j-1} - \sum_{a\in A_{\mathrm{pi}}} \eta_{\mathrm{m},a}^{j} - \sum_{a\in A_{\mathrm{pi}}} \eta_{\mathrm{d},a}^{j} \\
&= \sum_{a\in A_{\mathrm{pi}}\setminus(\mathscr{U}_j\cup\mathscr{R}_j)} \eta_{\mathrm{m},a}^{j-1} - \sum_{a\in A_{\mathrm{pi}}\setminus(\mathscr{U}_j\cup\mathscr{R}_j)} \eta_{\mathrm{m},a}^{j} + \sum_{a\in\mathscr{U}_j\setminus\mathscr{R}_j} \eta_{\mathrm{m},a}^{j-1} - \sum_{a\in\mathscr{U}_j\setminus\mathscr{R}_j} \eta_{\mathrm{m},a}^{j} \\
&\quad + \sum_{a\in\mathscr{R}_j\setminus\mathscr{U}_j} \eta_{\mathrm{m},a}^{j-1} - \sum_{a\in\mathscr{R}_j\setminus\mathscr{U}_j} \eta_{\mathrm{m},a}^{j} + \sum_{a\in\mathscr{R}_j\cap\mathscr{U}_j} \eta_{\mathrm{m},a}^{j-1} - \sum_{a\in\mathscr{R}_j\cap\mathscr{U}_j} \eta_{\mathrm{m},a}^{j} \\
&\quad + \sum_{a\in A_{\mathrm{pi}}\setminus(\mathscr{U}_j\cup\mathscr{R}_j)} \eta_{\mathrm{d},a}^{j-1} - \sum_{a\in A_{\mathrm{pi}}\setminus(\mathscr{U}_j\cup\mathscr{R}_j)} \eta_{\mathrm{d},a}^{j} + \sum_{a\in\mathscr{U}_j\setminus\mathscr{R}_j} \eta_{\mathrm{d},a}^{j-1} - \sum_{a\in\mathscr{U}_j\setminus\mathscr{R}_j} \eta_{\mathrm{d},a}^{j} \\
&\quad + \sum_{a\in\mathscr{R}_j\setminus\mathscr{U}_j} \eta_{\mathrm{d},a}^{j-1} - \sum_{a\in\mathscr{R}_j\setminus\mathscr{U}_j} \eta_{\mathrm{d},a}^{j} + \sum_{a\in\mathscr{R}_j\cap\mathscr{U}_j} \eta_{\mathrm{d},a}^{j-1} - \sum_{a\in\mathscr{R}_j\cap\mathscr{U}_j} \eta_{\mathrm{d},a}^{j} \\
&= \sum_{a\in\mathscr{U}_j} \eta_{\mathrm{m},a}^{j-1} - \sum_{a\in\mathscr{U}_j} \eta_{\mathrm{m},a}^{j} + \sum_{a\in\mathscr{R}_j} \eta_{\mathrm{d},a}^{j-1} - \sum_{a\in\mathscr{R}_j} \eta_{\mathrm{d},a}^{j} \\
&= \sum_{a\in\mathscr{U}_j} (\eta_{\mathrm{m},a}^{j-1} - \eta_{\mathrm{m},a}^{j}) + \frac{1}{2} \sum_{a\in\mathscr{R}_j} \eta_{\mathrm{d},a}^{j-1},
\end{aligned}
$$

where we use that $\eta_{\mathrm{m},a}^{j} = \eta_{\mathrm{m},a}^{j-1}$ for every $a \in \mathscr{R}_j \setminus \mathscr{U}_j$ since $\eta_{\mathrm{d},a}^{j-1} \ll \eta_{\mathrm{m},a}^{j-1}$ for every $a \in A_{\mathrm{pi}}$; see Lemma 6.3. Moreover, the discretization error estimator $\eta_{\mathrm{d},a}$ does not change after a switching up the model level.

Again, summing up over all $j = 1,\dots,\mu$ yields the overall error decrease after μ for-loop iterations of

$$
\begin{aligned}
&\sum_{j=1}^{\mu} \left(\sum_{a\in A_{\mathrm{pi}}} \eta_a^{j-1} - \sum_{a\in A_{\mathrm{pi}}} \eta_a^{j} \right) = \sum_{a\in A_{\mathrm{pi}}} \eta_a^{0} - \sum_{a\in A_{\mathrm{pi}}} \eta_a^{\mu} \\
&= \sum_{j=1}^{\mu} \left(\sum_{a\in\mathscr{U}_j} (\eta_{\mathrm{m},a}^{j-1} - \eta_{\mathrm{m},a}^{j}) + \frac{1}{2} \sum_{a\in\mathscr{R}_j} \eta_{\mathrm{d},a}^{j-1} \right).
\end{aligned}
$$

With similar arguments as before for Lines 11 and 12 we consider Lines 20 and 21 and obtain

$$
\begin{aligned}
&\sum_{a\in A_{\mathrm{pi}}} \eta_a^{\mu+1} - \sum_{a\in A_{\mathrm{pi}}} \eta_a^{\mu} \\
&= \sum_{a\in A_{\mathrm{pi}}} \eta_{\mathrm{d},a}^{\mu+1} + \sum_{a\in A_{\mathrm{pi}}} \eta_{\mathrm{m},a}^{\mu+1} - \sum_{a\in A_{\mathrm{pi}}} \eta_{\mathrm{d},a}^{\mu} - \sum_{a\in A_{\mathrm{pi}}} \eta_{\mathrm{m},a}^{\mu} \\
&= \sum_{a\in\mathscr{C}} \eta_{\mathrm{d},a}^{\mu+1} - \sum_{a\in\mathscr{C}} \eta_{\mathrm{d},a}^{\mu} + \sum_{a\in\mathscr{D}} \eta_{\mathrm{m},a}^{\mu+1} - \sum_{a\in\mathscr{D}} \eta_{\mathrm{m},a}^{\mu} \\
&= \sum_{a\in\mathscr{C}} \eta_{\mathrm{d},a}^{\mu} + \sum_{a\in\mathscr{D}} (\eta_{\mathrm{m},a}^{\mu+1} - \eta_{\mathrm{m},a}^{\mu}).
\end{aligned}
$$

Finally, it remains to prove that

$$\sum_{j=1}^{\mu}\left(\sum_{a\in\mathscr{U}_j}(\eta_{\mathrm{m},a}^{j-1}-\eta_{\mathrm{m},a}^{j})+\frac{1}{2}\sum_{a\in\mathscr{R}_j}\eta_{\mathrm{d},a}^{j-1}\right)-\sum_{a\in\mathscr{C}}\eta_{\mathrm{d},a}^{\mu}-\sum_{a\in\mathscr{D}}(\eta_{\mathrm{m},a}^{\mu+1}-\eta_{\mathrm{m},a}^{\mu})$$

is positive and uniformly bounded away from zero. Using the proofs of Lemmas 6.1 and 6.2 we have

$$\begin{aligned}
&\sum_{j=1}^{\mu}\sum_{a\in\mathscr{U}_j}(\eta_{\mathrm{m},a}^{j-1}-\eta_{\mathrm{m},a}^{j})+\frac{1}{2}\sum_{j=1}^{\mu}\sum_{a\in\mathscr{R}_j}\eta_{\mathrm{d},a}^{j-1}\\
&>\Theta_{\mathrm{m}}\mu\varepsilon+\frac{1}{2}\mu\Theta_{\mathrm{d}}\sum_{a\in A_{\mathrm{pi}}}\eta_{\mathrm{d},a}^{\mu}\\
&>\tau\Phi_{\mathrm{m}}\left|A_{\mathrm{pi}}\right|\varepsilon+C_2\varepsilon+(\Phi_{\mathrm{d}}+C_1)\sum_{a\in A_{\mathrm{pi}}}\eta_{\mathrm{d},a}^{\mu}\\
&>\sum_{a\in\mathscr{D}}(\eta_{\mathrm{m},a}^{\mu+1}-\eta_{\mathrm{m},a}^{\mu})+C_2\varepsilon+\sum_{a\in\mathscr{C}}\eta_{\mathrm{d},a}^{\mu}+C_1\left|A_{\mathrm{pi}}\right|\varepsilon,
\end{aligned}$$

which completes the proof. □

6.4.4 Remarks

Before we close this section we discuss some details and extensions regarding Alg. 6.1. First, we give an overview of the main computations that are performed in the algorithm. In Lines 2 and 13, the NLP (6.8) is solved using the current model level ℓ_a and the current stepsize h_a for every pipe $a\in A_{\mathrm{pi}}$. Most types of NLP algorithms are iterative methods. That is, the computational costs of the algorithms depend on the number of iterations required to converge to a (local) optimal solution and the costs per iteration. The latter mainly consist of the solution of a linear system (e.g., suitable forms of the KKT system for interior-point or active-set methods) for computing the search direction. The size of this linear system typically is $\mathscr{O}(n+m)$, where n is the number of variables and m is the number of constraints of the NLP. Both n and m are directly controlled by the stepsizes h_a that we use in our NLP models. The model level ℓ_a mainly determines the sparsity/density of the system matrices of the linear systems and the overall nonlinearity of the NLP, which typically influences the number of required iterations.

In Lines 3 and 14, the overall error estimator $\eta_a(y)$ is computed for every pipe $a\in A_{\mathrm{pi}}$. Thus, for all pipes, the solution of model (D_1) is computed with stepsize both $2h_a$ and $4h_a$ and the solution of model (D_{ℓ_a}) is computed with stepsize h_a. These solutions are obtained by solving the initial value problems consisting of the ordinary differential equations (M_1) and (M_{ℓ_a}) together with the initial value $p(x_0)$, which is contained in the optimal solution y of Problem (6.8). Continuing with the example of the implicit Euler method that we use as numerical integration scheme throughout this chapter, the initial value problems can be solved (i) by considering the implicit equations in (D_1) and (D_{ℓ_a}) and using, e.g., the Newton method to solve for p_k in every space

integration step or (ii) by using an existing software code and setting the order of the numerical integration scheme to one.

The subset $\mathscr{R}$ in Line 10 can be determined efficiently, since $\eta_{\mathrm{d},a}(y)$ has already been computed in Line 3 or 14 for every $a \in A_{\mathrm{pi}}$. For subset $\mathscr{U}$ in Line 10 and in (6.16) the error estimator $\eta_{\mathrm{m},a}(y)$ has also already been computed in Line 3 or 14 for every $a \in A_{\mathrm{pi}}$. Moreover, ℓ_a^{new} in (6.12) has to be computed in order to determine $\mathscr{U}$. For this, we compute $\eta_{\mathrm{m},a}(y;\ell_a-1)$ if and only if $\ell_a = 3$. In the case $\ell_a = 2$ we have $\eta_{\mathrm{m},a}(y;\ell_a-1) = 0$ and for $\ell_a = 1$ we have $\eta_{\mathrm{m},a}(y;\ell_a^{\mathrm{new}}) = \eta_{\mathrm{m},a}(y;\ell_a) = 0$. Subset $\mathscr{C}$ in Line 19 can also be computed efficiently, since $\eta_{\mathrm{d},a}(y)$ has already been computed in Line 3 or 14 for every $a \in A_{\mathrm{pi}}$. For subset $\mathscr{D}$ in Line 19 and in (6.18) the error estimator $\eta_{\mathrm{m},a}(y)$ has been computed already in Line 3 or 14 for every $a \in A_{\mathrm{pi}}$. If $\ell_a \in \{1,2\}$, then $\eta_{\mathrm{m},a}(y;\ell_a+1)$ has to be computed for every $a \in A_{\mathrm{pi}}$ in order to determine $\mathscr{D}$.

We note that the optimal solution y of Problem (6.8) contains, among others, the model level ℓ_a, stepsize h_a, and pressure $p^{\ell_a}(x_0)$ at the beginning of the pipe, for every $a \in A_{\mathrm{pi}}$. Using ℓ_a, h_a, and $p^{\ell_a}(x_0)$, the discretization and model error estimator for pipe $a \in A_{\mathrm{pi}}$ can be computed without information from other pipes. Hence, the error estimators, e.g., in Line 14, can be computed in parallel.

Up to now, we have discussed two types of errors: modeling and discretization errors. Both are handled by Alg. 6.1 and we have shown that the algorithm terminates with a combined model and discretization error that satisfies a user-specified error tolerance $\varepsilon > 0$. What we have ignored so far is that the NLPs are also solved by a numerical method that introduces numerical errors as well. However, it is easy to integrate the control of this additional error source into Alg. 6.1. Let $\varepsilon^{\mathrm{opt}} > 0$ be the optimality tolerance that we hand over to the optimization solver and suppose that the solver always satisfies this tolerance. Furthermore, let the tolerance ε considered so far now be denoted by $\varepsilon^{\mathrm{dm}}$. Using the triangle inequality we easily see that the upper bound of the total error (that is aggregated modeling, discretization, and optimization error) is $\varepsilon^{\mathrm{opt}} + \varepsilon^{\mathrm{dm}}$. Hence, in order to satisfy an overall error tolerance $\varepsilon > 0$, we have to ensure that $\varepsilon^{\mathrm{opt}} + \varepsilon^{\mathrm{dm}} \leq \varepsilon$ holds, which can be formally introduced in Alg. 6.1 by replacing ε with $\varepsilon^{\mathrm{opt}} + \varepsilon^{\mathrm{dm}}$.

Finally, note that this additional error source directly suggests itself for adaptive treatment as well. In the early iterations of Alg. 6.1 it is not important that $\varepsilon^{\mathrm{opt}}$ is small. That is, the optimization is allowed to produce coarser approximate local solutions. However, in the course of the algorithm, one can observe the achieved modeling and discretization error and can adaptively tighten the optimization tolerance. Since this strategy allows the optimization method to produce coarse approximate solutions in the beginning, it can be expected that this leads to a speed-up in the overall running times of Alg. 6.1.

The choice of the error tolerance ε that has to be provided in Alg. 6.1 will depend on the user requirements, however, one should be aware that due to the round-off errors committed during every single step of the procedure, and due to possible ill-conditioning of the linear systems solved by the NLP solver,

none of the three errors, the discretization error, the modeling error, and the NLP error can be chosen extremely small. Since the backward error and the associated condition number of the linear systems can be estimated during the procedure, see [49], and since the error estimates for the discretization method are at hand, it is just the modeling error which is not known a priori. To estimate this latter error (of the finest model) usually requires a comparison with experimental data. If these are available during a real-world process, then it is possible to adjust the required tolerances ε in a feedback loop using a standard PI controller, see, e.g., [84], i.e., if measured data are available that show that the finest model has a given accuracy, then ε should not be chosen smaller than this.

Finally, we want to stress that the described adaptive error control algorithm can be used with any number of model levels in the hierarchy, with any higher order discretization scheme, and with any number of grid refinement levels.

6.5 Computational Results

In this section we present numerical results obtained by the adaptive error control algorithm. To this end, we compare the efficiency of the method with an approach that directly solves an NLP that satisfies the same error tolerance and that is obtained without using adaptivity. Before we discuss the results in detail we briefly mention the computational setup and the gas transport network instances that we solve.

We implemented the adaptive error control algorithm 6.1 in Python 2.7.13 and used the scipy 0.14.0 module for solving the initial value problems. All nonlinear optimization models have been implemented using the C++ framework LaMaTTO++[1] for modeling and solving mixed-integer nonlinear optimization problems on networks. The computations have been done on a six-core AMD Opteron™ Processor 2435 with 2.20 GHz and 64 GB of main memory. The NLPs have been solved using Ipopt 3.12; see [97, 98].

For our computational study, we choose publicly available GasLib instances; see [88]. This has the advantage that, if desired, all numerical results can be reproduced on the same data. In what follows, we consider the networks GasLib-40 and GasLib-135, since these are the largest networks in the GasLib that only contain pipes and compressor stations as arc types. Detailed statistics are given in Table 6.1.

Next, we describe the parameterization of Alg. 6.1. We initialize every pipe $a \in A_{\text{pi}}$ with the coarsest model level $\ell_a = 3$ and with the coarsest possible discretization grid. In order to yield a well-defined algorithm, the number of discretization grid intervals has to be a multiple of 4; see Figure 6.2. Thus, we initially set $h_a = L_a/4$ and ensure in Step 21 of Alg. 6.1 that we never obtain a coarser grid size than the initial one. The overall tolerance is set to $\varepsilon =$

[1] http://www.mso.math.fau.de/edom/projects/lamatto.html

Table 6.1: Statistics for the instances

Network	# nodes	# pipes	# compressor stations	total pipe length (km)
GasLib-40	40	39	6	1112
GasLib-135	135	141	29	6935

10^{-4} bar. Moreover, we set $\Theta_d = \Theta_m = 0.7$, $\Phi_d = \Phi_m = 0.3$, $\tau = 1.1$, and $\mu = 4$. Here, we refrain from updating these parameters from iteration to iteration, which is possible in general. Note that our parameter choice violates the second inequality of Theorem 6.4. This could be fixed by simply increasing the hysteresis parameter μ. However, we refrain from using a larger μ in order to give the adaptive algorithm more chances to also switch down in the model hierarchy or to coarsen discretization grids. Our numerical experiments show that the violation of the second inequality of Theorem 6.4 does not harm convergence in practice but leads to slightly faster computations.

The same rationale holds for the relation between model and discretization error as assumed in Theorem 6.4; see also Lemma 6.3. To be fully compliant with the theory, the initial discretization grids need to be much finer. Again, coarser initial discretization grids do not harm convergence in our numerical experiments but yield much faster computations.

We now turn to the discussion of the numerical results. Both instances are solved using 8 iterations. Thus, together with the initially solved NLP, we have to solve 9 NLPs for solving both instances.

Using the adaptive control algorithm, it takes 3.82 s to solve the GasLib-40 instance and 7.50 s to solve the GasLib-135 instance. For the GasLib-40 network, the final NLP contains 2030 variables and 1990 constraints, whereas for the GasLib-135 the final NLP contains 3410 variables and 3270 constraints.

Most interesting is the speed-up that we obtain by using the adaptive control algorithm. Thus, we compare the above given solution times with the solution times for an NLP that satisfies the same error tolerances but that is obtained without using model level and discretization grid adaptivity. This NLP contains 40 000 variables and 40 000 constraints for the GasLib-40 instance and 145 000 variables as well as 145 000 constraints for the GasLib-135 instance. Compared to the final NLPs that have to be solved within the adaptive algorithm, the NLPs obtained without using adaptivity are quite large scale. This directly translates to solution times. The GasLib-40 instance requires 53.1 s and the GasLib-135 instance requires 122 s. Thus, we get a speed-up factor of 13.89 and 16.33, respectively.

Figure 6.4 illustrates the adaptivity of the algorithm by plotting how many pipe grids are refined ($|\mathscr{R}|$) and how many pipe models are switched up in the hierarchy ($|\mathscr{U}|$). It can be clearly seen that increasing the accuracy is only needed for a small fraction of the pipes. For the GasLib-40 network, we never refine grids for more than 9 pipes, whereas we never refine grids for more than

21 pipes for the GasLib-135 network. Thus, for the larger network, we never refine grids for more than 15 % of all pipes.

For both networks, the Lines 20 and 21 are only reached once. For the smaller network, only 1 pipe grid is coarsened, whereas 3 pipe grids are coarsened for the larger network. Moreover, the algorithm never switches down in the model hierarchy. Consequently, the NLPs get larger from iteration to iteration. This then yields increased running times for the NLP solver as depicted in Figure 6.5. It can be seen that the subsequent NLPs can be solved quite fast. There are two main reasons for this phenomenon. First, the NLP's size only increases moderately due to the adaptive control strategy. Second, the overall algorithm allows for warm-starting: When solving a single NLP we always use the last NLP's solution to set up the initial iterate.

Lastly, we consider the decrease in the respective errors. In Figure 6.6,

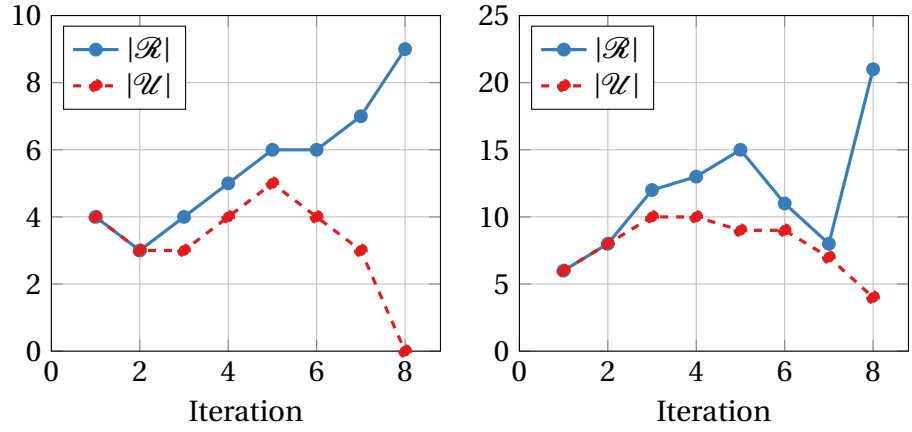

Figure 6.4: Number of pipes with refined grid (y-axis; $|\mathscr{R}|$) and number of pipes where the model is switched up in the model hierarchy (y-axis; $|\mathscr{U}|$) over the course of the iterations (x-axis). Left: GasLib-40, right: GasLib-135.

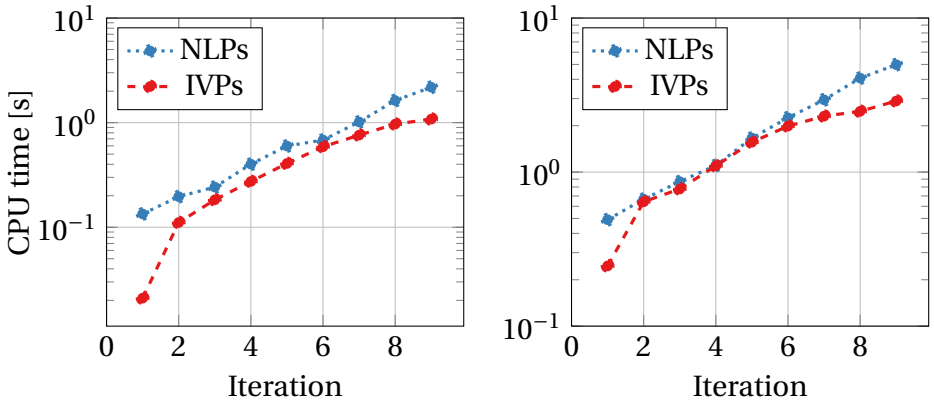

Figure 6.5: Aggregated run times (y-axis; in s) required for solving the nonlinear optimization problems (NLPs) and the initial value problems (IVPs) for the computation of the error estimates. Left: GasLib-40, right: GasLib-135.

the discretization, model, and total errors are plotted over the course of the iterations. Both profiles show the expected decrease in the errors.

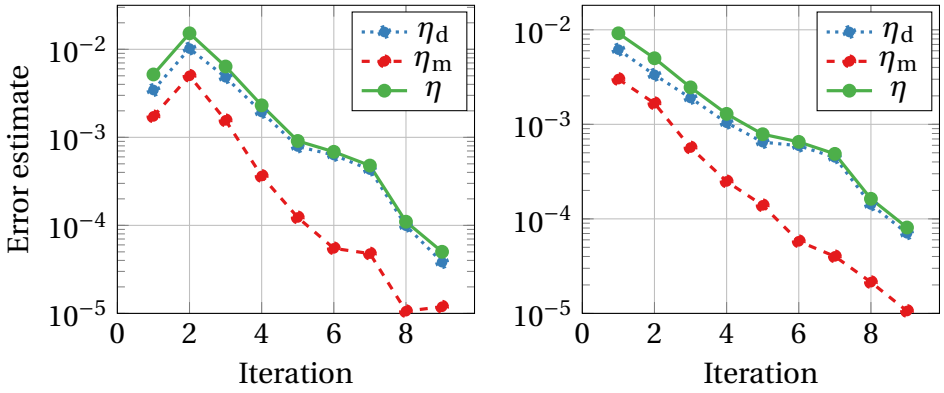

Figure 6.6: Discretization, model and total error estimates (y-axis) over the course of the iterations (x-axis). Left: GasLib-40, right: GasLib-135.

6.6 Summary of Chapter 6

We have considered the problem of operation cost minimization for gas transport networks. In this context, we have focused on stationary and isothermal models and developed an adaptive model and discretization error control algorithm for nonlinear optimization that uses a hierarchy of continuous and finite-dimensional models. Out of this hierarchy, the new method adaptively chooses different models in order to finally achieve an optimal solution that satisfies a prescribed combined model and discretization error tolerance. The algorithm is shown to be convergent and its performance is illustrated by several numerical results.

The results pave the way for future work in the context of model switching and discretization grid adaptation for nonlinear optimal control. On the one hand, it should be extended to non-isothermal and instationary models of gas transport, in particular, in a port-Hamiltonian formulation. On the other hand, it would be interesting to extend the new technique to mixed-integer nonlinear optimal control.

Chapter 7

Conclusions and Outlook

The numerical solution of a simulation or an optimization problem contains errors from all or some of the following sources: modeling, discretization, iteration, data uncertainty, and rounding errors. In this work, estimators for the different error sources have been derived and the errors have been adaptively controlled. As an example, natural gas networks have been considered. The gas flow through the pipes is modeled using a hierarchy of models based on the Euler equations of fluid dynamics. In order to obtain an appropriate trade-off between accuracy and computational complexity, detailed (and therefore computationally expensive) models should only be used in the network where this is necessary, e.g., right after a compressor, where the gas flow is dynamic. On the other hand, in parts of the network where the gas flow is steadier, simpler models, with a lower computational cost, can be applied. For many models in this hierarchy, we compute and analyze the magnitude of the different error sources within the state variables of a gas flow simulation using a backward error analysis. While modeling and discretization error estimators for gas flow simulations have already been extensively studied in the last decades, there is relatively few literature on iteration, data uncertainty, and rounding errors, which are therefore our main focus in Chapters 3 and 4. Moreover, if the total error exceeds a prescribed tolerance, then the different error components for every pipe have been adaptively controlled in Chapters 5 and 6 using Greedy-like strategies and techniques stemming from adaptive finite element methods. Both a synthetic experiment and applications to realistic gas networks have shown that the developed adaptive techniques significantly reduce the computational time as compared to classical methods, while maintaining the same accuracy.

We now shortly discuss the conclusions from the individual chapters. In Chapter 3, estimators have been derived for all the different error sources and they have been applied to a two-level model hierarchy for the simulation of gas flows. We find, e.g., that the componentwise condition numbers for nonlinear systems of equations reflect the sensitivity of the problem better than the classical normwise condition numbers. Moreover, spatial and temporal step-sizes are determined for which a well-conditioned problem is obtained. The

analysis in Chapter 3 was performed for a single pipe with a two-point spatial discretization scheme that is often used in gas flow optimization methods. The sensitivity analysis has been extended in Chapter 4 to an exemplary Y-shaped gas network that is discretized using the implicit box scheme, which is an effective discretization scheme for transient gas flow problems. The sensitivity of the network state with respect to perturbations in the boundary conditions has been computed using novel componentwise amplification vectors. We find that the mass flow rate in the first pipe is highly sensitive to perturbations in the inlet pressure. It is shown in Chapter 5 that the problem of finding an optimal refinement scheme is a generalization of the unbounded knapsack problem. New Greedy-like refinement strategies for the adaptive control of the error in space, time, and model have been developed, which have a network overview and take the behavior of the gas flow better into account than the strategy that is currently used in gas flow simulation software. Both a synthetic experiment on an abstract gas network and a realistic gas flow simulation show that the new strategies significantly outperform the current refinement strategy with respect to the computational cost incurred. Finally, in Chapter 6, the discretization and model error in every pipe are adaptively controlled within an optimization algorithm using bulk criteria. It is proven that, also when one allows for coarsening, an ε-feasible solution is found after a finite number of grid and model adaptations. Numerical experiments show that the use of adaptive error control reduces the computational time substantially as compared to solving the optimization problem without adaptivity, while retaining the same accuracy.

Although error estimators have been developed for all the different error sources in Chapter 3, only the discretization and model error have been adaptively controlled in Chapter 5 and 6. Thus, future work should consist of incorporating the iteration, data uncertainty, and rounding errors into the adaptive controllers. Further, note that we have chosen the example of gas networks. However, the developed error estimators and adaptive control strategies can be easily adapted to other applications on networks, like water flow, electricity, and traffic flow problems.

Appendix A

Forecast Error Analysis using ANACONDA

In this appendix, we analyze the effect of forecast errors in the gas demand on a certain quantity of interest. First, some regulatory rules concerning the trading of natural gas are discussed in Section A.1. The gas flow model used within the simulation software ANACONDA is given in Section A.2. In Section A.3, a network with one compressor is simulated, where the quantity of interest is the volume flow rate at the source. A network with three compressors is considered in Section A.4, with the total fuel gas consumption as the quantity of interest.

A.1 Rules for using Gas Networks

Before the German gas market liberalization in 2005, there were only a few German gas companies that were both gas traders and network operators [64]. After the liberalization, the trading and the shipping of gas were separated. Because of the high importance of gas in the German energy supply, the trading and shipping of gas are subject to strict regulations. In [64, p. 49], the process before the actual transportation of the gas is described. First, capacity contracts, which are rights to inject or withdraw gas within certain limits, can be booked by a transport customer to be allowed to transport gas through the network. Second, on the day before the transportation the nomination takes place, i.e., the transport customer has to fix the share of the capacity contracts it wants to use. Finally, until two hours before the transportation, the customer is allowed to renominate the initial nomination, e.g., if the supply or demand has unexpectedly changed. Besides this process, there is a daily auction on which freely available capacities are sold one day before the transportation, which do not have the right of a renomination.

A.2 ANACONDA Gas Flow Model

The code ANACONDA [65] simulates the gas flow through pipeline networks. It uses the volume flow rate under standard conditions, which is given by [33]

$$q_0 = \frac{A\rho v}{\rho_0},$$

with unit m^3/s, where A is the cross-sectional area of the pipe and ρ_0 the density under standard conditions. By standard conditions, an air pressure of 1 atm = 1.01325 bar and a temperature of 0 °C = 273.15 K is meant [33]. The nonlinear model in ANACONDA to simulate gas flow through pipes is given by [39, Eq. (5)]

$$\frac{\partial p}{\partial t} + \frac{\rho_0 c^2}{A}\frac{\partial q_0}{\partial x} = 0, \tag{A.1a}$$

$$\frac{\partial q_0}{\partial t} + \frac{\partial}{\partial x}\left(\frac{A}{\rho_0}p + \frac{\rho_0 c^2}{A}\frac{q_0^2}{p}\right) = -\frac{\lambda \rho_0 c^2 |q_0| q_0}{2DAp}. \tag{A.1b}$$

This nonlinear model is derived from the isothermal Euler equations, the first two equations of (3.1), by assuming both the compressibility factor z to be constant and the pipe to be horizontal, i.e., $h' = 0$.

A.3 Network with One Compressor

A small example gas network with one compressor and one pipe is given in Figure A.1. The gas flow in this network is simulated with ANACONDA [65] using the nonlinear model (A.1) for the gas flow in the pipe. The compressor is set to increase the pressure p of the gas with 4 bar and the bypass valve is closed. The time horizon for the simulation is set to $t_f = 4\,\mathrm{h}$. As boundary values, the pressure at the source (so) is prescribed by $p(\mathrm{so}, t) = 60\,\mathrm{bar}$ for every time $t \in [0, t_f]$ and the volume flow rate at the sink (si) is prescribed by

$$\begin{aligned} &q_0(\mathrm{si}, 0) = 0, \quad q_0(\mathrm{si}, 1\,\mathrm{h}) = 139, \quad q_0(\mathrm{si}, 2\,\mathrm{h}) = 194, \\ &q_0(\mathrm{si}, 3\,\mathrm{h}) = 83, \quad q_0(\mathrm{si}, 4\,\mathrm{h}) = 139, \end{aligned} \tag{A.2}$$

with a linear interpolation between these time points. The main result of the simulation is the volume flow rate at the source $q_0(\mathrm{so}, t)$ at the different time points t_i, given by

$$\begin{aligned} &q_0(\mathrm{so}, 0) = 0, \quad q_0(\mathrm{so}, 1\,\mathrm{h}) = 141, \quad q_0(\mathrm{so}, 2\,\mathrm{h}) = 194, \\ &q_0(\mathrm{so}, 3\,\mathrm{h}) = 84, \quad q_0(\mathrm{so}, 4\,\mathrm{h}) = 139. \end{aligned} \tag{A.3}$$

The result shows the amount of gas that should be inserted into the source such that the demand at the sink, given by the boundary values (A.2), is fulfilled. The flow rates in (A.2) are forecasted demands for gas at the sink. However,

forecast errors are involved in these demands. A customer could change his mind due to unexpected circumstances and would like to withdraw a different gas flow rate at the sink as originally stated. Customers are allowed to change their demand until two hours before the withdrawal using a renomination; see Section A.1. Thus, uncertainty is involved in the boundary values.

We investigate how the errors in the boundary values influence the result (A.3) by perturbing the flow rates at the sink with ±5%. We find a linear dependence between $q_0(\mathrm{so}, t_i)$ and $q_0(\mathrm{si}, t_i)$ with a slope of one, i.e., $\frac{\partial q_0(\mathrm{so},t_i)}{\partial q_0(\mathrm{si},t_i)} = 1$. This holds for all four different times $t_i \in \{1\,\mathrm{h}, 2\,\mathrm{h}, 3\,\mathrm{h}, 4\,\mathrm{h}\}$. It means that the error in the result (A.3) is equal to the forecast error in the flow rates (A.2). For example, if we know from experience that the forecast error for the volume flow rate at the sink $q_0(\mathrm{si}, t)$, $t \in [0, t_f]$, is less than or equal to 10%, then we know that the volume flow rate at the source $q_0(\mathrm{so}, t)$ can also maximally change with 10%. Hence, ten per cent more gas should be kept ready at the source than the result of the simulation shows in order to satisfy the possible increase in demand at the sink.

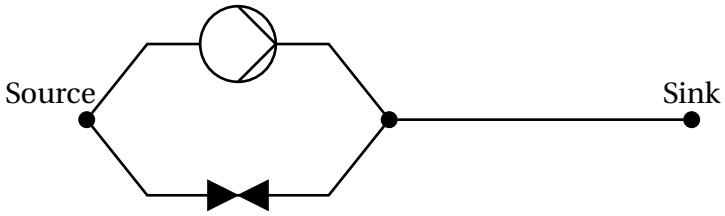

Figure A.1: A small gas network with (from left to right) a source, a compressor including a bypass valve, a pipe, and a sink [39].

A.4 Network with Three Compressors

We again consider the realistic pipe network depicted in Figure 5.3. It consists of twelve pipes P01–P12 with lengths between 30 km and 100 km, three compressors, one control valve, two sources, and four sinks. The target functional M is given by the total fuel gas consumption of the compressors [33, p. 106]

$$M(u) = \sum_{c \in \mathscr{J}_c} \int_0^{t_f} F_c(u, t)\,\mathrm{d}t, \tag{A.4}$$

where $u = [p, q]^T$ is the state vector, $\mathscr{J}_c$ is the set of compressor stations, $t_f = 86\,400\,\mathrm{s}\,(24\,\mathrm{h})$ the simulation time, and F_c the fuel gas consumption of compressor c. The unit of target functional M is m^3. The fuel gas consumption F_c is given by [55], [33, Eq. (1.29)]

$$F_c = d_{F,c}\, q_{0,\mathrm{in}} \left(\left(\frac{p_{\mathrm{out}}}{p_{\mathrm{in}}} \right)^{\frac{\gamma-1}{\gamma}} - 1 \right),$$

where the coefficient $d_{F,c}$ is a compressor specific parameter, $q_{0,\text{in}}$ is the volume flow rate at the compressor inlet, p_{out} and p_{in} are the pressures at the compressor outlet and inlet, respectively, and γ is the isentropic coefficient of the gas. The unit of the fuel gas consumption F_c is m^3/s. The initial conditions are set to the stationary state of the network and the boundary conditions are set to

$$p(\text{So01}, t) = 60, \quad \forall\, t \in [0, t_f], \tag{A.5a}$$

$$q_0(\text{So02}, t) = \begin{cases} 200 + \frac{1}{2880}\, t, & \text{for } t \leq 14\,400, \\ 205, & \text{for } t > 14\,400, \end{cases} \tag{A.5b}$$

$$q_0(\text{Si01}, t) = 100, \quad \forall\, t \in [0, t_f], \tag{A.5c}$$

$$q_0(\text{Si02}, t) = 50, \quad \forall\, t \in [0, t_f], \tag{A.5d}$$

$$q_0(\text{Si03}, t) = 100, \quad \forall\, t \in [0, t_f], \tag{A.5e}$$

$$q_0(\text{Si04}, t) = 100, \quad \forall\, t \in [0, t_f]. \tag{A.5f}$$

The gas flow through this pipeline network is again simulated using the software ANACONDA [65], which results in a target functional value M in (A.4). The boundary values at the four sinks in (A.5c)–(A.5f) are predicted demands by the customers for the coming 24 hours. Again, it could happen that the customers' wishes change during this time period. In this case, the customer is allowed to modify his or her demand at time t_i for time $t_i + 2\,\text{h}$ onward using a renomination; see Section A.1. Hence, the boundary values in (A.5c)–(A.5f) again contain uncertainties during the simulation time of 24 hours.

We determine the effect that the uncertainties in the boundary conditions have on the total fuel gas consumption M. For this, the volume flow rates q_0 at the four sinks are perturbed with $\pm 10\%$ for every time $t \in [0, t_f]$ and the total fuel gas consumption is computed as a function of the flow rates within this range. We find a linear relation between the fuel gas consumption and the gas flow rate at all four sinks. The slopes of the linear functions are 0.12 for sink Si01 and 0.22 for sinks Si02–Si04. This means that changes in the flow rates of sinks Si02–Si04 have a larger effect on the total fuel gas consumption than a change in the flow rate of sink Si01.

Bibliography

[1] M. A. Adewumi and J. Zhou. Simulation of transient flow in natural gas pipelines. 27th Annual Meeting of PSIG (Pipeline Simulation Interest Group), Albuquerque, NM, 1995. URL: https://www.onepetro.org/conference-paper/PSIG-9508.

[2] P. Bales. Hierarchische Modellierung der Eulerschen Flussgleichungen in der Gasdynamik. Diplomarbeit. TU Darmstadt, 2005.

[3] M. K. Banda and M. Herty. Multiscale modeling for gas flow in pipe networks. *Math. Methods Appl. Sci.*, 31(8):915–936, 2008. DOI: 10.1002/mma.948.

[4] M. K. Banda, M. Herty, and A. Klar. Coupling conditions for gas networks governed by the isothermal Euler equations. *Netw. Heterog. Media*, 1(2):295–314, 2006. DOI: 10.3934/nhm.2006.1.295.

[5] M. K. Banda, M. Herty, and A. Klar. Gas flow in pipeline networks. *Netw. Heterog. Media*, 1(1):41–56, 2006. DOI: 10.3934/nhm.2006.1.41.

[6] R. Becker, H. Kapp, and R. Rannacher. Adaptive finite element methods for optimal control of partial differential equations: basic concept. *SIAM J. Control Optim.*, 39(1):113–132, 2000. DOI: 10.1137/S0363012999351097.

[7] R. Becker and R. Rannacher. An optimal control approach to a posteriori error estimation in finite element methods. *Acta Numer.*, 10:1–102, 2001. DOI: 10.1017/S0962492901000010.

[8] J. Bell, M. J. Berger, J. Saltzman, and M. Welcome. Three-dimensional adaptive mesh refinement for hyperbolic conservation laws. *SIAM J. Sci. Comput.*, 15(1):127–138, 1994. DOI: 10.1137/0915008.

[9] M. J. Berger and P. Colella. Local adaptive mesh refinement for shock hydrodynamics. *J. Comput. Phys.*, 82(1):64–84, 1989. DOI: 10.1016/0021-9991(89)90035-1.

[10] M. J. Berger and A. Jameson. Automatic adaptive grid refinement for the Euler equations. *AIAA J.*, 23(4):561–568, 1985. DOI: 10.2514/3.8951.

[11] M. J. Berger and J. Oliger. Adaptive mesh refinement for hyperbolic partial differential equations. *J. Comput. Phys.*, 53(3):484–512, 1984. DOI: 10.1016/0021-9991(84)90073-1.

[12] M. Besier and R. Rannacher. Goal-oriented space-time adaptivity in the finite element Galerkin method for the computation of nonstationary incompressible flow. *Int. J. Numer. Meth. Fl.*, 70(9):1139–1166, 2012. DOI: 10.1002/fld.2735.

[13] L. T. Biegler. *Nonlinear Programming: Concepts, Algorithms, and Applications to Chemical Processes*. MOS-SIAM Series on Optimization. SIAM, Philadelphia, PA, 2010. DOI: 10.1137/1.9780898719383.

[14] H. G. Bock, M. Diehl, E. Kostina, and J. P. Schlöder. Constrained optimal feedback control of systems governed by large differential algebraic equations. In: *Real-Time PDE-Constrained Optimization*. SIAM, Philadelphia, PA, 2007, pp. 3–24. DOI: 10.1137/1.9780898718935.ch1.

[15] M. Bollhöfer and V. Mehrmann. *Numerische Mathematik – Eine projektorientierte Einführung für Ingenieure, Mathematiker und Naturwissenschaftler*. Grundkurs Mathematik. Vieweg+Teubner Verlag, Wiesbaden, 2004. DOI: 10.1007/978-3-322-80242-2.

[16] M. Braack and A. Ern. A posteriori control of modeling errors and discretization errors. *Multiscale Model. Simul.*, 1(2):221–238, 2003. DOI: 10.1137/S1540345902410482.

[17] S. C. Brenner and L. R. Scott. *The Mathematical Theory of Finite Element Methods*. Third edition. Texts in Applied Mathematics. Springer, New York, 2008. DOI: 10.1007/978-0-387-75934-0.

[18] R. W. Brockett. *Finite Dimensional Linear Systems*. Classics in Applied Mathematics. SIAM, Philadelphia, PA, 2015. DOI: 10.1137/1.9781611973884.

[19] J. Brouwer, I. Gasser, and M. Herty. Gas pipeline models revisited: model hierarchies, nonisothermal models, and simulations of networks. *Multiscale Model. Simul.*, 9(2):601–623, 2011. DOI: 10.1137/100813580.

[20] Bundesministerium für Wirtschaft und Energie. Primärenergieverbrauch nach Energieträgern. URL: www.bmwi.de.

[21] Bundesverband der Energie- und Wasserwirtschaft e.V. Gas pipelines in Europe. URL: www.bdew.de.

[22] C. Carstensen and R. H. W. Hoppe. Error reduction and convergence for an adaptive mixed finite element method. *Math. Comp.*, 75(255):1033–1042, 2006. DOI: 10.1090/S0025-5718-06-01829-1.

[23] C. Carstensen and R. H. W. Hoppe. Convergence analysis of an adaptive nonconforming finite element method. *Numer. Math.*, 103(2):251–266, 2006. DOI: 10.1007/s00211-005-0658-6.

[24] F. Chaitin-Chatelin and V. Frayssé. *Lectures on Finite Precision Computations*. Software, Environments and Tools. SIAM, Philadelphia, PA, 1996. DOI: 10.1137/1.9780898719673.

[25] K. S. Chapman, P. Krishniswami, V. Wallentine, M. Abbaspour, R. Ranganathan, R. Addanki, J. Sengupta, and L. Chen. *Virtual Pipeline System Testbed to Optimize the U.S. Natural Gas Transmission Pipeline System*. Tech. rep. DE-FC26-01NT41322. The National Gas Machinery Laboratory, Kansas State University, 2005.

[26] N. H. Chen. An explicit equation for friction factor in pipe. *Ind. Eng. Chem. Fund.*, 18(3):296–297, 1979. DOI: 10.1021/i160071a019.

[27] O. Christensen. *Functions, Spaces, and Expansions: Mathematical Tools in Physics and Engineering*. Applied and Numerical Harmonic Analysis. Birkhäuser, Boston, MA, 2010.

[28] R. M. Colombo and M. Garavello. A well-posed Riemann problem for the p-system at a junction. *Netw. Heterog. Media*, 1(3):495–511, 2006. DOI: 10.3934/nhm.2006.1.495.

[29] G. B. Dantzig. Discrete-variable extremum problems. *Operations Res.*, 5:266–277, 1957.

[30] P. Deuflhard and A. Hohmann. *Numerical Analysis, A First Course in Scientific Computation*. De Gruyter Textbook. Walter de Gruyter & Co., Berlin, 1995.

[31] M. Diehl, H. G. Bock, and J. P. Schlöder. A real-time iteration scheme for nonlinear optimization in optimal feedback control. *SIAM J. Control Optim.*, 43(5):1714–1736, 2005. DOI: 10.1137/S0363012902400713.

[32] M. Diehl, H. G. Bock, and J. P. Schlöder. Newton-type methods for the approximate solution of nonlinear programming problems in real-time. In: *High Performance Algorithms and Software for Nonlinear Optimization*. Ed. by G. Di Pillo and A. Murli. Springer, Boston, MA, 2003, pp. 177–200. DOI: 10.1007/978-1-4613-0241-4_8.

[33] P. Domschke. Adjoint-Based Control of Model and Discretization Errors for Gas Transport in Networked Pipelines. PhD thesis. TU Darmstadt, 2011.

[34] P. Domschke, A. Dua, J. J. Stolwijk, J. Lang, and V. Mehrmann. Adaptive refinement strategies for the simulation of gas flow in networks using a model hierarchy. *Electron. Trans. Numer. Anal.*, 48:97–113, 2018. URL: http://etna.mcs.kent.edu/volumes/2011-2020/vol48/abstract.php?vol=48&pages=97-113.

[35] P. Domschke, B. Geißler, O. Kolb, J. Lang, A. Martin, and A. Morsi. Combination of nonlinear and linear optimization of transient gas networks. *INFORMS J. Comput.*, 23(4):605–617, 2011. DOI: 10.1287/ijoc.1100.0429.

[36] P. Domschke, B. Hiller, J. Lang, and C. Tischendorf. *Modellierung von Gasnetzwerken: Eine Übersicht*. Preprint 2717. TU Darmstadt, 2017. URL: http://www3.mathematik.tu-darmstadt.de/fb/mathe/preprints.html.

[37] P. Domschke, O. Kolb, and J. Lang. Adjoint-based control of model and discretisation errors for gas and water supply networks. In: *Computational Optimization and Applications in Engineering and Industry*. Ed. by X. Yang and S. Koziel. Springer, Berlin Heidelberg, 2011, pp. 1–17. DOI: 10.1007/978-3-642-20986-4.

[38] P. Domschke, O. Kolb, and J. Lang. Adjoint-based control of model and discretisation errors for gas flow in networks. *Int. J. Mathematical Modelling and Numerical Optimisation*, 2(2):175–193, 2011. DOI: 10.1504/IJMMNO.2011.039427.

[39] P. Domschke, O. Kolb, and J. Lang. Adjoint-based error control for the simulation and optimization of gas and water supply networks. *Appl. Math. Comput.*, 259:1003–1018, 2015. DOI: 10.1016/j.amc.2015.03.029.

[40] P. Domschke, O. Kolb, and J. Lang. An adaptive model switching and discretization algorithm for gas flow on networks. *Procedia Comput. Sci.*, 1(1):1331–1340, 2010. DOI: 10.1016/j.procs.2010.04.148.

[41] W. Dörfler and M. Rumpf. An adaptive strategy for elliptic problems including a posteriori controlled boundary approximation. *Math. Comp.*, 67(224):1361–1382, 1998. DOI: 10.1090/S0025-5718-98-00993-4.

[42] W. Dörfler. A convergent adaptive algorithm for Poisson's equation. *SIAM J. Numer. Anal.*, 33(3):1106–1124, 1996. DOI: 10.1137/0733054.

[43] K. Ehrhardt and M. C. Steinbach. Nonlinear optimization in gas networks. In: *Modeling, Simulation and Optimization of Complex Processes*. Ed. by H. G. Bock, E. Kostina, H. X. Phu, and R. Ranacher. Springer, Berlin Heidelberg, 2005, pp. 139–148. DOI: 10.1007/3-540-27170-8_11.

[44] K. Ehrhardt and M. C. Steinbach. KKT systems in operative planning for gas distribution networks. *Proc. Appl. Math. Mech.*, 4(1):606–607, 2004. DOI: 10.1002/pamm.200410284.

[45] M. Feistauer. *Mathematical Methods in Fluid Dynamics*. Pitman Monographs and Surveys in Pure and Applied Mathematics Series. Longman Scientific & Technical, Harlow, UK, 1993.

[46] A. Fügenschuh, B. Geißler, R. Gollmer, A. Morsi, M. E. Pfetsch, J. Rövekamp, M. Schmidt, K. Spreckelsen, and M. C. Steinbach. Physical and technical fundamentals of gas networks. In: *Evaluating Gas Network Capacities*. Ed. by T. Koch, B. Hiller, M. E. Pfetsch, and L. Schewe. MOS-SIAM Series on Optimization. SIAM, Philadelphia, PA, 2015, pp. 17–44. DOI: 10.1137/1.9781611973693.ch2.

[47] B. Geißler, A. Martin, A. Morsi, and L. Schewe. Using piecewise linear functions for solving MINLPs. In: *Mixed Integer Nonlinear Programming*. Ed. by J. Lee and S. Leyffer. IMA Vol. Math. Appl. Springer, New York, 2012, pp. 287–314. DOI: 10.1007/978-1-4614-1927-3.

[48] B. Geißler, A. Morsi, and L. Schewe. A new algorithm for MINLP applied to gas transport energy cost minimization. In: *Facets of Combinatorial Optimization*. Springer, Heidelberg, 2013, pp. 321–353. DOI: 10.1007/978-3-642-38189-8_14.

[49] G. H. Golub and C. F. Van Loan. *Matrix Computations*. Third edition. Johns Hopkins Studies in the Mathematical Sciences. Johns Hopkins University Press, Baltimore, MD, 1996.

[50] C. Grossmann and H. Roos. *Numerical Treatment of Partial Differential Equations*. Universitext. Translated and revised from the 3rd (2005) German edition by Martin Stynes. Springer, Berlin, 2007. DOI: 10.1007/978-3-540-71584-9.

[51] M. Gugat, F. M. Hante, M. Hirsch-Dick, and G. Leugering. Stationary states in gas networks. *Netw. Heterog. Media*, 10(2):295–320, 2015. DOI: 10.3934/nhm.2015.10.295.

[52] M. Gugat, R. Schultz, and D. Wintergerst. Networks of pipelines for gas with nonconstant compressibility factor: stationary states. *Comp. Appl. Math.*, 2016. DOI: 10.1007/s40314-016-0383-z.

[53] E. Hairer, S. P. Nørsett, and G. Wanner. *Solving Ordinary Differential Equations I*. Second edition. Springer Series in Computational Mathematics. Springer, Berlin, 1993. DOI: 10.1007/978-3-540-78862-1.

[54] F. M. Hante, G. Leugering, A. Martin, L. Schewe, and M. Schmidt. Challenges in optimal control problems for gas and fluid flow in networks of pipes and canals: from modeling to industrial applications. In: *Industrial Mathematics and Complex Systems: Emerging Mathematical Models, Methods and Algorithms*. Ed. by P. Manchanda, R. Lozi, and A. H. Siddiqi. Industrial and Applied Mathematics. Springer, Singapore, 2017, pp. 77–122. DOI: 10.1007/978-981-10-3758-0_5.

[55] M. Herty. Modeling, simulation and optimization of gas networks with compressors. *Netw. Heterog. Media*, 2(1):81–97, 2007. DOI: 10.3934/nhm.2007.2.81.

[56] M. Herty, J. Mohring, and V. Sachers. A new model for gas flow in pipe networks. *Math. Methods Appl. Sci.*, 33(7):845–855, 2010. DOI: 10.1002/mma.1197.

[57] N. J. Higham. *Accuracy and Stability of Numerical Algorithms*. Second edition. SIAM, Philadelphia, PA, 2002. DOI: 10.1137/1.9780898718027.

[58] International Organization for Standardization. ISO 6976:1995 Natural gas – Calculation of calorific values, density, relative density and Wobbe index from composition. URL: https://www.iso.org/obp/ui/#iso:std:iso:6976:ed-2:v2:en (visited on 04/20/2016).

[59] N. Jacobson. *Basic Algebra I*. Second edition. Basic Algebra. Dover Publications, Mineola, NY, 2009.

[60] I. Joormann, M. Schmidt, M. C. Steinbach, and B. M. Willert. What does "feasible" mean? In: *Evaluating Gas Network Capacities*. Ed. by T. Koch, B. Hiller, M. E. Pfetsch, and L. Schewe. MOS-SIAM Series on Optimization. SIAM, Philadelphia, PA, 2015, pp. 211–232. DOI: 10.1137/1.9781611973693.ch11.

[61] S. L. Ke and H. C. Ti. Transient analysis of isothermal gas flow in pipeline networks. *Chem. Eng. J.*, 76(2):169–177, 2000. DOI: 10.1016/S1385-8947(99)00122-9.

[62] H. Kellerer, U. Pferschy, and D. Pisinger. *Knapsack Problems*. Springer, Berlin, 2004. DOI: 10.1007/978-3-540-24777-7.

[63] C. T. Kelley. *Iterative Methods for Linear and Nonlinear Equations*. Frontiers in Applied Mathematics. SIAM, Philadelphia, PA, 1995. DOI: 10.1137/1.9781611970944.

[64] T. Koch, B. Hiller, M. E. Pfetsch, and L. Schewe, eds. *Evaluating Gas Network Capacities*. MOS-SIAM Series on Optimization. SIAM, Philadelphia, PA, 2015. DOI: 10.1137/1.9781611973693.

[65] O. Kolb. Simulation and Optimization of Gas and Water Supply Networks. PhD thesis. TU Darmstadt, 2011.

[66] O. Kolb, J. Lang, and P. Bales. An implicit box scheme for subsonic compressible flow with dissipative source term. *Numer. Algorithms*, 53(2-3):293–307, 2010. DOI: 10.1007/s11075-009-9287-y.

[67] M. Konstantinov, D. W. Gu, V. Mehrmann, and P. Petkov. *Perturbation Theory for Matrix Equations*. Studies in Computational Mathematics. Elsevier, Amsterdam, 2003.

[68] A. Kröner, K. Kunisch, and B. Vexler. Semismooth Newton methods for optimal control of the wave equation with control constraints. *SIAM J. Control Optimization*, 49(2):830–858, 2011. DOI: 10.1137/090766541.

[69] R. Le Veque. *Finite Volume Methods for Hyperbolic Problems*. Cambridge Texts in Applied Mathematics. Cambridge University Press, Cambridge, 2002.

[70] D. Leykekhman and B. Vexler. A priori error estimates for three dimensional parabolic optimal control problems with pointwise control. *SIAM J. Control Optimization*, 54(5):2403–2435, 2016. DOI: 10.1137/15M1028042.

[71] F. Liu, W. W. Hager, and A. V. Rao. Adaptive mesh refinement method for optimal control using nonsmoothness detection and mesh size reduction. *J. of the Franklin Institute*, 352(10):4081–4106, 2015. DOI: 10.1016/j.jfranklin.2015.05.028.

[72] M. V. Lurie. *Modeling of Oil Product and Gas Pipeline Transportation*. Wiley-VCH, Weinheim, 2008. DOI: 10.1002/9783527626199.

[73] A. Martin, M. Möller, and S. Moritz. Mixed integer models for the stationary case of gas network optimization. *Math. Program.*, 105(2):563–582, 2006. DOI: 10.1007/s10107-005-0665-5.

[74] V. Mehrmann, M. Schmidt, and J. J. Stolwijk. Model and discretization error adaptivity within stationary gas transport optimization. *Vietnam J. Math.*, 46(4):779–801, 2018. DOI: 10.1007/s10013-018-0303-1.

[75] V. Mehrmann and J. J. Stolwijk. *Error analysis for the Euler equations in purely algebraic form*. Preprint 6–2015. TU Berlin, Institut für Mathematik, 2015. URL: https://www3.math.tu-berlin.de/cgi-bin/IfM/show_abstract.cgi?Report-06-2015.rdf.html.

[76] S. Moritz. A Mixed Integer Approach for the Transient Case of Gas Network Optimization. PhD thesis. TU Darmstadt, 2006.

[77] A. S. Morse, D. Q. Mayne, and G. C. Goodwin. Applications of hysteresis switching in parameter adaptive control. *IEEE Trans. Automat. Control*, 37(9):1343–1354, 1992. DOI: 10.1109/9.159571.

[78] Z. Nagy, S. Agachi, F. Allgöwer, R. Findeisen, M. Diehl, H. G. Bock, and J. P. Schlöder. The tradeoff between modelling complexity and real-time feasibility in nonlinear model predictive control. In: *Proceedings of the 6th World Multiconference on Systemics, Cybernetics and Informatics*. International Institute of Informatics and Systemics, Orlando, FL, 2002.

[79] J. T. Oden, S. Prudhomme, A. Romkes, and P. T. Bauman. Multiscale modeling of physical phenomena: adaptive control of models. *SIAM J. Sci. Comput.*, 28(6):2359–2389, 2006. DOI: 10.1137/050632488.

[80] A. J. Osiadacz. Different transient flow models – limitations, advantages, and disadvantages. 28th Annual Meeting of PSIG (Pipeline Simulation Interest Group), San Francisco, CA, 1996. URL: https://www.onepetro.org/conference-paper/PSIG-9606.

[81] A. J. Osiadacz. *Simulation and Analysis of Gas Networks*. E. & F.N. Spon, London, 1987.

[82] A. J. Osiadacz and M. Chaczykowski. Comparison of isothermal and non-isothermal pipeline gas flow models. *Chem. Eng. J.*, 81(1–3):41–51, 2001. DOI: 10.1016/S1385-8947(00)00194-7.

[83] M. Padulo, M. S. Campobasso, and M. D. Guenov. Novel uncertainty propagation method for robust aerodynamic design. *AIAA J.*, 49(3):530–543, 2011. DOI: 10.2514/1.J050448.

[84] P. H. Petkov, N. D. Christov, and M. M. Konstantinov. *Computational Methods for Linear Control Systems*. Prentice Hall International Ltd., Hertfordshire, UK, 1991.

[85] J. R. Rice. *Numerical Methods, Software, and Analysis*. Second edition. Academic Press, San Diego, CA, 1993.

[86] D. Rose, M. Schmidt, M. C. Steinbach, and B. M. Willert. Computational optimization of gas compressor stations: MINLP models versus continuous reformulations. *Math. Meth. Oper. Res.*, 83(3):409–444, 2016. DOI: 10.1007/s00186-016-0533-5.

[87] L. Schewe, T. Koch, A. Martin, and M. E. Pfetsch. Mathematical optimization for evaluating gas network capacities. In: *Evaluating Gas Network Capacities*. MOS-SIAM Series on Optimization. SIAM, Philadelphia, PA, 2015, pp. 87–102. DOI: 10.1137/1.9781611973693.ch5.

[88] M. Schmidt, D. Aßmann, R. Burlacu, J. Humpola, I. Joormann, N. Kanelakis, T. Koch, D. Oucherif, M. E. Pfetsch, L. Schewe, R. Schwarz, and M. Sirvent. GasLib – A library of gas network instances. *Data*, 2(4):40, 2017. DOI: 10.3390/data2040040.

[89] M. Schmidt, M. C. Steinbach, and B. M. Willert. High detail stationary optimization models for gas networks. *Optim. Eng.*, 16(1):131–164, 2015. DOI: 10.1007/s11081-014-9246-x.

[90] M. Schmidt, M. C. Steinbach, and B. M. Willert. High detail stationary optimization models for gas networks: validation and results. *Optim. Eng.*, 17(2):437–472, 2016. DOI: 10.1007/s11081-015-9300-3.

[91] M. C. Steinbach. On PDE solution in transient optimization of gas networks. *J. Comput. Appl. Math.*, 203(2):345–361, 2007. DOI: 10.1016/j.cam.2006.04.018.

[92] J. Stoer and R. Bulirsch. *Introduction to Numerical Analysis*. Springer, New York-Heidelberg, 1980.

[93] J. J. Stolwijk and V. Mehrmann. *Error Analysis and Model Adaptivity for Flows in Gas Networks*. Preprint 2–2017. TU Berlin, Institut für Mathematik, 2017. URL: https://www3.math.tu-berlin.de/cgi-bin/IfM/show_abstract.cgi?Report-02-2017.rdf.html.

[94] J. J. Stolwijk and V. Mehrmann. Error analysis and model adaptivity for flows in gas networks. *An. Ştiinţ. Univ. "Ovidius" Constanţa Ser. Mat.*, 26(2):231–266, 2018. DOI: 10.2478/auom-2018-0027.

[95] G. Strang. *Linear Algebra and its Applications*. Second edition. Academic Press, New York, 1980.

[96] N. N. Taleb. *The Black Swan: The Impact of the Highly Improbable*. Second edition. Incerto. Random House Publishing Group, New York, 2010.

[97] A. Wächter and L. T. Biegler. Line search filter methods for nonlinear programming: motivation and global convergence. *SIAM J. Optim.*, 16(1):1–31, 2005. DOI: 10.1137/S1052623403426556.

[98] A. Wächter and L. T. Biegler. On the implementation of an interior-point filter line-search algorithm for large-scale nonlinear programming. *Math. Program.*, 106(1):25–57, 2006. DOI: 10.1007/s10107-004-0559-y.

[99] B. Wendroff. On centered difference equations for hyperbolic systems. *J. Soc. Indust. Appl. Math.*, 8:549–555, 1960.

[100] J. F. Wilkinson, D. V. Holliday, E. H. Batey, and K. W. Hannah. *Transient Flow in Natural Gas Transmission Systems*. American Gas Association, New York, 1964.

[101] J. H. Wilkinson. *Rounding Errors in Algebraic Processes*. Prentice-Hall, Inc., Englewood Cliffs, NJ, 1963.

[102] H. Woźniakowski. Numerical stability for solving nonlinear equations. *Numer. Math.*, 27(4):373–390, 1976. DOI: 10.1007/BF01399601.

[103] T. J. Ypma. The effect of rounding errors on Newton-like methods. *IMA J. Numer. Anal.*, 3(1):109–118, 1983. DOI: 10.1093/imanum/3.1.109.